

Higgs Phenomenology in the Two Higgs Doublet Model of type II

*A dissertation submitted to
the University of San Francisco-Quito
in partial fulfillment of
the requirements for the degree of
Doctor of Philosophy*

By
Carlos A. Marín

20 July 2004

Supervisor: Dr. Bruce Hoeneisen

Contents

1	Introduction	1
2	Limits on the Two Higgs Doublet Model from meson decay, mixing and CP violation	
2.1	Introduction	1
2.2	Feynman rules of the charged Higgs in the Two Higgs Doublet Model.	2
2.3	Theory	2
2.4	Limits	5
2.5	Conclusions	5
3	Mass constraints, production cross sections, and decay rates in the Two Higgs Doublet Model	
3.1	Introduction	1
3.2	Masses	1
3.3	Feynman rules	4
3.4	Decay rates of h^0	8
3.5	Branching fractions of h^0	9
3.6	Decay rates of H^\pm	10
3.7	Decays of H^0	11
3.8	Decay rates of A^0	13
3.9	Decay $Z \rightarrow h^0\gamma$	22
3.10	Vertex with four particles	23
3.11	Production of h^0 , H^0 and A^0	23
3.12	Production of h^0Z^0X	25
3.13	Production of H^+	27
3.14	Production of h^0W^+X	29
3.15	Numerical examples	31
3.16	Running coupling constants and GrandUnification	33
3.17	Conclusions	35
4	Higgs production at a muon collider in the Two Higgs Doublet Model of type II	38
4.1	Introduction	1
4.2	Higgs bosons masses and radiative corrections	2

4.3	Production of h^0 , H^0	5
4.4	Production of A^0	11
4.5	Production of H^\pm	14
4.6	Production of charged Higgs boson pairs	16
4.7	$\mu^-\mu^+ \rightarrow t\bar{t}$ annihilation	20
4.8	$H^\mp W^\pm$ production at a Hadron Collider	22
4.8.1	$q\bar{q} \rightarrow H^-W^+$ interaction	22
4.8.2	$gg \rightarrow H^-W^+$ interaction	25
4.8.3	Differential cross section $p\bar{p} \rightarrow H^\mp W^\pm X$	26
4.9	Comparison between $\mu^-\mu^+ \rightarrow H^\mp W^\pm$ and $p\bar{p}, pp \rightarrow H^\mp W^\pm X$ for large values of $\tan\beta$	30
4.10	Conclusions	31
A Functions S^{WW}, S^{HW} and S^{HH}		1
B Calculation of the box diagrams corresponding to charged Higgs contributions to B		
B.1	Invariant amplitude M^{HH}	3
B.2	Invariant amplitude M^{HW}	7
B.3	Invariant amplitude M^{WW}	10
B.4	Mass difference Δm_B	11
C Integrals		12
C.1	$I_\alpha^{HH}(i, j)$	12
C.2	$(I_\alpha^{HW})^{(1)}(i, j)$	13
C.3	$(I_\alpha^{HW})^{(2)}(i, j)$	13
C.4	$I^{HW}(i, j)$	14
C.5	$I_{\alpha\beta}^{HW}(i, j)$	14
D $A^0 \rightarrow Z^0\gamma$ decay		16
D.1	(a) $i = e^-, \mu^-, \tau^-, d, s, b$	16
D.2	b) $i = u, c, t$	21
D.3	Width decay	21

Chapter 1

Introduction

The Standard Model of quarks and leptons is based on some basic principles: special relativity, locality, quantum mechanics, local symmetries and renormalizability [1]. Therefore the predictions of the Standard Model “are precise and unambiguous, and generally cannot be modified ‘a little bit’ except in very limited specific ways. This feature makes the experimental success especially meaningful, since it becomes hard to imagine that the theory could be approximately right without in some sense being exactly right.” [1] The Standard Model predicts the existence of a massive spin zero boson called Higgs particle. The Higgs mechanism is responsible for the masses of the weak interaction gauge bosons W^\pm and Z^0 , and is also sufficient to give masses to the leptons and quarks. The discovery of the Standard Model Higgs is then one of the principal goals of experimental and theoretical particle physicists. We could say that the Higgs mechanism is a cornerstone of the Standard Model.

Among the extensions of the Standard Model that respect its principles and symmetries, that are compatible with present data within a region of parameter space, and are of interest at the large particle colliders, is the addition of a second doublet of Higgs fields. Higgs doublets can be added to the Standard Model without upsetting the Z/W mass ratio; higher dimensional representations upset this ratio [2].

In the Two Higgs Doublet Model there are two choices for the Higgs-quark interactions. In Model I, the quarks and leptons do not couple to the first Higgs doublet (Φ_1), but couple to the second Higgs doublet (Φ_2). In Model II, Φ_1 couples only to down-type quarks and leptons and Φ_2 couples only to up-type quarks and neutrinos. If we consider the neutrinos as massless particles, there are no couplings between neutrinos and neutral Higgs bosons. The Model II choice for the Higgs-fermion couplings is the required structure for the Minimal Supersymmetric Model.

After the electroweak symmetry-breaking mechanism, three of the eight degrees of freedom are absorbed by the W^\pm and Z^0 gauge bosons, leading to the existence of five elementary Higgs particles. The physical spectrum of the Two Higgs Doublet Model (Model II) contains five Higgs bosons: one pseudoscalar A^0 (CP-odd scalar), two neutral scalars H^0 and h^0 (CP-even scalars), and two charged scalars H^+ and H^- . In the most general model, the masses of the Higgs bosons, the mixing angle α ($-\pi/2 < \alpha \leq 0$) between the two neutral scalar Higgs fields, and the ratio of the vacuum expectation values of the two neutral components of the Higgs doublets, $\tan \beta$ ($0 \leq \beta < \frac{\pi}{2}$), are all independent parameters of the theory [3]. However, in the Minimal Supersymmetric Model the conditions on the potential imposed by supersymmetry reduces the number of parameters to two, which may be chosen to be $\tan \beta$ and m_H [3].

$$\Phi_1 = \begin{pmatrix} \Phi_1^{o*} \\ -\Phi_1^- \end{pmatrix}, \quad \Phi_2 = \begin{pmatrix} \Phi_2^+ \\ \Phi_2^o \end{pmatrix}, \quad \tan \beta \equiv \frac{\langle \Phi_2^o \rangle}{\langle \Phi_1^{o*} \rangle}.$$

In this thesis we study the Two Higgs Doublet Model of type II, set limits to the parameter $\tan \beta$ as a function of the mass of the charged Higgs m_H , and find interesting discovery channels in hadron colliders or muon colliders.

All the analysis in this thesis are based on the “tree-level Higgs potential” [3].

The plan in my thesis is the following:

In the second Chapter[4], using the experimental data on meson decay rates, mixing and CP violation in the K^0 and B^0 systems, we set limits to the parameter $\tan \beta$ as a function of the mass of the charged Higgs m_H . Recent measurements of $\sin(2\beta_{CKM})$ by the B-factories Belle [5] and BaBar [6] permit us to set more stringent limits on $\tan \beta$. β_{CKM} is an angle of the “unitarity triangle”. [7]

In the third Chapter[8], we present graphically the corresponding limits on m_{H^0} , m_{h^0} and m_{A^0} as a function of the mass of the charged Higgs, without considering the influence of radiative corrections. Then we calculate production cross sections, decay rates and branching fractions of the Higgs particles. Next, we obtain the running coupling constants and discuss Grand Unification. Finally, in the Conclusions, we list interesting discovery channels.

In Chapter four [9], we analyze the possibility of the construction of a $\mu^-\mu^+$ collider to detect charged or neutral Higgs bosons. The reason for this is that in a muon collider, the signal could be cleaner than in a hadron collider. Some of the production cross sections that we study are: $\mu^-\mu^+ \rightarrow h^0 Z^0, H^0 Z^0, H^- H^+, A^0 Z^0$ and $H^\mp W^\pm$. Then, we compare

the channel $\mu^-\mu^+ \rightarrow H^\mp W^\pm$ (at $\sqrt{s} = 500\text{GeV}/c$ and for large values of $\tan\beta$) with the production processes $p\bar{p} \rightarrow H^\mp W^\pm X$ (at the Tevatron) and $pp \rightarrow H^\mp W^\pm X$ (at the LHC), taking into account the $t\bar{t}$ background, to check the feasibility of detecting H^\pm using a muon collider. The influence of radiative corrections in the masses of the Higgs bosons is considered in all the calculations. Finally, in the Conclusions, we also check the process $\mu^-\mu^+ \rightarrow A^0 h^0$.

NOTE : The results presented in this thesis (width decays, production cross sections, etc.) are calculated in detail in reference [10].

Bibliography

- [1] Frank Wilczek, “Beyond the Standard Model: an answer and twenty questions”, hep-ph/9802400 (1998).
- [2] Bruce Hoeneisen, Serie de Documentos USFQ **26**, Universidad San Francisco de Quito, Ecuador (2001).
- [3] Vernon Barger and Roger Phillips, Collider Physics (Addison Wesley, 1988); S. Dawson, J.F. Gunion, H.E. Haber and G. Kane, The Higgs Hunter’s Guide (Addison Wesley, 1990).
- [4] Carlos A. Marín and Bruce Hoeneisen, hep-ph/0210167 (2002).
- [5] K. Abe *et.al.* (Belle Collaboration), Belle Preprint 2002-6 and hep-ex/0202027v2, 2002.
- [6] B. Aubert *et.al.*, SLAC preprint SLAC-PUB-9153, 2002 and hep-ex/0203007.
- [7] 2002 Review of Particle Physics, The Particle Data Group, K. Hagiwara *et.al.*, Phys. Rev. D **66** (2002) 010001.
- [8] C. Marín and B. Hoeneisen, hep-ph/0402061 v1 (2004).
- [9] C. Marín, hep-ph/0405021 v1 (2004).
- [10] C. Marín, Higgs Phenomenology in the Two Higgs Doublet Model of type II (personal notes), Volumen I, II and III, Universidad San Francisco de Quito (2004).

Chapter 2

Limits on the Two Higgs
Doublet Model from meson
decay, mixing and CP violation

Abstract

We calculate the rate of π^+ , K^+ , D^+ and $B^+ \rightarrow \mu^+ \nu_\mu$ decays, the branching ratio corresponding to $H^+ \rightarrow \tau^+ \nu_\tau$, and the box diagrams of $B^o \leftrightarrow \bar{B}^o$, $K^o \leftrightarrow \bar{K}^o$ and $D^o \leftrightarrow \bar{D}^o$ mixing in the Two Higgs Doublet Model (Model II). Using the experimental data on meson decay rates, mixing, and CP violation in the K^o and B^o systems we set competitive upper and lower limits to the parameter $\tan \beta$ as a function of the mass of the charged Higgs m_H .

2.1 Introduction

The Standard Model of quarks and leptons is here to stay. This theory is based on principles: special relativity, locality, quantum mechanics, local symmetries and renormalizability[1]. Therefore the predictions of the Standard Model “are precise and unambiguous, and generally cannot be modified ‘a little bit’ except in very limited specific ways. This feature makes the experimental success especially meaningful, since it becomes hard to imagine that the theory could be approximately right without in some sense being exactly right.”[1] Among the extensions of the Standard Model that respect its principles and symmetries, that are compatible with present data within a region of parameter space, and are of interest at the large particle colliders, is the addition of a second doublet of Higgs fields. Higgs doublets can be added to the Standard Model without upsetting the Z/W mass ratio; higher dimensional representations upset this ratio. A second Higgs doublet could make the three running coupling constants of the Standard Model meet at the Grand Unified Theory (GUT) scale. A second Higgs doublet is necessary in Supersymmetric extensions of the Standard Model[2]. In this article we explore the limits that present data place on the parameters of the Two Higgs Doublet Model (Model II).[3] In particular we consider meson decay, mixing and CP violation.

All of our analysis is based on the “tree-level Higgs potential”[3]. The physical spectrum of the Two Higgs Doublet Model (Model II) contains five Higgs bosons: one pseudoscalar A^o (CP-odd scalar), two neutral scalars H^o and h^o (CP-even scalars), and two charged scalars H^+ and H^- . In the most general model, the masses of the Higgs bosons, the mixing angle α between the two neutral scalar Higgs fields, and the ratio of the vacuum expectation values of the two neutral components of the Higgs doublets, $\tan \beta > 0$, are all independent parameters of the theory. However, in the Minimal Supersymmetric Model the conditions on the potential imposed by supersymmetry reduces the number of parameters to two, which may be chosen to be $\tan \beta$ and m_H [3].

$$\Phi_1 = \begin{pmatrix} \Phi_1^{o*} \\ -\Phi_1^- \end{pmatrix}, \quad \Phi_2 = \begin{pmatrix} \Phi_2^+ \\ \Phi_2^o \end{pmatrix}, \quad \tan \beta \equiv \frac{\langle \Phi_2^o \rangle}{\langle \Phi_1^{o*} \rangle}.$$

Using the experimental data on meson decay rates, mixing and CP violation we set limits to the parameter $\tan \beta$ as a function of the mass of the charged Higgs m_H . Recent measurements of $\sin(2\beta_{CKM})$ by the B-factories Belle[5] and BaBar[6] permit us to set more stringent limits on $\tan \beta$. β_{CKM} is an angle of the “unitarity triangle”. [7]

2.2 Feynman rules of the charged Higgs in the Two Higgs Doublet Model.

The effective Lagrangian corresponding to the $H^\pm f \bar{f}'$ vertex is:

$$\begin{aligned} \mathcal{L}_{H^\pm f f'} = & \frac{g}{2\sqrt{2}m_W} \{ H^+ V_{ff'} \bar{u}_f (A + B\gamma^5) v_{\bar{f}'} \\ & + H^- V_{ff'}^* \bar{u}_{f'} (A - B\gamma^5) v_{\bar{f}} \} \end{aligned} \quad (2.1)$$

where

$$A \equiv (m_{f'} \tan \beta + m_f \cot \beta) \quad (2.2)$$

and

$$B \equiv (m_{f'} \tan \beta - m_f \cot \beta), \quad (2.3)$$

f = fermion (quark or lepton) and \bar{f}' = antifermion (antiquark or antilepton). $V_{ff'}$ is an element of the CKM matrix.

The charged-Higgs propagator is: $i/(K^2 - m_H^2 + i\varepsilon)$.

2.3 Theory

Consider the (B^o, \bar{B}^o) system. $B^o \leftrightarrow \bar{B}^o$ mixing occurs because of the box diagrams illustrated in Figure 2.1. The difference in mass of the two eigenstates that diagonalize the hamiltonian can be written in the form

$$\begin{aligned} \Delta m_B = & \frac{\beta_B G_F^2 m_W^2 f_B^2 m_B}{6\pi^2} \\ & \times \left| \sum_{i,j} \xi_i \xi_j \left[S^{WW} - 2 \cot^2 \beta \cdot S^{HW} + \frac{1}{4} \cot^4 \beta \cdot S^{HH} \right] \right|. \end{aligned} \quad (2.4)$$

The functions

$$S^{WW}(x_W^i, x_W^j), \quad S^{HW}(x_W^i, x_W^j, x_H^i, x_H^j, x_H^W) \quad \text{and} \quad S^{HH}(x_H^i, x_H^j, x_H^W)$$

are obtained from the box diagrams and are written in Appendix A. The Feynman rules for H^\pm are listed in Section 2.2. We have derived[8] S^{WW} in agreement with the literature[9]. The derivation of S^{HW} and S^{HH} is given in Appendices B and C [10]. The variables of these functions are

$$x_W^i \equiv \frac{m_i^2}{m_W^2}, \quad x_H^i \equiv \frac{m_i^2}{m_H^2}, \quad \text{and} \quad x_H^W \equiv \frac{m_W^2}{m_H^2}$$

where $i = u, c, t$. $\xi_i \equiv V_{ib}V_{id}^*$. The notation for the remaining symbols in (2.4) is standard[7]. To obtain the Standard Model[9], omit S^{HW} and S^{HH} . β_B is a factor of order 1. Estimates of β_B using “vacuum intermediate state insertion”[9], “PCAC and vacuum saturation”[9], “bag model”[9], “QCD corrections”[11, 12], and the “free particles in a box”[8] models span the range ≈ 0.4 to ≈ 1 . f_B is the decay constant that appears in the decay rate for $B^+ \rightarrow \mu^+\nu_\mu$ [7] which at tree level in the Two Higgs Doublet Model (Model II) is:

$$\Gamma_{B^+} = \frac{|V_{ub}|^2}{8\pi} G_F^2 m_\mu^2 m_{B^+} \left(1 - \frac{m_\mu^2}{m_{B^+}^2}\right)^2 \left[f_B - g_B \frac{m_{B^+}^2}{m_H^2} \tan^2 \beta\right]^2 \quad (2.5)$$

In the derivation of (2.5) we have substituted

$$\begin{aligned} \bar{v}(\bar{b}) \gamma^\mu (1 - \gamma^5) u(u) &\rightarrow p^\mu f_B, \\ \bar{v}(\bar{b}) (1 - \gamma^5) u(u) &\rightarrow -\frac{m_{B^+}^2}{m_b} g_B \end{aligned}$$

which defines the decay constants f_B and g_B . $\bar{v}(\bar{b})$ and $u(u)$ are spinors, see Section 2. We expect $f_B \approx g_B$: for a scalar meson with the quark and antiquark at rest $f_B = \frac{m_{B^+}}{m_b} g_B$. The decays $B^+ \rightarrow \mu^+\nu_\mu$ and $D^+ \rightarrow \mu^+\nu_\mu$ are not yet accessible to experiment so that f_B and f_D are unknown. f_B is estimated using sum rules[13], or the $B^* - B$ mass difference[14], or a phenomenological model[15], or the MIT bag model[16]. These estimates span the range $\approx 0.06\text{GeV}$ to $\approx 0.2\text{GeV}$ with the convention used in reference [7] and in Equation (2.5).

In the “free particles in a box”[8] model $\beta_B = 1$ (after correcting [8] by a color factor $4/3$) and the volume of the box, *i.e.* the meson, is $V = 8/(\beta_B m_B f_B^2)$.

For the (B_s^0, \bar{B}_s^0) system: $\xi_i \equiv V_{ib}V_{is}^*$ where $i = u, c, t$; in (2.4) replace subscript B by B_s . For the (K^0, \bar{K}^0) system: $\xi_i \equiv V_{is}V_{id}^*$ where $i = u, c, t$; in (2.4) replace subscript B by K . The CP violation parameter ε [9, 7] in the (K^0, \bar{K}^0) system in the Two Higgs Doublet Model is given by:

$$\varepsilon = e^{i\frac{\pi}{4}} \cdot \frac{\text{Im} \left(\sum_{i,j} \xi_i \xi_j [S^{WW} - 2 \cot^2 \beta \cdot S^{HW} + \frac{1}{4} \cot^4 \beta \cdot S^{HH}] \right)}{2\sqrt{2} \cdot \left| \sum_{i,j} \xi_i \xi_j [S^{WW} - 2 \cot^2 \beta \cdot S^{HW} + \frac{1}{4} \cot^4 \beta \cdot S^{HH}] \right|} \quad (2.6)$$

For the (D^0, \bar{D}^0) system: $\xi_i \equiv V_{ci}V_{ui}^*$ where $i = d, s, b$; in (2.4) replace subscript B by D and replace $\cot \beta$ by $\tan \beta$ (leave $\tan \beta$ as is in (2.5)).

The branching ratio for $H^+ \rightarrow \tau^+\nu_\tau$ for $m_H < m_t$ is given by

$$B(H^+ \rightarrow \tau^+\nu_\tau) \approx \frac{m_\tau^2 \tan^2 \beta}{|V_{cs}|^2 a + |V_{cb}|^2 b + m_\tau^2 \tan^2 \beta} \quad (2.7)$$

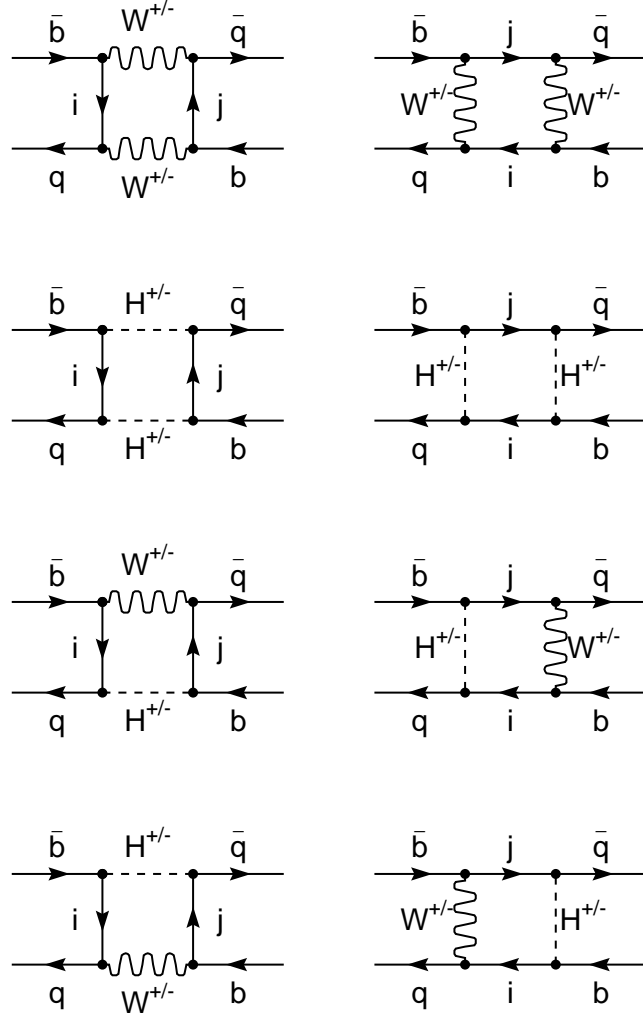


Figure 2.1: Feynman diagrams corresponding to $B^0 \leftrightarrow \bar{B}^0$ mixing in the Two Higgs Doublet Model. $q = d$ or s and $i, j = u, c, t$. The diagrams on the right side interfere with a “-” sign.

with $a \equiv 3[m_s^2 \tan^2 \beta + m_c^2 \cot^2 \beta]$ and $b \equiv 3[m_b^2 \tan^2 \beta + m_c^2 \cot^2 \beta]$. From the measured limit[17] on m_H as a function of the branching ratio and (2.7) we obtain a lower bound of m_H for each $\tan \beta$.

Let us finally mention that the time-dependent CP-violating asymmetry $A \equiv (\Gamma - \bar{\Gamma})/(\Gamma + \bar{\Gamma})$, where Γ ($\bar{\Gamma}$) is the rate of the decay $B^o \rightarrow J/\psi + K_s$ ($\bar{B}^o \rightarrow J/\psi + K_s$), measured by CDF, Belle and BaBar is given by $\sin(2\beta_{CKM}) \cdot \sin(\Delta M t)$ in both the Standard Model and in the Two Higgs Doublet Model (Model II). This is because the dominating terms of $\xi_i \xi_j S^{HW}$ and $\xi_i \xi_j S^{HH}$ have $i = j = t$.

2.4 Limits

All experimental data are taken from [7]. In order to obtain limits we assume conservatively $0.4 < \beta_x < 1.8$, and $f_x = g_x$ with $x = B, B_s, D, K, \pi$. These assumptions are not critical since the upper (lower) limits on $\tan \beta$ depend on terms $\propto \tan^4 \beta$ ($\propto \cot^4 \beta$) in (2.4) or (2.5). We take the magnitude of the elements of the CKM matrix from [7] and leave the phase $\angle V_{ub}$ as a free parameter. The following calculations are made for each $(m_H, \tan \beta)$. The measured value of the parameter ε determines the phase $\angle V_{ub}$ of the CKM matrix, and hence β_{CKM} . This phase is required to be within the experimental bounds: $0.325 < \tan(\beta_{CKM}) < 0.862$ at 95% confidence level [7]. The measured decay rates Γ_K and Γ_π determine f_K and f_π using (2.5). The experimental upper bounds on Γ_B and Γ_D determine upper bounds on f_B and f_D using (2.5). The measured Δm_B and Δm_K determine $\beta_B f_B^2$ and $\beta_K f_K^2$ using (2.4). The experimental upper bound on Δm_D determines an upper bound on $\beta_D f_D^2$. The experimental lower bound on Δm_{B_s} determines a lower bound on $\beta_{B_s} f_{B_s}^2$. From the preceding information we obtain β_K and a lower bound on β_B . Then the requirements $0.4 < \beta_K < 1.8$, $\beta_B < 1.8$ and $0.325 < \tan(\beta_{CKM}) < 0.862$ place limits on $\tan \beta$ for each m_H as listed in Table 2.1. The confidence level of these limits is 95%. It turns out that the lower limit on $\tan \beta$ is determined by the experimental lower limit of $\tan(\beta_{CKM})$, and the upper limit on $\tan \beta$ is determined by $\beta_B < 1.8$.

2.5 Conclusions

Using measured meson decay rates, mixing and CP violation we have obtained lower and upper bounds of $\tan \beta$ for each m_H . These limits are compared with the results of direct searches in Figures 2.2. Note that the measurements of $\sin(2\beta_{CKM})$ by the Belle and BaBar collaborations have raised

$m_H = 100\text{GeV}$	$1.74 < \tan \beta < 67$
$m_H = 200\text{GeV}$	$1.36 < \tan \beta < 134$
$m_H = 300\text{GeV}$	$1.13 < \tan \beta < 202$
$m_H = 1000\text{GeV}$	$0.58 < \tan \beta < 672$

Table 2.1: Limits on $\tan \beta$ for several m_H from measurements of meson decay, mixing and CP violation. These limits correspond to 95% confidence.

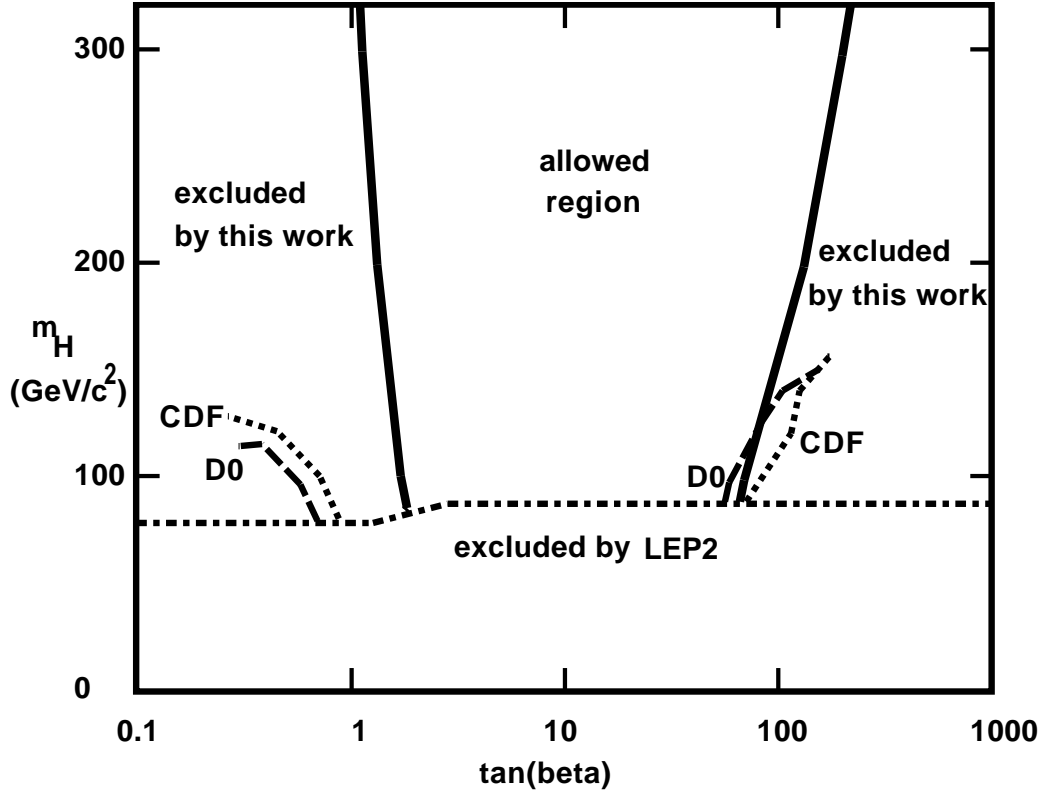


Figure 2.2: Lower and upper limits on $\tan \beta$ as a function of the mass of the charged Higgs m_H from meson decay, mixing and CP violation (continuous curve) compared to limits obtained by CDF[18], D0[19] and LEP2[20], all at 95% confidence.

the lower bound on $\tan\beta$ by a factor ≈ 5 with respect to our previous calculation [4]. It is important to mention that an indirect limit by the CLEO collaboration [21] obtained from the measurements of the $b \rightarrow s\gamma$ transition, limits the Two Higgs Doublet Model of type II to have a charged Higgs mass in excess of about $264\text{GeV}/c^2$ (it is a slow function of $\tan\beta$).

Bibliography

- [1] Frank Wilczek, “Beyond the Standard Model: an answer and twenty questions”, hep-ph/9802400 (1998) .
- [2] R.D. Peccei, “Physics beyond the Standard Model”, hep-ph/9909233 (1999).
- [3] Vernon Barger and Roger Phillips, Collider Physics (Addison Wesley, 1988), pages 452-454; S. Dawson, J. F. Gunion, H.E. Haber and G. Kane, The Higgs Hunter’s Guide (Addison Wesley, 1990), p. 383.
- [4] Carlos A. Marín and Bruce Hoeneisen, Revista Colombiana de Física, **31**, No. 1, 34 (1999).
- [5] K. Abe *et.al.* (Belle Collaboration), Belle Preprint 2002-6 and hep-ex/0202027v2, 2002.
- [6] B. Aubert *et.al.*, SLAC preprint SLAC-PUB-9153, 2002 and hep-ex/0203007.
- [7] 2002 Review of Particle Physics, The Particle Data Group, K. Hagiwara *et.al.*, Phys. Rev. **D 66** (2002) 010001.
- [8] Carlos Marín and Bruce Hoeneisen, POLITECNICA **XVI**, No. 2, 33 (1991), Escuela Politécnica Nacional, Quito, Ecuador.
- [9] Ling-Lie Chau, Physics Reports **95**, No. 1, 1 (1983).
- [10] Carlos Marín and Bruce Hoeneisen, Serie Documentos USFQ No. 15 (1996), Universidad San Francisco de Quito.
- [11] Yosef Nir, Nucl. Phys. **B306**, 14 (1988).
- [12] A. J. Buras, M. Jamin and P. H. Weisz, Nucl. Phys. **B347**, 491 (1990).
- [13] L. J. Reinders, Phys. Rev. **D 38**, 947 (1988).

- [14] M. Suzuki, Phys. Lett. **162B**, 392 (1985).
- [15] M. Suzuki, Nucl. Phys. **B177**, 413 (1981); Phys. Lett. **142B**, 207 (1984).
- [16] E. Golowich, Phys. Lett. **91B**, 271 (1980); M. Claudson, Harvard University preprint HUTP-81/A016.
- [17] A. Heister *et. al.* (ALEPH), hep-ex/0207054 v1 (2002).
- [18] CDF Collab., Phys. Rev. Lett. **79**, 357 (1997).
- [19] D0 Collab., Phys. Rev. Lett. **82**, 4975 (1999); FERMILAB-Conf-00-294-E.
- [20] LEP Higgs Working Group, <http://lephiggs.web.cern.ch/LEPHIGGS/papers/index.html>; LHWG Note/2001-05.
- [21] M. S. Alam et al., Phys. Rev. Lett. **74**, 2885 (1995).

Chapter 3

Mass constraints, production
cross sections, and decay rates
in the Two Higgs Doublet
Model of type II

Abstract

We calculate masses, production cross sections, and decay rates in the Two Higgs Doublet Model of type II. We also discuss running coupling constants and Grand Unification. The most interesting production channels are $gg \rightarrow h^0, H^0, A^0$ on mass shell, and $q\bar{q}, gg \rightarrow h^0 Z$ and $q\bar{q}' \rightarrow h^0 W^\pm$ in the continuum (tho there may be peaks at m_{A^0}). The most interesting decays are $h^0, H^0, A^0 \rightarrow b\bar{b}$ -jets and $\tau^+\tau^-$, and, if above threshold, $H^0 \rightarrow ZZ, W^+W^-$ and $h^0 h^0$. The following final states should be compared with the Standard Model cross section: $b\bar{b}Z, b\bar{b}W^\pm, \tau^+\tau^-Z, \tau^+\tau^-W^\pm, b\bar{b}, \tau^+\tau^-, ZZ, W^+W^-, 3$ and 4 b -jets, $2\tau^+ + 2\tau^-, b\bar{b}\tau^+\tau^-, ZW^+W^-, 3Z, ZZW^\pm$ and $3W^\pm$. Mass peaks should be searched in the following channels: $Zb\bar{b}, ZZ, ZZZ, b\bar{b}, 4b$ -jets and, just in case, $Z\gamma$.

3.1 Introduction

Among the extensions of the Standard Model that respect its principles and symmetries, and are compatible with present data within a region of parameter space, and are of interest at the large particle colliders, is the addition of a second doublet of Higgs fields. In this article we consider the Two Higgs Doublet Model of type II[1]. The Higgs sector of the Minimal Supersymmetric Standard Model (MSSM) is of this type (tho the model of type II does not require Supersymmetry). The physical spectrum of the model contains five Higgs bosons: one pseudoscalar A^o (CP-odd scalar), two neutral scalars H^o and h^o (CP-even scalars), and two charged scalars H^+ and H^- . The masses of the charged Higgs bosons m_H , and the ratio of the vacuum expectation values of the two neutral components of the Higgs doublets, $\tan\beta > 0$, are free parameters of the theory.

In [2] we obtained limits in the $(m_H, \tan\beta)$ plane using measured decay rates, mixing and CP violation of mesons. In this article we present graphically the corresponding limits on m_{H^0} , m_{h^0} and m_{A^0} . Then we calculate production cross sections, decay rates and branching fractions of the Higgs particles. Next, we obtain the running coupling constants and discuss Grand Unification. Finally, in the Conclusions, we list interesting discovery channels.

3.2 Masses

The masses of the neutral Higgs particles as a function of the masses of the charged Higgs m_H , $\tan\beta$ and the masses of Z and W , calculated at tree level, are:

$$m_{A^0}^2 = m_H^2 - m_W^2, \quad (3.1)$$

$$2m_{H^0}^2 = m_H^2 - m_W^2 + m_Z^2 + \left[(m_H^2 - m_W^2 + m_Z^2)^2 - 4m_Z^2 (m_H^2 - m_W^2) \left(\frac{\tan^2\beta - 1}{\tan^2\beta + 1} \right)^2 \right]^{\frac{1}{2}} \quad (3.2)$$

$$2m_{h^0}^2 = m_H^2 - m_W^2 + m_Z^2 - \left[(m_H^2 - m_W^2 + m_Z^2)^2 - 4m_Z^2 (m_H^2 - m_W^2) \left(\frac{\tan^2\beta - 1}{\tan^2\beta + 1} \right)^2 \right]^{\frac{1}{2}} \quad (3.3)$$

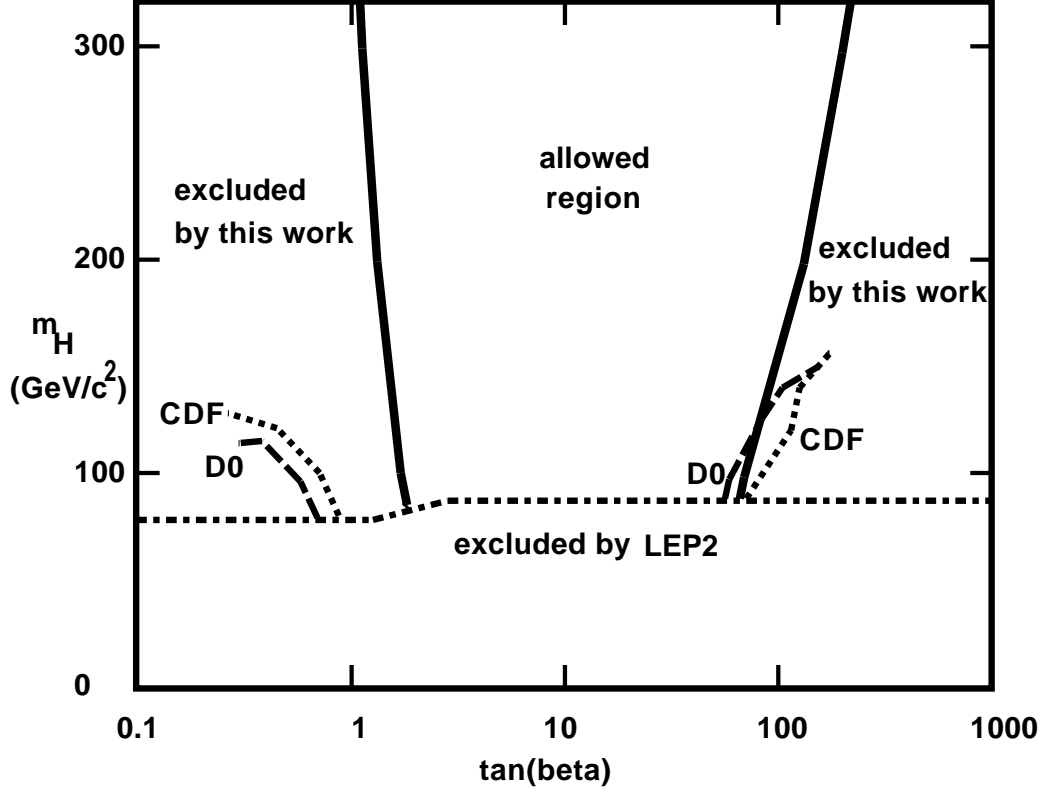


Figure 3.1: Lower and upper limits on $\tan \beta$ as a function of the mass of the charged Higgs m_H from meson decay, mixing and CP violation (continuous curve) compared to limits obtained by CDF[3], D0[4] and LEP2[5], all at 95% confidence. Taken from [2].

We have re derived these equations in agreement with the literature.[1]

In Chapter two [2] we obtained the limits in the $(\tan \beta, m_H)$ plane shown in Figure 3.1. From that figure and Equations 3.1, 3.2 and 3.3 we obtain the limits on the masses of the neutral Higgs particles shown in Figure 3.2.

Radiative corrections can be very large. In the MSSM the largest contributions arise from the incomplete cancellation between top and stop loops. The corresponding plot similar to Figure 3.2 with radiative corrections can be found in [6].

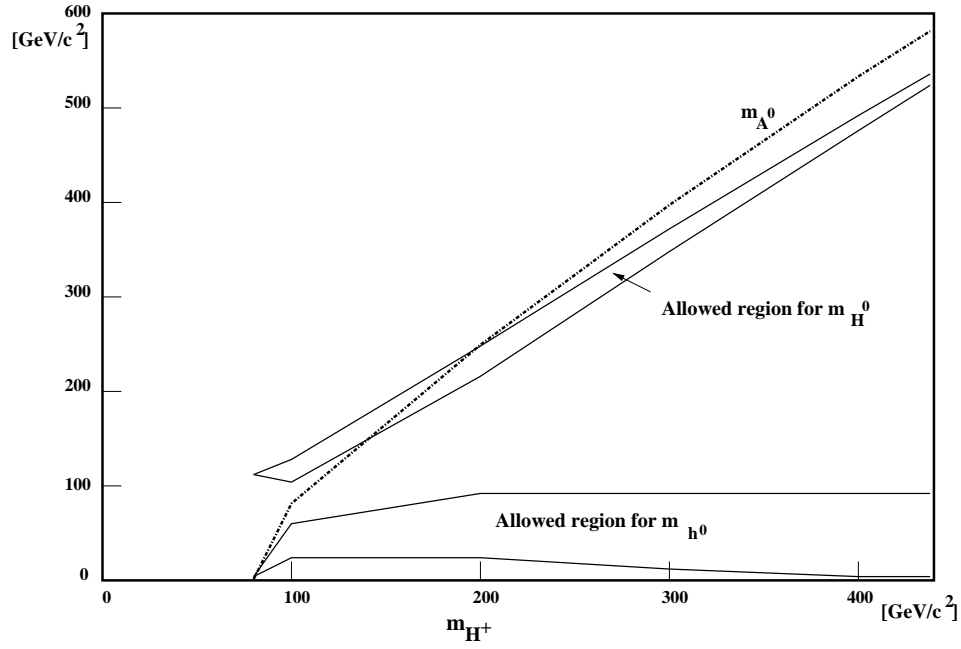


Figure 3.2: Allowed regions of the masses of the neutral Higgs h^0 , H^0 and A^0 as a function of the mass m_H of the charged Higgs H^\pm . From Figure 3.1 and the tree level Equations 3.1, 3.2 and 3.3. Radiative corrections raise the allowed region of h^0 . [6]

3.3 Feynman rules

The Lagrangian for the VHH interaction is:[1]

$$\begin{aligned}\mathcal{L}_{VHH} = & \frac{-ig}{2}W_\mu^+ \cdot H^- \overleftrightarrow{\partial}^\mu [H^0 \sin(\alpha - \beta) + h^0 \cos(\alpha - \beta) + iA^0] + \text{h.c.} \\ & - \frac{ig}{2\cos\theta_W}Z_\mu \{iA^0 \overleftrightarrow{\partial}^\mu [H^0 \sin(\alpha - \beta) + h^0 \cos(\alpha - \beta)] \\ & - (2\sin^2\theta_W - 1) \cdot H^- \overleftrightarrow{\partial}^\mu H^+\} \end{aligned} \quad (3.4)$$

where

$$A \overleftrightarrow{\partial}^\mu B = A(\partial^\mu B) - (\partial^\mu A)B. \quad (3.5)$$

The Lagrangian for the VVH interaction is:

$$\begin{aligned}\mathcal{L}_{VVH} = & \left(gm_W W_\mu^+ W^{-\mu} + \frac{gm_Z}{2\cos\theta_W} Z_\mu Z^\mu \right) \\ & \times [H^0 \cos(\beta - \alpha) + h^0 \sin(\beta - \alpha)]. \end{aligned} \quad (3.6)$$

There are no vertices ZH^0H^0 , Zh^0h^0 , ZA^0A^0 , ZW^+H^- or ZH^0h^0 . The interactions of neutral Higgs bosons with up and down quarks are given by:

$$\begin{aligned}\mathcal{L}_{AHhff'} = & \frac{-gm_f}{2m_W \sin\beta} [\bar{u}_f v_{\bar{f}} (H^0 \sin\alpha + h^0 \cos\alpha) - i \cos\beta \cdot \bar{u}_f \gamma^5 v_{\bar{f}} A^0] \\ & - \frac{gm_{f'}}{2m_W \cos\beta} \\ & \times [\bar{u}_{f'} v_{\bar{f}'} (H^0 \cos\alpha - h^0 \sin\alpha) - i \sin\beta \cdot \bar{u}_{f'} \gamma^5 v_{\bar{f}'} A^0] \end{aligned} \quad (3.7)$$

where $f = u, c, t, \nu_e, \nu_\mu, \nu_\tau$ and $f' = d, s, b, e^-, \mu^-, \tau^-$. The Lagrangian corresponding to the $H^\pm f \bar{f}'$ vertex is:

$$\begin{aligned}\mathcal{L}_{H^\pm f f'} = & \frac{g}{2\sqrt{2}m_W} \{ H^+ V_{ff'} \bar{u}_f (A + B\gamma^5) v_{\bar{f}'} \\ & + H^- V_{ff'}^* \bar{u}_{f'} (A - B\gamma^5) v_{\bar{f}} \} \end{aligned} \quad (3.8)$$

where $A \equiv (m_{f'} \tan\beta + m_f \cot\beta)$ and $B \equiv (m_{f'} \tan\beta - m_f \cot\beta)$. $V_{ff'}$ is an element of the CKM matrix. The Lagrangian corresponding to three Higgs

bosons is:

$$\begin{aligned}
\mathcal{L}_{3h} = & -gH^0\{H^+H^-\left[m_W\cos(\beta-\alpha)-\frac{m_Z}{2\cos\theta_W}\cos(2\beta)\cos(\beta+\alpha)\right] \\
& +\frac{m_Z}{4\cos\theta_W}H^0H^0\cos(2\alpha)\cos(\beta+\alpha) \\
& +\frac{m_Z}{4\cos\theta_W}h^0h^0[2\sin(2\alpha)\sin(\beta+\alpha)-\cos(\beta+\alpha)\cos(2\alpha)] \\
& -\frac{m_Z}{4\cos\theta_W}A^0A^0\cos(2\beta)\cos(\beta+\alpha)\} \\
& -gh^0\{H^+H^-\left[m_W\sin(\beta-\alpha)+\frac{m_Z}{2\cos\theta_W}\cos(2\beta)\sin(\beta+\alpha)\right] \\
& +\frac{m_Z}{4\cos\theta_W}h^0h^0\cos(2\alpha)\sin(\beta+\alpha) \\
& -\frac{m_Z}{4\cos\theta_W}H^0H^0[2\sin(2\alpha)\cos(\beta+\alpha)+\sin(\beta+\alpha)\cos(2\alpha)] \\
& +\frac{m_Z}{4\cos\theta_W}A^0A^0\cos(2\beta)\sin(\beta+\alpha)\}. \tag{3.9}
\end{aligned}$$

Vertexes with four partons including two Higgs bosons are

$$\begin{aligned}
\mathcal{L}_4 = & e^2A_\mu A^\mu H^+H^- + \frac{eg\cos(2\theta_W)}{\cos\theta_W}A_\mu Z^\mu H^+H^- \\
& -\frac{eg}{2}\sin(\beta-\alpha)A_\mu W^{\pm\mu}H^0H^\mp + \frac{eg}{2}\cos(\beta-\alpha)A_\mu W^{\pm\mu}h^0H^\mp \\
& \pm \frac{ige}{2}A_\mu W^{\pm\mu}A^0H^\mp, \tag{3.10}
\end{aligned}$$

The $H^+H^-\gamma$ vertex is

$$\mathcal{L}_{H^+H^-\gamma} = -ig\sin\theta_W A_\mu H^-\overleftrightarrow{\partial}^\mu H^+ \tag{3.11}$$

The Higgs propagators are: $i/(k^2 - m^2 + i\varepsilon)$.

Feynman diagrams corresponding to the production of Zh^0 are shown in Figures 3.3, 3.4 and 3.5. Note that the invariant mass of Zh^0 can have a resonance at m_{A^0} which is an interesting experimental signature. Feynman diagrams corresponding to the production of $W^\pm h^0$ or $W^\pm H^0$ are shown in Figure 3.6.

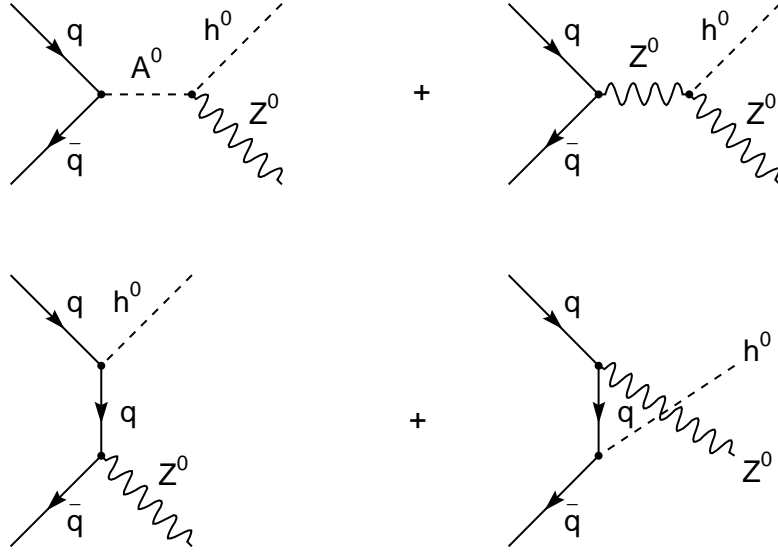


Figure 3.3: Feynman diagrams corresponding to the production of h^0 in the channel $q\bar{q} \rightarrow h^0 Z^0$.

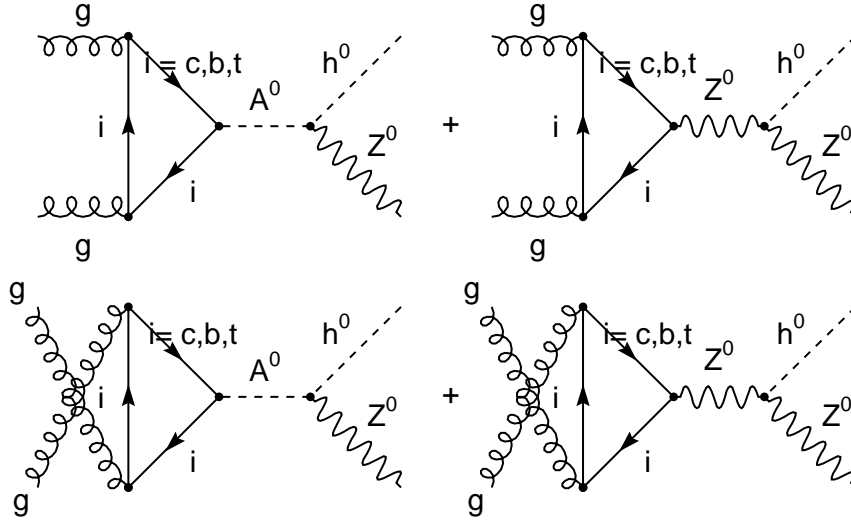


Figure 3.4: Feynman diagrams corresponding to the production of h^0 in the channel $gg \rightarrow h^0 Z^0$. Continued in Figure 3.5.

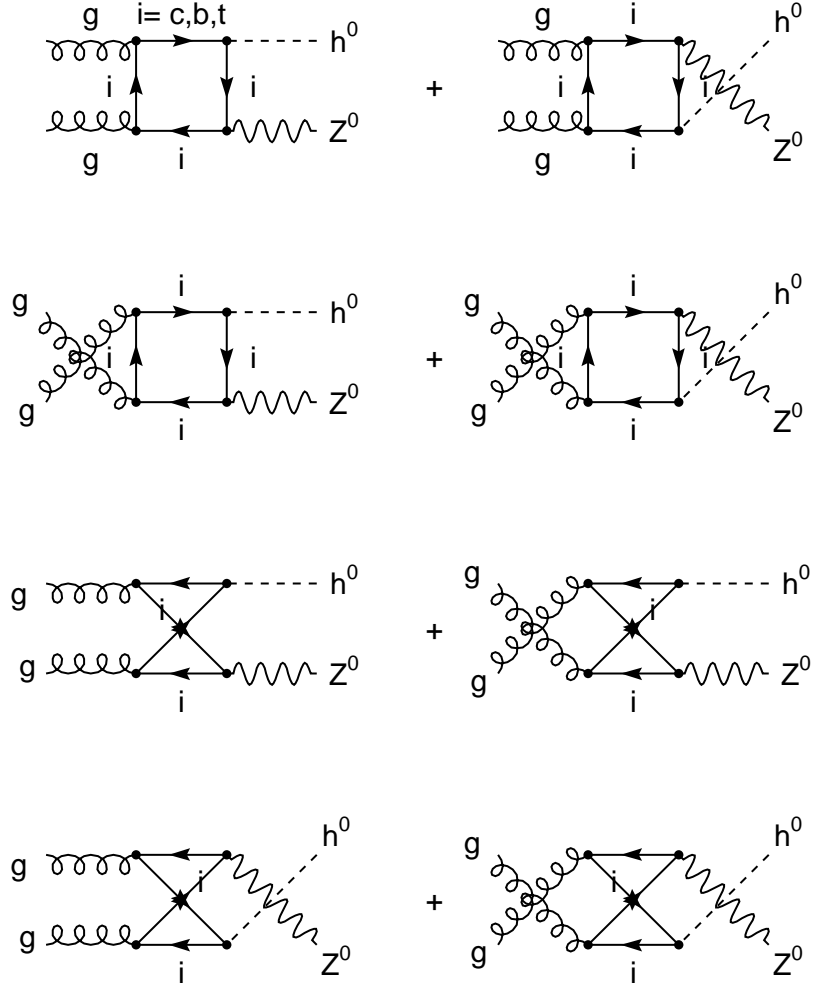


Figure 3.5: Continued from Figure 3.4.

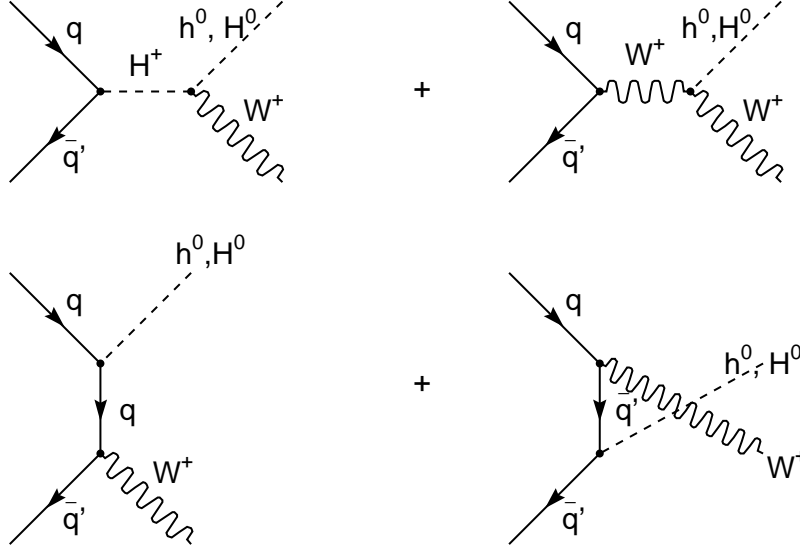


Figure 3.6: Feynman diagrams corresponding to the production of $h^0 W^\pm$ and $H^0 W^\pm$.

3.4 Decay rates of h^0

Calculating the Feynman diagrams of Figure 3.7 we obtain the decay rate corresponding to $h^0 \rightarrow gg$:

$$\Gamma(h^0 \rightarrow gg) = \frac{\sqrt{2}G_F\alpha_s^2 m_{h^0}^3 \cos^2 \alpha}{64\pi^3 \sin^2 \beta} |\tan \beta \tan \alpha \tau_b [(\tau_b - 1)f(\tau_b) + 2] - \tau_t [(\tau_t - 1)f(\tau_t) + 2]|^2 \quad (3.12)$$

where

$$\tau_i = \frac{4m_i^2}{m_{h^0}^2}, \quad (3.13)$$

(note that τ_i will change from Section to Section),

$$f(\tau_i) = \begin{cases} -2 \left[\arcsin \left(\tau_i^{-1/2} \right) \right]^2 & \text{if } \tau_i > 1 \\ \frac{1}{2} \left[\ln \left(\frac{1+(1-\tau_i)^{1/2}}{1-(1-\tau_i)^{1/2}} \right) - i\pi \right]^2 & \text{if } \tau_i \leq 1, \end{cases} \quad (3.14)$$

$$\tan \alpha = - \left\{ \frac{1+F}{1-F} \right\}^{\frac{1}{2}}, \quad (3.15)$$

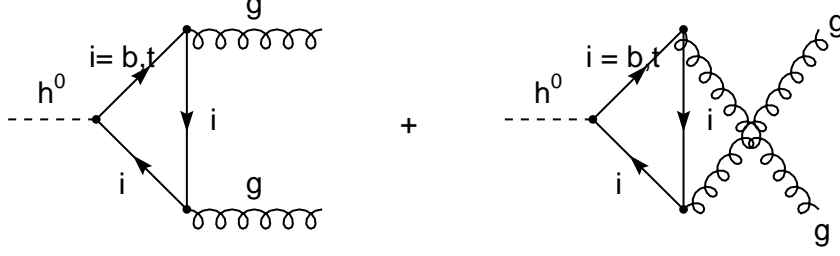


Figure 3.7: Feynman diagrams corresponding to the decay $h^0 \rightarrow gg$.

$$F = \frac{1 - \tan^2 \beta}{(1 + \tan^2 \beta) G} \left[1 - \frac{m_Z^2}{m_H^2} - \frac{m_W^2}{m_H^2} \right], \quad (3.16)$$

$$G = \left[\left(1 + \frac{m_Z^2}{m_H^2} - \frac{m_W^2}{m_H^2} \right)^2 - 4 \frac{m_Z^2}{m_H^2} \left(1 - \frac{m_W^2}{m_H^2} \right) \left(\frac{\tan^2 \beta - 1}{\tan^2 \beta + 1} \right)^2 \right]^{\frac{1}{2}}. \quad (3.17)$$

Calculating the Feynman diagrams of Figure 3.8 we obtain:

$$\Gamma(h^0 \rightarrow c\bar{c}) = \frac{3G_F m_c^2 m_{h^0} \cos^2 \alpha}{\sqrt{2} \cdot 4\pi \sin^2 \beta} \left(1 - \frac{4m_c^2}{m_{h^0}^2} \right)^{\frac{3}{2}}, \quad (3.18)$$

$$\Gamma(h^0 \rightarrow b\bar{b}) = \frac{3G_F m_b^2 m_{h^0} \sin^2 \alpha}{\sqrt{2} \cdot 4\pi \cos^2 \beta} \left(1 - \frac{4m_b^2}{m_{h^0}^2} \right)^{\frac{3}{2}}, \quad (3.19)$$

and

$$\Gamma(h^0 \rightarrow \tau^- \tau^+) = \frac{G_F m_\tau^2 m_{h^0} \sin^2 \alpha}{\sqrt{2} \cdot 4\pi \cos^2 \beta} \left(1 - \frac{4m_\tau^2}{m_{h^0}^2} \right)^{\frac{3}{2}}. \quad (3.20)$$

3.5 Branching fractions of h^0

From the preceding decay rates we obtain the following branching fractions for the case $m_b, m_c, m_\tau \ll m_{h^0} < 120 \text{ GeV}/c^2$:

$$B(h^0 \rightarrow b\bar{b}) = \frac{3m_b^2 \sin^2 \alpha}{3m_b^2 \sin^2 \alpha + 3m_c^2 \cos^2 \alpha \cot^2 \beta + m_\tau^2 \sin^2 \alpha + J} \quad (3.21)$$

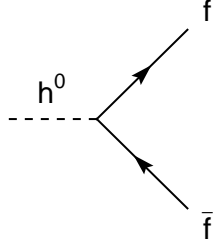


Figure 3.8: Feynman diagram corresponding to the decays $h^0 \rightarrow b\bar{b}, c\bar{c}, \tau\bar{\tau}$.

and

$$B(h^0 \rightarrow \tau^+\tau^-) = \frac{m_\tau^2 \sin^2 \alpha}{3m_b^2 \sin^2 \alpha + 3m_c^2 \cos^2 \alpha \cot^2 \beta + m_\tau^2 \sin^2 \alpha + J} \quad (3.22)$$

where

$$J = \frac{\alpha_s^2 m_{h^0}^2 \cos^2 \alpha}{8\pi^2 \tan^2 \beta} |\tan \beta \tan \alpha \left[\tau_b \left(-\frac{1}{2} \left\{ \ln \left(\frac{\tau_b}{4} \right) + i\pi \right\}^2 + 2 \right) \right. \\ \left. - \tau_t \{(\tau_t - 1) f(\tau_t) + 2\} \right]^2. \quad (3.23)$$

For $90 < m_H < 1000 \text{ GeV}/c^2$, $B(h^0 \rightarrow b\bar{b})$ varies from 0.856 to 0.944. Neglecting $B(h^0 \rightarrow gg)$ and the contribution of $c\bar{c}$ we obtain

$$B(h^0 \rightarrow b\bar{b}) = \frac{3m_b^2}{3m_b^2 + m_\tau^2} = 0.944 \quad (3.24)$$

and

$$B(h^0 \rightarrow \tau^+\tau^-) = \frac{m_\tau^2}{3m_b^2 + m_\tau^2} = 0.056. \quad (3.25)$$

3.6 Decay rates of H^\pm

The tree level Feynman diagram of Figure 3.9 gives the following decay rate:

$$\Gamma(H^\pm \rightarrow W^\pm h^0) = \frac{\sqrt{2} G_F \cos^2 \alpha}{16\pi m_H^3 (1 + \tan^2 \beta)} [1 + \tan \beta \tan \alpha]^2 \\ \times \Lambda^{3/2}(m_H^2, m_W^2, m_{h^0}^2) \quad (3.26)$$

where

$$\Lambda(a, b, c) = a^2 + b^2 + c^2 - 2ab - 2bc - 2ca. \quad (3.27)$$

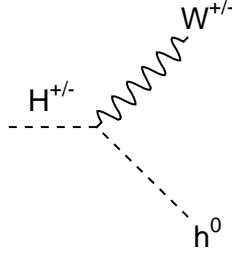


Figure 3.9: Feynman diagram corresponding to the decay $H^{\pm} \rightarrow W^{\pm} h^0$.

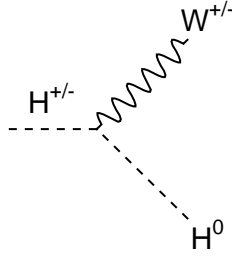


Figure 3.10: Feynman diagram corresponding to the decay $H^{\pm} \rightarrow W^{\pm} H^0$.

Similarly from the Feynman diagrams of Figures 3.10 and 3.11 we obtain

$$\Gamma(H^{\pm} \rightarrow W^{\pm} H^0) = \frac{\sqrt{2}G_F (\tan \beta - \tan \alpha)^2}{16\pi m_H^3 (1 + \tan^2 \beta) (1 + \tan^2 \alpha)} \times \Lambda^{3/2}(m_H^2, m_W^2, m_{H^0}^2), \quad (3.28)$$

$$\Gamma(H^{\pm} \rightarrow W^{\pm} A^0) = \frac{\sqrt{2}G_F}{16\pi m_H^3} \Lambda^{3/2}(m_{A^0}^2, m_W^2, m_H^2). \quad (3.29)$$

3.7 Decays of H^0 .

The tree level Feynman diagrams of Figure 3.12 give the following decay rates:

$$\Gamma(H^0 \rightarrow f\bar{f}) = \frac{\sqrt{2}G_F m_f^2 m_{H^0}}{8\pi} \left(1 - \frac{4m_f^2}{m_{H^0}^2}\right)^{3/2} N_f B_f^2 \quad (3.30)$$

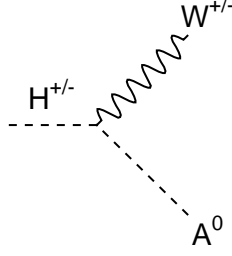


Figure 3.11: Feynman diagram corresponding to the decay $H^\pm \rightarrow W^\pm A^0$.

where $N_f = 3$ for quarks, $N_f = 1$ for leptons, $B_f^2 = \sin^2 \alpha (1 + \cot^2 \beta)$ for $f = u, c, t$, and $B_f^2 = \cos^2 \alpha (1 + \tan^2 \beta)$ for $f = d, s, b, e^-, \mu^-, \tau^-$.

From the Feynman diagrams of Figure 3.13 we obtain

$$\begin{aligned} \Gamma(H^0 \rightarrow gg) &= \frac{\sqrt{2}G_F\alpha_s^2 m_{H^0}^3}{64\pi^3} \sin^2 \alpha (1 + \cot^2 \beta) \\ &\times \left| \frac{\tan \beta}{\tan \alpha} \tau_b [(\tau_b - 1)f(\tau_b) + 2] \right. \\ &\left. + \tau_t [(\tau_t - 1)f(\tau_t) + 2] \right|^2 \end{aligned} \quad (3.31)$$

where

$$\tau_i = \frac{4m_i^2}{m_{H^0}^2}. \quad (3.32)$$

From the Feynman diagram of Figure 3.14 we obtain

$$\begin{aligned} \Gamma(H^0 \rightarrow h^0 h^0) &= \frac{\sqrt{2}G_F m_Z^4}{32\pi m_{H^0}} \\ &\times \left(1 - \frac{4m_{h^0}^2}{m_{H^0}^2} \right)^{1/2} \frac{(1 - \tan^2 \alpha)^2}{(1 + \tan^2 \alpha)^3 (1 + \tan^2 \beta)} \\ &\times \left[\frac{4 \tan \alpha}{1 - \tan^2 \alpha} (\tan \alpha + \tan \beta) - (1 - \tan \alpha \tan \beta) \right]^2. \end{aligned} \quad (3.33)$$

From the Feynman diagrams of Figures 3.15 and 3.16 we obtain

$$\begin{aligned} \Gamma(H^0 \rightarrow A^0 A^0) &= \frac{\sqrt{2}G_F m_Z^4}{32\pi m_{H^0}} \left(1 - \frac{4m_{A^0}^2}{m_{H^0}^2} \right)^{1/2} \\ &\times \frac{(\tan^2 \beta - 1)^2}{(1 + \tan^2 \alpha) (1 + \tan^2 \beta)^3} [1 - \tan \alpha \tan \beta]^2, \end{aligned} \quad (3.34)$$

$$\begin{aligned}\Gamma(H^0 \rightarrow ZZ) &= \frac{\sqrt{2}G_F(1 + \tan\beta \tan\alpha)^2 m_{H^0}^3}{32\pi(1 + \tan^2\beta)(1 + \tan^2\alpha)} \\ &\times (12x^2 - 4x + 1)(1 - 4x)^{1/2}\end{aligned}\quad (3.35)$$

where

$$x = \frac{m_Z^2}{m_{H^0}^2}.\quad (3.36)$$

Similarly, from the diagram of Figure 3.17 we obtain

$$\begin{aligned}\Gamma(H^0 \rightarrow W^+W^-) &= \frac{\sqrt{2}G_F(1 + \tan\beta \tan\alpha)^2 m_{H^0}^3}{16\pi(1 + \tan^2\beta)(1 + \tan^2\alpha)} \\ &\times (12y^2 - 4y + 1)(1 - 4y)^{1/2}\end{aligned}\quad (3.37)$$

where

$$y = \frac{m_W^2}{m_{H^0}^2}.\quad (3.38)$$

From the Feynman diagram of Figure 3.18 we obtain

$$\begin{aligned}\Gamma(H^0 \rightarrow W^\pm H^\mp) &= \frac{\sqrt{2}G_F(\tan\alpha - \tan\beta)^2}{16\pi m_{H^0}^3(1 + \tan^2\alpha)(1 + \tan^2\beta)} \\ &\times \Lambda^{3/2}(m_{H^0}^2, m_W^2, m_H^2).\end{aligned}\quad (3.39)$$

From the Feynman diagram of Figure 3.19 we obtain

$$\begin{aligned}\Gamma(H^0 \rightarrow H^+H^-) &= \frac{\sqrt{2}G_F m_W^4}{4\pi m_{H^0}(1 + \tan^2\beta)(1 + \tan^2\alpha)} \\ &\times \left[(1 + \tan\beta \tan\alpha) - \frac{(1 - \tan\beta \tan\alpha)}{2\cos^2\theta_W} \frac{1 - \tan^2\beta}{1 + \tan^2\beta} \right]^2 \\ &\times \left(1 - \frac{4m_H^2}{m_{H^0}^2} \right)^{1/2}.\end{aligned}\quad (3.40)$$

The Feynman diagrams corresponding to $h^0, H^0 \rightarrow \gamma\gamma$ are shown in Figure 3.20.

$$\Gamma(H^0 \rightarrow h^0 Z) = 0.\quad (3.41)$$

3.8 Decay rates of A^0

From the tree level Feynman diagram of Figure 3.21 we obtain

$$\begin{aligned}\Gamma(A^0 \rightarrow Zh^0) &= \frac{\sqrt{2}G_F \cos^2\alpha}{16\pi m_{A^0}^3(1 + \tan^2\beta)} \\ &\times [1 + \tan\beta \tan\alpha]^2 \Lambda^{3/2}(m_{A^0}^2, m_{h^0}^2, m_Z^2)\end{aligned}\quad (3.42)$$

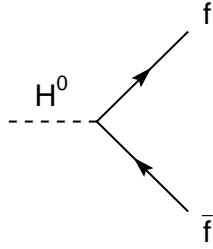


Figure 3.12: Feynman diagram corresponding to the decay $H^0 \rightarrow f\bar{f}$.

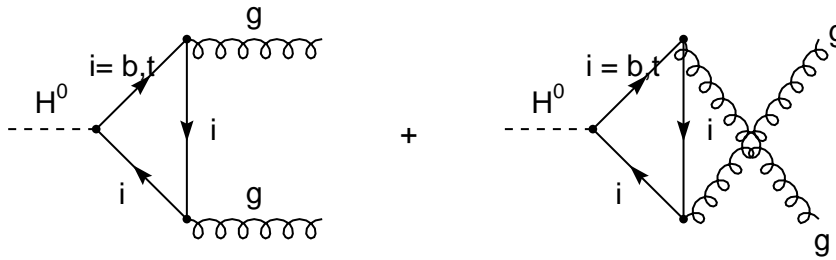


Figure 3.13: Feynman diagrams corresponding to the decay $H^0 \rightarrow gg$.

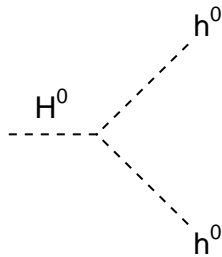


Figure 3.14: Feynman diagram corresponding to the decay $H^0 \rightarrow h^0 h^0$.

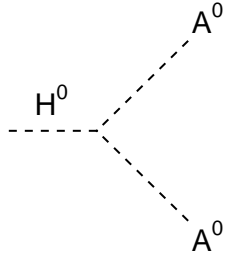


Figure 3.15: Feynman diagram corresponding to the decay $H^0 \rightarrow A^0 A^0$.

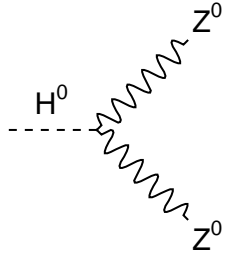


Figure 3.16: Feynman diagram corresponding to the decay $H^0 \rightarrow Z Z$.

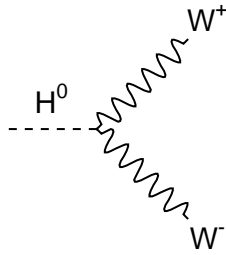


Figure 3.17: Feynman diagram corresponding to the decay $H^0 \rightarrow W^+ W^-$.

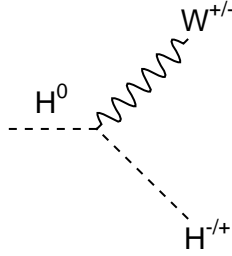


Figure 3.18: Feynman diagram corresponding to the decay $H^0 \rightarrow W^\pm H^\mp$.

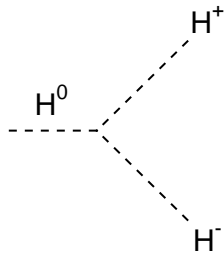


Figure 3.19: Feynman diagram corresponding to the decay $H^0 \rightarrow H^+ H^-$.

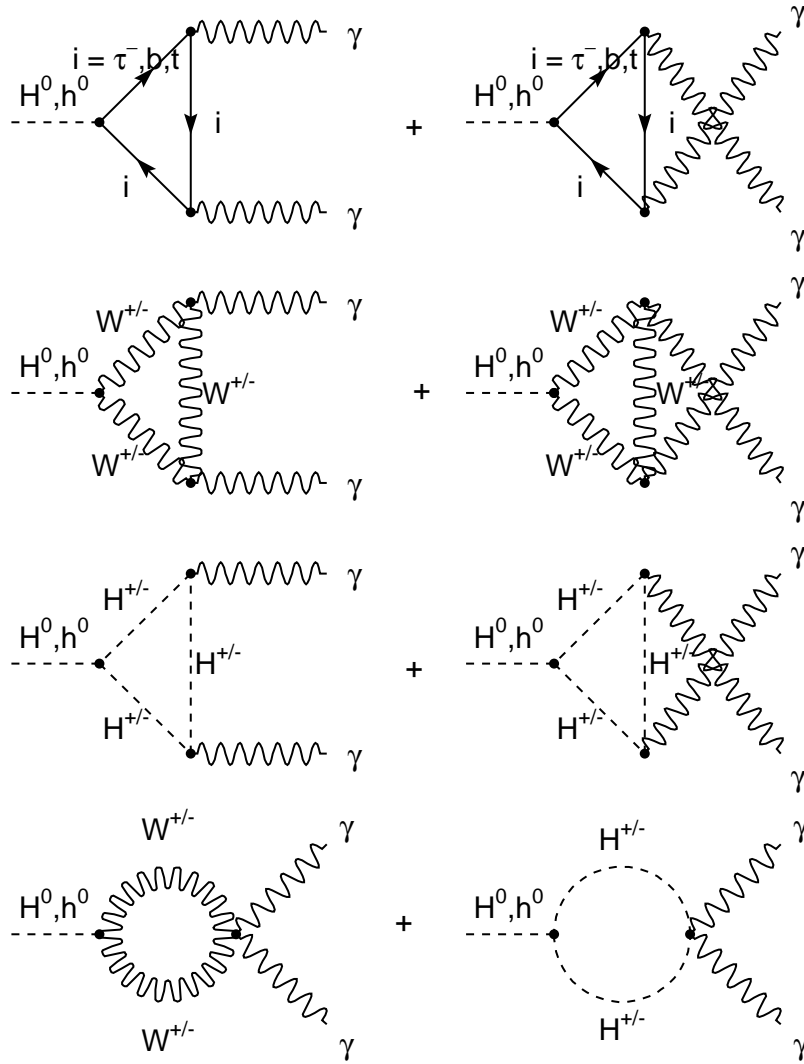


Figure 3.20: Feynman diagrams corresponding to $h^0, H^0 \rightarrow \gamma\gamma$.

From the tree level diagram of Figure 3.22 we obtain

$$\Gamma(A^0 \rightarrow f\bar{f}) = \frac{\sqrt{2}G_F}{8\pi} m_{A^0} m_f^2 A_f^2 \left(1 - \frac{4m_f^2}{m_{A^0}^2}\right)^{1/2} N_f \quad (3.43)$$

where $N_f = 3$ for quarks, $N_f = 1$ for leptons, $A_f = \cot \beta$ for $f = u, c, t$, and $A_f = \tan \beta$ for $f = d, s, b, e^-, \mu^-, \tau^-$.

From the Feynman diagrams shown in Figure 3.23 we obtain (see Appendix D):

$$\begin{aligned} \Gamma(A^0 \rightarrow Z\gamma) &= \frac{\sqrt{2}G_F \alpha_{em}^2 m_{A^0}^3}{512\pi^3 \sin^2 \theta_W \cos^2 \theta_W} \left(1 - \frac{m_Z^2}{m_{A^0}^2}\right)^3 \\ &\times |\tan \beta \left\{ \left(\frac{1}{2} - \frac{2}{3} \sin^2 \theta_W\right) I(\tau_b, \Lambda_b) \right. \\ &+ \left. \left(\frac{1}{2} - 2 \sin^2 \theta_W\right) I(\tau_\tau, \Lambda_\tau) \right\} \\ &+ 2 \cot \beta \left(\frac{1}{2} - \frac{4}{3} \sin^2 \theta_W\right) I(\tau_t, \Lambda_t)|^2 \end{aligned} \quad (3.44)$$

where

$$\tau_i = \frac{4m_i^2}{m_{A^0}^2}, \quad \Lambda_i = \frac{4m_i^2}{m_Z^2}, \quad (3.45)$$

and

$$I(\tau_i, \Lambda_i) = \frac{\tau_i \Lambda_i}{\Lambda_i - \tau_i} \{f(\tau_i) - f(\Lambda_i)\}. \quad (3.46)$$

From the Feynman diagrams of Figure 3.24 we obtain the decay rate:

$$\Gamma(A^0 \rightarrow gg) = \frac{\sqrt{2}G_F \alpha_s^2 m_{A^0}^3}{128\pi^3} |\tan \beta \tau_b f(\tau_b) + \cot \beta \tau_t f(\tau_t)|^2. \quad (3.47)$$

$$\Gamma(A^0 \rightarrow h^0 h^0) = \Gamma(A^0 \rightarrow H^0 H^0) = 0. \quad (3.48)$$

From the Feynman diagram 3.25 we obtain

$$\Gamma(A^0 \rightarrow W^\pm H^\mp) = \frac{\sqrt{2}G_F}{16\pi m_{A^0}^3} \Lambda^{3/2}(m_{A^0}^2, m_W^2, m_H^2). \quad (3.49)$$

From the Feynman diagram 3.26 we obtain

$$\begin{aligned} \Gamma(A^0 \rightarrow ZH^0) &= \frac{\sqrt{2}G_F (\tan \beta - \tan \alpha)^2}{16\pi m_{A^0}^3 (1 + \tan^2 \alpha) (1 + \tan^2 \beta)} \\ &\times \Lambda^{3/2}(m_{A^0}^2, m_{H^0}^2, m_Z^2). \end{aligned} \quad (3.50)$$

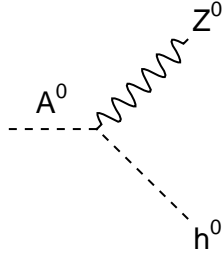


Figure 3.21: Feynman diagram corresponding to the decay $A^0 \rightarrow Zh^0$.

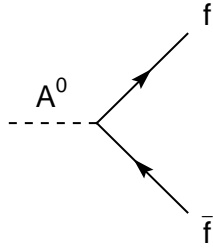


Figure 3.22: Feynman diagram corresponding to the decay $A^0 \rightarrow f\bar{f}$.

From the Feynman diagrams of 3.27 we obtain:

$$\begin{aligned} \Gamma(A^0 \rightarrow \gamma\gamma) = & \frac{\sqrt{2}G_F\alpha_{em}^2 m_{A^0}^3}{256\pi^3} \left| \tan\beta \left[\frac{1}{3}\tau_b f(\tau_b) + \tau_\tau f(\tau_\tau) \right] \right. \\ & \left. + \cot\beta \left[\frac{4}{3}\tau_t f(\tau_t) \right] \right|^2 \end{aligned} \quad (3.51)$$

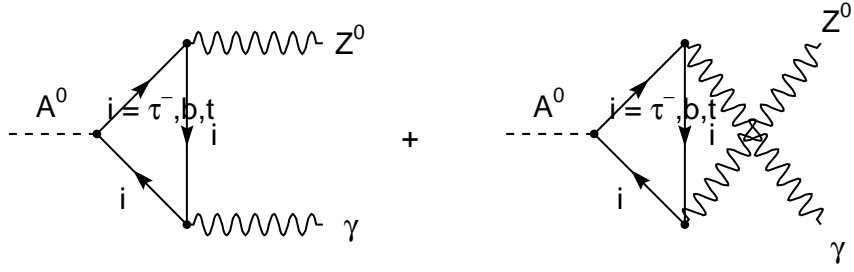


Figure 3.23: Feynman diagrams corresponding to the decay $A^0 \rightarrow Z\gamma$.

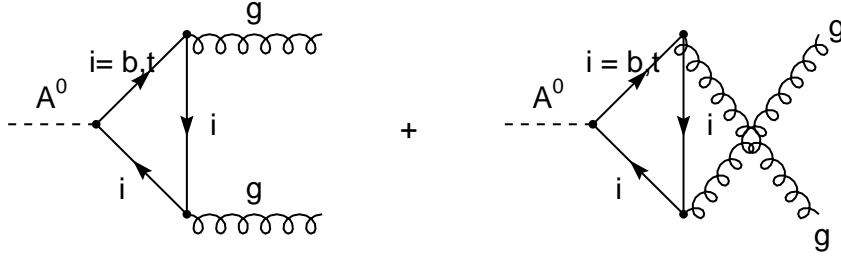


Figure 3.24: Feynman diagrams of $A^0 \rightarrow gg$.

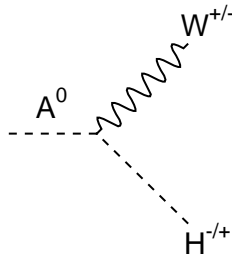


Figure 3.25: Feynman diagram of $A^0 \rightarrow W^\pm H^\mp$.

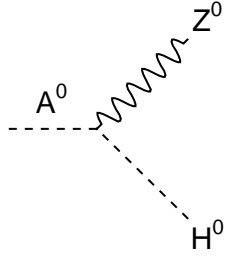


Figure 3.26: Feynman diagram of $A^0 \rightarrow ZH^0$.

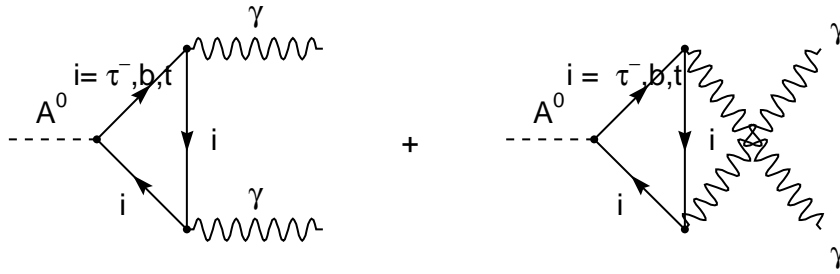


Figure 3.27: Feynman diagrams for $A^0 \rightarrow \gamma\gamma$.

3.9 Decay $Z \rightarrow h^0 \gamma$

From the Feynman diagrams of Figure 3.28 we obtain:

$$\begin{aligned}
\Gamma(Z \rightarrow h^0 \gamma) &= \frac{\sqrt{2} G_F \alpha_{em}^2 m_Z^3}{64 \pi^3 \sin^2 \theta_W \cos^2 \theta_W} \left(1 - \frac{m_{h^0}^2}{m_Z^2}\right)^3 \cos^2 \alpha \cos^2 \beta \\
&\times \left| \frac{1}{\cos \beta \sin \beta} [\tan \alpha \tan \beta \left(\frac{1}{2} - \frac{2}{3} \sin^2 \theta_W\right) F(\tau_b, \Lambda_b) \right. \right. \\
&+ \tan \alpha \tan \beta \left(\frac{1}{2} - 2 \sin^2 \theta_W\right) F(\tau_\tau, \Lambda_\tau) \\
&- 2 \left(\frac{1}{2} - \frac{4}{3} \sin^2 \theta_W\right) F(\tau_t, \Lambda_t)] \\
&+ \left[\tan \beta - \tan \alpha + \frac{1 - \tan^2 \beta \tan \beta + \tan \alpha}{1 + \tan^2 \beta} \frac{1}{2 \cos^2 \theta_W} \right] \\
&\times \frac{m_W^2}{2 m_H^2} (1 - 2 \sin^2 \theta_W) I(\tau_H, \Lambda_H) \\
&- \frac{1}{2} (\tan \beta - \tan \alpha) \cos^2 \theta_W [4 (3 - \tan^2 \theta_W) K(\tau_W, \Lambda_W) \\
&+ \left\{ \left(1 + \frac{2}{\tau_W}\right) \tan^2 \theta_W - \left(5 + \frac{2}{\tau_W}\right) \right\} \\
&\times I(\tau_W, \Lambda_W)]|^2
\end{aligned} \tag{3.52}$$

where

$$\tau_i = \frac{4m_i^2}{m_{h^0}^2}, \quad \Lambda_i = \frac{4m_i^2}{m_Z^2}, \quad \tau_H = \frac{4m_H^2}{m_{h^0}^2}, \quad \Lambda_H = \frac{4m_H^2}{m_Z^2}, \tag{3.53}$$

$$\begin{aligned}
F(\tau_i, \Lambda_i) &= -\frac{1}{2} \frac{\tau_i \Lambda_i}{\tau_i - \Lambda_i} - \frac{\tau_i^2 \Lambda_i}{(\tau_i - \Lambda_i)^2} \{g(\tau_i) - g(\Lambda_i)\} \\
&+ \frac{1}{4} \frac{\tau_i \Lambda_i}{\tau_i - \Lambda_i} \left[1 + \frac{\tau_i \Lambda_i}{\tau_i - \Lambda_i}\right] \{f(\tau_i) - f(\Lambda_i)\},
\end{aligned} \tag{3.54}$$

$$g(x) = \begin{cases} (x-1)^{1/2} \arcsin(x^{-1/2}) & \text{if } x \geq 1 \\ \frac{1}{2} (1-x)^{1/2} \left[\ln \left\{ \frac{1+(1-x)^{1/2}}{1-(1-x)^{1/2}} \right\} - i\pi \right] & \text{if } x < 1, \end{cases} \tag{3.55}$$

$$\begin{aligned}
I(\tau_H, \Lambda_H) &= -\frac{1}{2} \frac{\tau_H \Lambda_H}{(\tau_H - \Lambda_H)} - \frac{\tau_H^2 \Lambda_H}{(\tau_H - \Lambda_H)^2} [g(\tau_H) - g(\Lambda_H)] \\
&+ \frac{1}{4} \frac{\tau_H^2 \Lambda_H^2}{(\tau_H - \Lambda_H)^2} [f(\tau_H) - f(\Lambda_H)],
\end{aligned} \tag{3.56}$$

$$\tau_W = \frac{4m_W^2}{m_{h^0}^2}, \quad \Lambda_W = \frac{4m_W^2}{m_Z^2}, \quad (3.57)$$

$$K(\tau_W, \Lambda_W) = -\frac{\tau_W \Lambda_W}{4(\tau_W - \Lambda_W)} [f(\tau_W) - f(\Lambda_W)]. \quad (3.58)$$

The decay width of Equation 3.52 turns out to be negligible compared to the full width of Z so we can not use it to constrain the mass of h^0 .

3.10 Vertex with four particles

The decay rate corresponding to the Feynman diagram 3.29 is:

$$\begin{aligned} \Gamma(H^\pm \rightarrow W^\pm \gamma h^0) &= \frac{3G_F^2 \sin^2 \theta_W (1 + \tan \beta \tan \alpha)^2 m_W^5}{32 (1 + \tan^2 \beta) (1 + \tan^2 \alpha) \pi^3 (x_H^W)^{1/2}} \\ &\times \left\{ \frac{1}{2} \Lambda^{\frac{1}{2}} \left(1, x_H^W, x_H^{h^0} \right) \left(1 + x_H^W + x_H^{h^0} \right) \right. \\ &+ \left(2x_H^W x_H^{h^0} - x_H^W - x_H^{h^0} \right) \times \ln \left| \frac{\Lambda^{\frac{1}{2}} \left(1, x_H^W, x_H^{h^0} \right) + 1 - x_H^W - x_H^{h^0}}{2 (x_H^W x_H^{h^0})^{1/2}} \right| \\ &- \left| x_H^{h^0} - x_H^W \right| \times \\ &\left. \ln \left| \frac{\left| x_H^{h^0} - x_H^W \right| \Lambda^{\frac{1}{2}} \left(1, x_H^W, x_H^{h^0} \right) - \left(x_H^W + x_H^{h^0} \right) + \left(x_H^W - x_H^{h^0} \right)^2}{2 (x_H^W x_H^{h^0})^{1/2}} \right| \right\} \quad (3.59) \end{aligned}$$

where

$$x_H^W = \frac{m_W^2}{m_H^2}, \quad x_H^{h^0} = \frac{m_{h^0}^2}{m_H^2}. \quad (3.60)$$

3.11 Production of h^0 , H^0 and A^0

From the Feynman diagrams in Figure 3.30 we obtain

$$\begin{aligned} \sigma(p\bar{p} \rightarrow AX) &= \frac{\pi^2 \Gamma(A \rightarrow 2g) \gamma_A}{8m_A^3} \\ &\times \int_{\gamma_A}^1 \frac{dx_a}{x_a} g(x_a, m^2) g\left(\frac{\gamma_A}{x_a}, m^2\right) + \frac{4\pi^2 \gamma_A}{3m_A^3} \\ &\times \left[\sum_{q=u,d,s,c,b} \Gamma(A \rightarrow q\bar{q}) \int_{\gamma_A}^1 \frac{dx_a}{x_a} f_q(x_a, m^2) f_q\left(\frac{\gamma_A}{x_a}, m^2\right) \right] \quad (3.61) \end{aligned}$$

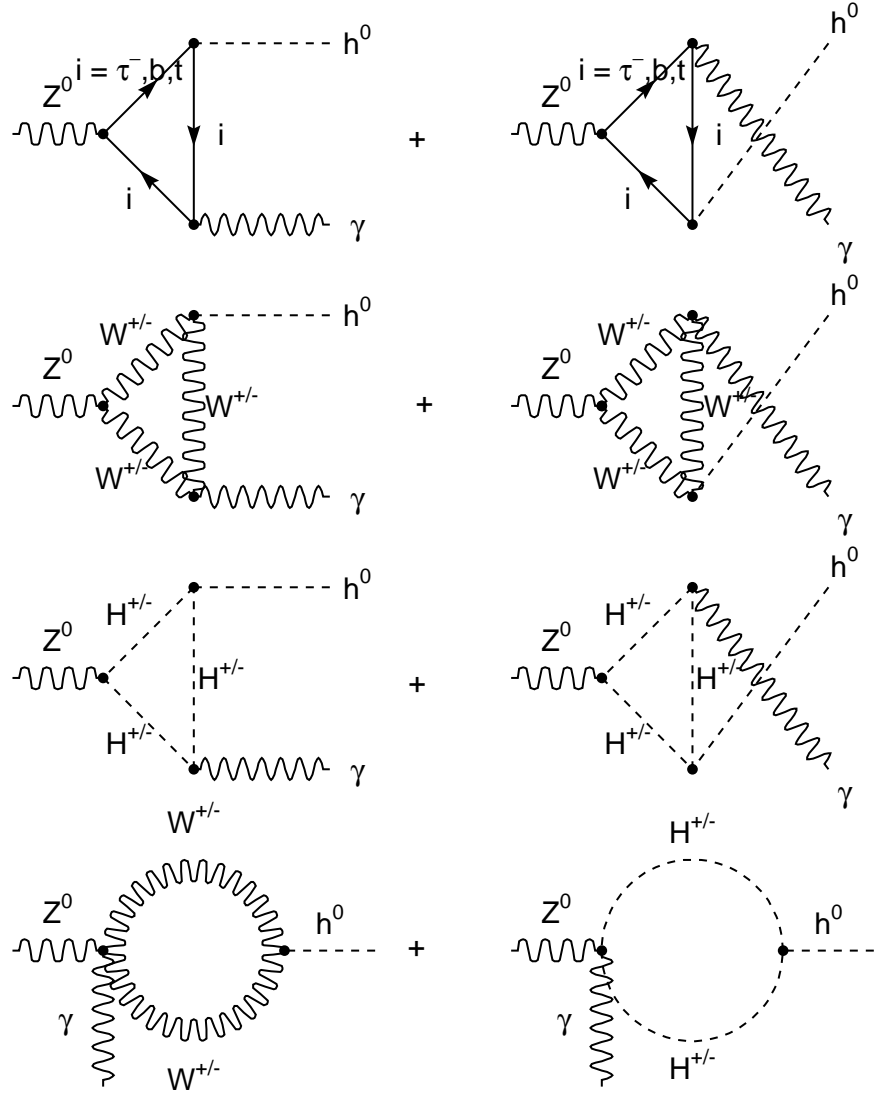


Figure 3.28: Feynman diagrams for $Z \rightarrow h^0 \gamma$.

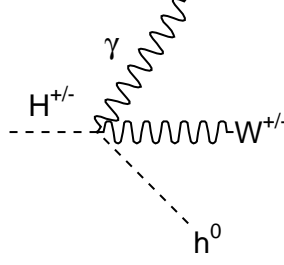


Figure 3.29: Diagram for $H^{\pm} \rightarrow W^{\pm} \gamma h^0$.

where $A \equiv h^0, H^0, A^0$ and $\gamma_A \equiv m_A^2/s$. Here f_q is the unpolarized parton distribution function for quark or anti-quark q and g is the parton distribution function for gluons. m^2 is the factorization scale. $\Gamma(h^0 \rightarrow gg)$ is given by (3.12), $\Gamma(H^0 \rightarrow gg)$ by (3.31), $\Gamma(A^0 \rightarrow gg)$ by (3.47), $\Gamma(h^0 \rightarrow c\bar{c})$ by (3.18), $\Gamma(h^0 \rightarrow b\bar{b})$ by (3.19), $\Gamma(H^0 \rightarrow q\bar{q})$ by (3.30), and finally, $\Gamma(A^0 \rightarrow q\bar{q})$ is given by (3.43).

3.12 Production of $h^0 Z^0 X$

A production channel with interesting experimental signature is $p\bar{p} \rightarrow h^0 Z^0 X$. The differential cross section obtained from the Feynman diagrams in Figure 3.3 is

$$\begin{aligned} \frac{d^2\sigma}{dy d(p_T)^2} &= \sum_f \int_{x_{amin}}^1 dx_a f_f(x_a, m_a^2) f_f(x_b, m_b^2) \frac{x_b \hat{s}}{m_{h^0}^2 - \hat{u}} \\ &\times \frac{d\sigma}{dt}(f\bar{f} \rightarrow h^0 Z^0) \end{aligned} \quad (3.62)$$

where f is q or g ,

$$x_{amin} = \frac{\sqrt{s}m_T e^y + m_{h^0}^2 - m_Z^2}{s - \sqrt{s}m_T e^{-y}}, \quad (3.63)$$

$$m_T = (m_Z^2 + p_T^2)^{\frac{1}{2}}, \quad (3.64)$$

$$x_b = \frac{x_a \sqrt{s}m_T e^{-y} + m_{h^0}^2 - m_Z^2}{x_a s - \sqrt{s}m_T e^y}, \quad (3.65)$$

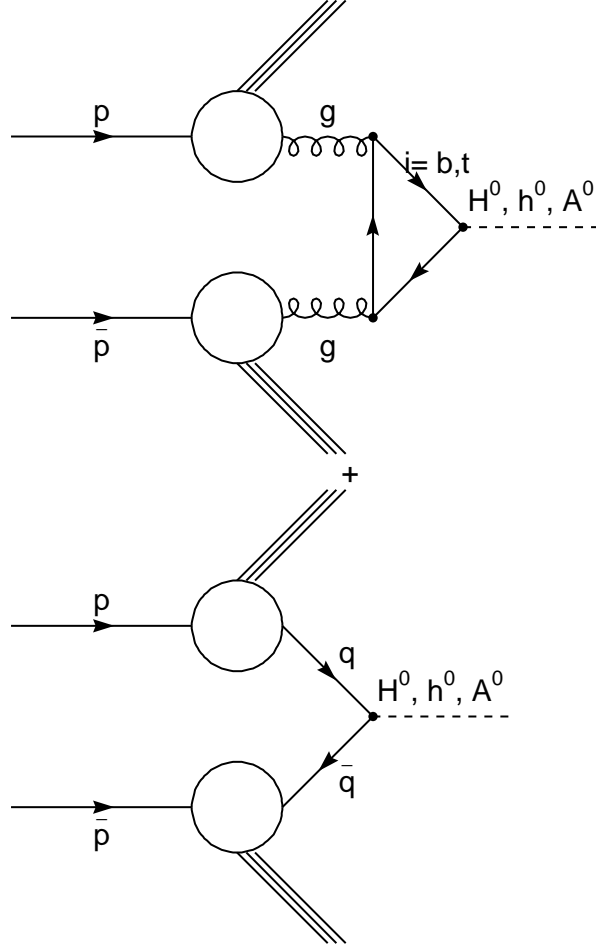


Figure 3.30: Feynman diagrams for $p\bar{p} \rightarrow AX$ with $A \equiv h^0, H^0, A^0$.

f	$t_{3L}(f)$	q_f	g_A^f	g_V^f
e^-, μ^-, τ^-	$-\frac{1}{2}$	-1	$-\frac{1}{2}$	$-\frac{1}{2} + 2 \sin^2 \theta_W$
u, c, t	$\frac{1}{2}$	$\frac{2}{3}$	$\frac{1}{2}$	$\frac{1}{2} - \frac{4}{3} \sin^2 \theta_W$
d, s, b	$-\frac{1}{2}$	$-\frac{1}{3}$	$-\frac{1}{2}$	$-\frac{1}{2} + \frac{2}{3} \sin^2 \theta_W$

Table 3.1: Coefficients in Equation (3.70).

$$\hat{s} = x_a x_b s, \quad (3.66)$$

$$p_T^2 = \frac{\Lambda(\hat{s}, m_{h^0}^2, m_Z^2) \sin^2 \theta}{4\hat{s}}, \quad (3.67)$$

$$\hat{u} = \frac{1}{2} (m_{h^0}^2 + m_Z^2 - \hat{s} - \cos \theta \Lambda^{1/2}(\hat{s}, m_{h^0}^2, m_Z^2)) \quad (3.68)$$

and

$$\hat{u}\hat{t} = m_{h^0}^2 m_Z^2 + \hat{s} p_T^2. \quad (3.69)$$

y is the rapidity, θ is the angle of dispersion, and p_T is the transverse momentum of Z^0 . For the light quarks u, d and s we obtain

$$\begin{aligned} \frac{d\sigma}{d\hat{t}} &= \frac{1}{48\pi\hat{s}} G_F^2 m_Z^4 \frac{\sin^2(\beta - \alpha)}{(\hat{s} - m_Z^2)^2 + m_Z^2 \Gamma_Z^2} \left[(g_V^f)^2 + (g_A^f)^2 \right] \\ &\times \left[8m_Z^2 + \frac{\Lambda(\hat{s}, m_{h^0}^2, m_Z^2)}{\hat{s}} \sin^2 \theta \right] \end{aligned} \quad (3.70)$$

where $g_A^f \equiv t_{3L}(f)$ and $g_V^f \equiv t_{3L}(f) - 2q_f \sin^2 \theta_W$. Coefficients in Equation (3.70) are given in Table 3.1. The Standard Model cross section is obtained by omitting the factor $\sin^2(\beta - \alpha)$ in Equation (3.70). The contributions to the cross section from the heavy quarks c and b are negligible. Γ_Z is the total decay width of the Z^0 .

3.13 Production of H^+

From the diagrams in Figures 3.31 and 3.32 we obtain

$$\begin{aligned} \sigma(p\bar{p} \rightarrow H^+ X) &= \frac{4\pi^2 \gamma_H}{3m_H^3} \sum_{q, q'} \Gamma(H^+ \rightarrow q\bar{q}') \\ &\int_{\gamma_H}^1 \frac{dx_a}{x_a} \left[f_q^p(x_a, m^2) \cdot f_{\bar{q}'}^{\bar{p}}\left(\frac{\gamma_H}{x_a}, m^2\right) + f_{\bar{q}'}^p(x_a, m^2) \cdot f_q^{\bar{p}}\left(\frac{\gamma_H}{x_a}, m^2\right) \right] \end{aligned} \quad (3.71)$$

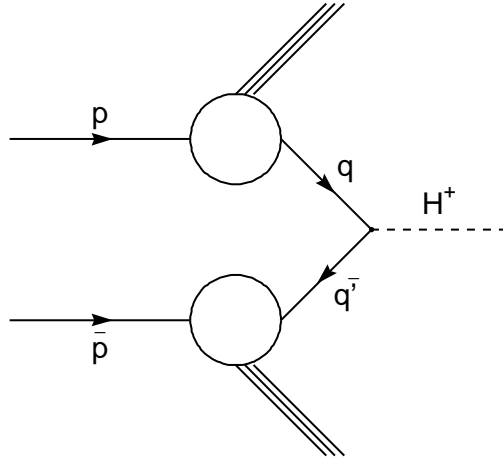


Figure 3.31: Feynman diagram for $p\bar{p} \rightarrow H^+ X$.

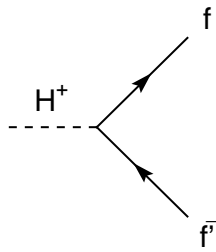


Figure 3.32: Feynman diagram for $H^+ \rightarrow f\bar{f}$.

where

$$\gamma_H = \frac{m_H^2}{s} \quad (3.72)$$

and

$$\begin{aligned} \Gamma(H^+ \rightarrow f \bar{f}') &= \Gamma(H^- \rightarrow f' \bar{f}) \\ &= \frac{\sqrt{2} G_F |V_{ff'}|^2 N_c}{16\pi m_H} \cdot \Lambda^{1/2} \left(\frac{m_f^2}{m_H^2}, \frac{m_{f'}^2}{m_H^2}, 1 \right) \\ &\times \left\{ A^2 [m_H^2 - (m_f + m_{f'})^2] + B^2 [m_H^2 - (m_f - m_{f'})^2] \right\} \end{aligned} \quad (3.73)$$

with $N_c = 3$ for quarks, $N_c = 1$ for leptons,

$$A = m_{f'} \tan \beta + m_f \cot \beta \quad (3.74)$$

$$B = m_{f'} \tan \beta - m_f \cot \beta \quad (3.75)$$

$f = u, c, t, \nu_e, \nu_\mu, \nu_\tau$, and $f' = d, s, b, e^-, \mu^-, \tau^-$. [7]

3.14 Production of $h^0 W^+ X$

Let us now consider the channel $p\bar{p} \rightarrow h^0 W^+ X$. We obtain:

$$\begin{aligned} \frac{d^2 \sigma}{dy d(p_T)^2} &= \sum_{q, q'} \int_{x_{amin}}^1 dx_a [f_q^p(x_a, m_a^2) f_{q'}^{\bar{p}}(x_b, m_b^2) \\ &+ f_{q'}^p(x_a, m_a^2) f_q^{\bar{p}}(x_b, m_b^2)] \frac{x_b \hat{s}}{m_{h^0}^2 - \hat{u}} \frac{d\sigma}{d\hat{t}}(qq' \rightarrow h^0 W^+) \end{aligned} \quad (3.76)$$

where

$$f_{q'}^p = f_{q'}^p, \quad f_{\bar{q}}^{\bar{p}} = f_{\bar{q}}^{\bar{p}}, \quad f_q^p = f_q^p, \quad f_{q'}^{\bar{p}} = f_{q'}^{\bar{p}}, \quad (3.77)$$

$$x_{amin} = \frac{\sqrt{s} m_T e^y + m_{h^0}^2 - m_W^2}{s - \sqrt{s} m_T e^{-y}}, \quad (3.78)$$

$$m_T = (m_W^2 + p_T^2)^{\frac{1}{2}}, \quad (3.79)$$

$$x_b = \frac{x_a \sqrt{s} m_T e^{-y} + m_{h^0}^2 - m_W^2}{x_a s - \sqrt{s} m_T e^y}, \quad (3.80)$$

$$\hat{s} = x_a x_b s, \quad (3.81)$$

$$p_T^2 = \frac{\Lambda(\hat{s}, m_{h^0}^2, m_W^2) \sin^2 \theta}{4\hat{s}}, \quad (3.82)$$

$$\hat{u} = \frac{1}{2} [m_{h^0}^2 + m_W^2 - \hat{s} - \cos \theta \Lambda^{1/2}(\hat{s}, m_{h^0}^2, m_W^2)], \quad (3.83)$$

$$\hat{t} = \frac{1}{2} [m_{h^0}^2 + m_W^2 - \hat{s} + \cos \theta \Lambda^{1/2}(\hat{s}, m_{h^0}^2, m_W^2)], \quad (3.84)$$

$$\cos \theta = \left(1 - \frac{4\hat{s}p_T^2}{\Lambda(\hat{s}, m_{h^0}^2, m_W^2)}\right)^{1/2} \quad (3.85)$$

and

$$\hat{u}\hat{t} = m_{h^0}^2 m_W^2 + \hat{s}p_T^2. \quad (3.86)$$

y is the rapidity of W^+ and p_T is the transverse momentum of W^+ . From the Feynman diagrams of Figure 3.6 we obtain for $f\bar{f}' \rightarrow h^0 W^+$:

$$\begin{aligned} \frac{d\sigma}{d\hat{t}} = & \frac{1}{16\pi\hat{s}^2} |V_{ff'}|^2 G_F^2 \{ |C_{H^+}|^2 \hat{s}\Lambda \\ & \times [m_{f'}^2 \tan^2 \beta + m_f^2 \cot^2 \beta] + m_W^4 |C_W|^2 [8\hat{s}m_W^2 + \Lambda \sin^2 \theta] \\ & - 2C_{H^+} \Re(C_W) [m_{f'}^2 \tan \beta (\hat{s}\Lambda + 2m_W^2 \hat{u} (\hat{s} - m_{h^0}^2) \\ & + 2m_W^4 (2m_{h^0}^2 - \hat{t})) - m_f^2 \cot \beta (\hat{s}\Lambda + 2m_W^2 \hat{t} (\hat{s} - m_{h^0}^2) \\ & + 2m_W^4 (2m_{H^0}^2 - \hat{u}))] \\ & + \frac{1}{2} m_W^2 \Lambda \sin^2 \theta \left[\frac{m_f^2 C_f^2}{\hat{t}^2} + \frac{m_{f'}^2 C_{f'}^2}{\hat{u}} \right] + \hat{s} [m_f^2 C_f^2 + m_{f'}^2 C_{f'}^2] \\ & + 2C_{H^+} \hat{s} \left[m_{h^0}^2 m_W^2 - \frac{1}{4} \Lambda \sin^2 \theta \right] \left[\frac{m_f^2 \cot \beta C_f}{\hat{t}} - \frac{m_{f'}^2 \tan \beta C_{f'}}{\hat{u}} \right] \\ & + 2C_{H^+} \hat{s} [m_{f'}^2 \tan \beta C_{f'} \hat{u} - m_f^2 \cot \beta C_f \hat{t}] \\ & - 2\Re(C_W) \left[\frac{1}{2} \Lambda \sin^2 \theta \left(m_W^2 + \frac{\hat{s}}{2} \right) - \hat{s} m_{h^0}^2 m_W^2 + 4\hat{s} m_W^4 + 4m_W^6 \right] \\ & \times \left[\frac{m_f^2 C_f}{\hat{t}} + \frac{m_{f'}^2 C_{f'}}{\hat{u}} \right] - 2\Re(C_W) m_f^2 C_f [-2m_W^4 + \hat{t} (\hat{s} - 2m_W^2)] \\ & - 2\Re(C_W) m_{f'}^2 C_{f'} [-2m_W^4 + \hat{u} (\hat{s} - 2m_W^2)] \} \end{aligned} \quad (3.87)$$

where Λ stands for $\Lambda(\hat{s}, m_{h^0}^2, m_W^2)$,

$$C_{H^+} = \frac{\cos(\beta - \alpha)}{\hat{s} - m_H^2}, \quad (3.88)$$

partons	$\tan(\beta) = 100$	$\tan(\beta) = 10$	$\tan(\beta) = 2$
gg	0.20E+1	0.13E-1	0.35E-1
$b\bar{b}$	0.31E+2	0.31E+0	0.12E-1
$c\bar{c}$	0.73E-7	0.73E-5	0.18E-3
$s\bar{s}$	0.20E+0	0.20E-2	0.81E-4
$d\bar{d}$	0.10E-1	0.10E-3	0.41E-5
$u\bar{u}$	0.18E-9	0.18E-7	0.46E-6

Table 3.2: Production cross section [pb] for $p\bar{p} \rightarrow A^0$ from the indicated partons. $m_{A^0} = 200\text{GeV}/c^2$, $\sqrt{s} = 1960\text{GeV}/c^2$.

$$C_W = \frac{\sin(\beta - \alpha)(\hat{s} - m_W^2 - im_W\Gamma_W)}{(\hat{s} - m_W^2)^2 + m_W^2\Gamma_W^2}, \quad (3.89)$$

$$C_f = -\frac{\cos\alpha}{\sin\beta}, \quad C_{f'} = \frac{\sin\alpha}{\cos\beta}. \quad (3.90)$$

For $p\bar{p} \rightarrow h^0 W^- X$ interchange $\hat{u} \leftrightarrow \hat{t}$.

For the Standard Model we obtain the differential cross section (3.87) with h^0 replaced by the Standard Model Higgs, $C_{H^+} = 0$, $C_f = C_{f'} = -1$, and $\sin(\beta - \alpha) = 1$ in (3.89).

3.15 Numerical examples

Two sensitive channels for the search of the Standard Model Higgs are $p\bar{p} \rightarrow h^0 ZX$ and $p\bar{p} \rightarrow h^0 W^\pm X$. The cross section for $p\bar{p} \rightarrow h^0 ZX$ off resonance in the Doublet model differs from the Standard Model by a factor $\sin^2(\beta - \alpha)$ (see Equation (3.70)) and it will be hard to obtain both m_{h^0} and $\tan(\beta)$. We are therefore interested in the production of $h^0 Z$ on resonance. In particular $p\bar{p} \rightarrow A^0$ followed by $A^0 \rightarrow h^0 Z \rightarrow b\bar{b}l^-l^+$ where $l = \mu, e$. A peak should be observed in the $h^0 Z$ invariant mass. From Equation (3.61) we obtain the cross sections listed in Tables 3.2 and 3.3.

Let us now consider the decays of A^0 . As an example we take $m_{h^0} = 120\text{GeV}/c^2$, $m_{H^0} = 250\text{GeV}/c^2$, $m_H = 200\text{GeV}/c^2$ and $m_{A^0} = 250\text{GeV}/c^2$. The corresponding branching fractions are listed in Table 3.4. From Tables 3.3 and 3.4 we obtain a production cross section times branching fraction for the process $p\bar{p} \rightarrow A^0 \rightarrow h^0 Z$ of 0.018pb for $\tan(\beta) = 2$, and 0.0045pb for $\tan(\beta) = 10$.

From Equations (3.71) and (3.73) we obtain the production cross sections for $p\bar{p} \rightarrow H^\pm X$ shown in Table 3.5.

partons	$\tan(\beta) = 100$	$\tan(\beta) = 10$	$\tan(\beta) = 2$
gg	0.42E+0	0.22E-2	0.19E-1
$b\bar{b}$	0.82E+1	0.82E-1	0.33E-2
$c\bar{c}$	0.19E-7	0.19E-5	0.49E-4
$s\bar{s}$	0.57E-1	0.57E-3	0.23E-4
$d\bar{d}$	0.44E-2	0.44E-4	0.18E-5
$u\bar{u}$	0.89E-10	0.89E-8	0.22E-6

Table 3.3: Production cross section [pb] for $p\bar{p} \rightarrow A^0$ from the indicated partons. $m_{A^0} = 250\text{GeV}/c^2$, $\sqrt{s} = 1960\text{GeV}/c^2$.

partons	$\tan(\beta) = 100$	$\tan(\beta) = 10$	$\tan(\beta) = 2$
$A \rightarrow gg$	3.0E-4	1.5E-4	2.0E-3
$A \rightarrow b\bar{b}$	1.0E+0	9.4E-1	5.9E-2
$A \rightarrow c\bar{c}$	8.0E-10	7.5E-6	2.9E-4
$A \rightarrow s\bar{s}$	8.0E-4	7.5E-4	4.7E-5
$A \rightarrow Zh^0$	6.1E-6	5.5E-2	9.4E-1
$A \rightarrow Z\gamma$	1.9E-8	6.0E-9	1.2E-6
$A \rightarrow \gamma\gamma$	1.2E-7	8.1E-8	7.5E-6

Table 3.4: Branching fractions for A^0 assuming $m_H = 200\text{GeV}/c^2$, $m_{H^0} = 250\text{GeV}/c^2$, $m_{A^0} = 250\text{GeV}/c^2$ and $m_{h^0} = 120\text{GeV}/c^2$.

partons	$\tan(\beta) = 100$	$\tan(\beta) = 10$	$\tan(\beta) = 2$
ud	0.82E-2	0.82E-4	0.34E-5
$u\bar{s}$	0.66E-1	0.66E-3	0.26E-4
$u\bar{b}$	0.89E-2	0.89E-4	0.36E-5
$c\bar{s}$	0.31E-1	0.32E-3	0.91E-4
$c\bar{b}$	0.24E-1	0.24E-3	0.96E-5

Table 3.5: Production cross section [pb] for $p\bar{p} \rightarrow H^+X$ from the indicated partons. $m_H = 250\text{GeV}/c^2$, $\sqrt{s} = 1960\text{GeV}/c^2$.

process	$\tan(\beta) = 100$	$\tan(\beta) = 50$	$\tan(\beta) = 2$
$b + g \rightarrow b + h^0$	0.021	0.021	0.011
$u + \bar{u} \rightarrow b + \bar{b} + h^0$	0.002	0.001	0.0004
$d + \bar{d} \rightarrow b + \bar{b} + h^0$	0.0005	0.0005	0.0001
$g + g \rightarrow b + \bar{b} + h^0$	0.015	0.015	0.008

Table 3.6: Production cross section [pb] for $p\bar{p} \rightarrow bh^0X$ from the indicated processes. $m_{h^0} = 120\text{GeV}/c^2$, $m_{A^0} = 250\text{GeV}/c^2$, $\sqrt{s} = 1960\text{GeV}/c^2$.

Other channels of experimental interest are the production of 3 or more b -jets as in Figure 3.33. Some numerical calculations using the CompHEP program[8] are presented in Table 3.6.

3.16 Running coupling constants and Grand Unification

The coupling constants of the Two Higgs Doublet Model of type II are $g_s(\mu)$ for SU(3), $g(\mu)$ for SU(2), and $g'(\mu)$ for U(1). These coupling constants depend on the energy scale μ as follows:

$$\frac{1}{g_s^2(\mu)} = \frac{1}{g_s^2(m_x)} + \frac{1}{8\pi^2} \left(-11 + \frac{4}{3}n_F \right) \ln \left(\frac{m_x}{\mu} \right), \quad (3.91)$$

$$\frac{1}{g^2(\mu)} = \frac{1}{g^2(m_x)} + \frac{1}{8\pi^2} \left(-\frac{22}{3} + \frac{4}{3}n_F + \frac{1}{6}n_S \right) \ln \left(\frac{m_x}{\mu} \right), \quad (3.92)$$

$$\frac{1}{g'^2(\mu)} = \frac{1}{g'^2(m_x)} + \frac{1}{8\pi^2} \left(\frac{20}{9}n_F + \frac{1}{6}n_S \right) \ln \left(\frac{m_x}{\mu} \right), \quad (3.93)$$

where n_F is the number of families of quarks and leptons, and n_S is the number of higgs doublets. For the Two Higgs Doublet Model of type II considered in this article, $n_F = 3$ and $n_S = 2$. In terms of the elementary electric charge and the Weinberg angle, $g(m_Z) = e(m_Z)/\sin\theta_W(m_Z)$, $g'(m_Z) = e(m_Z)/\cos\theta_W(m_Z)$. The fine structure constant is $\alpha(m_Z) = e^2(m_Z)/(4\pi)$.

Let us now assume that a Grand Unified Theory (GUT) breaks its symmetry to SU(3) \times SU(2) \times U(1) at the energy scale m_x . At this scale we take

$$g_s^2(m_x) = g^2(m_x) = \frac{5}{3}g'^2(m_x), \quad (3.94)$$

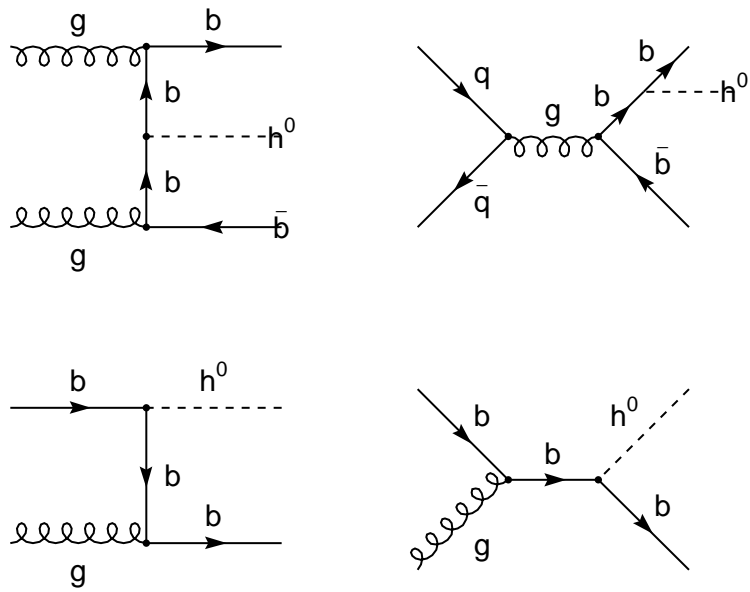


Figure 3.33: Some Feynman diagrams for the production of three or more b -jets.

	Doublet Model		MSSM	
n_S	$\sin^2 \theta_W(m_Z)$	m_x	$\sin^2 \theta_W(m_Z)$	m_x
0	0.2037	$1.0 \cdot 10^{15}$	0.2037	$8.0 \cdot 10^{17}$
2	0.2118	$4.2 \cdot 10^{14}$	0.2311	$2.0 \cdot 10^{16}$
4	0.2194	$1.8 \cdot 10^{14}$	0.2536	$1.0 \cdot 10^{15}$
6	0.2266	$8.3 \cdot 10^{13}$	0.2722	$8.3 \cdot 10^{13}$
8	0.2334	$3.9 \cdot 10^{13}$	0.2880	$1.0 \cdot 10^{13}$

Table 3.7: Predicted $\sin^2 \theta_W(m_Z)$ and m_x for the Two Higgs Doublet Model of type II, and the Minimum Supersymmetric Model as a function of the number of doublets n_S .

and obtain

$$\sin^2 \theta_W = \frac{11 + \frac{1}{2}n_S + \frac{5e^2}{3g_s^2} (22 - \frac{1}{5}n_S)}{66 + n_S}, \quad (3.95)$$

$$\ln \left(\frac{m_x}{m_Z} \right) = \frac{24\pi^2}{e^2} \frac{1 - \frac{8e^2}{3g_s^2}}{66 + n_S}, \quad (3.96)$$

with all running couplings evaluated at m_Z .

The corresponding equations of the Minimum Supersymmetry Model[9] are

$$\sin^2 \theta_W = \frac{18 + 3n_S + \frac{e^2}{g_s^2} (60 - 2n_S)}{108 + 6n_S}, \quad (3.97)$$

$$\ln \left(\frac{m_x}{m_Z} \right) = \frac{8\pi^2}{e^2} \left[\frac{1 - \frac{8e^2}{3g_s^2}}{18 + n_S} \right]. \quad (3.98)$$

Some numerical results are presented in Table 3.7. From the Table we conclude that the Two Higgs Doublet Model of type II is in disagreement with the measured value of $\sin^2 \theta_W(m_Z)$, and with the non-observation of proton decay (m_x is too low). Raising the number of doublets to ≈ 7 would bring $\sin^2 \theta_W(m_Z)$ into agreement with observations, but m_x is still too low. The MSSM with $n_S = 2$ (which includes the Two Higgs Doublet Model of type II) is in agreement with both the observed $\sin^2 \theta_W(m_Z)$, and with the non-observation of proton decay.

3.17 Conclusions

One of the major efforts at the Fermilab Tevatron in Run II, and at the future LHC, is the search for the Standard Model Higgs h_{SM} . The four

channels with largest production cross section are[6] $gg \rightarrow h_{SM}$, $q\bar{q}' \rightarrow h_{SM}W$, $q\bar{q} \rightarrow h_{SM}Z$ and $qq \rightarrow h_{SM}qq$. The decay modes of h_{SM} with largest branching fraction[6] are $b\bar{b}$ for $m_{h_{SM}} \lesssim 137\text{GeV}/c^2$ and W^+W^- for $m_{h_{SM}} \gtrsim 137\text{GeV}/c^2$.

The search for the Standard Model Higgs will also constrain or discover particles of the Two Higgs Doublet Model of type II.

The most interesting production channels are $gg \rightarrow h^0, H^0, A^0$ on mass shell, and $q\bar{q}, gg \rightarrow h^0Z$ and $q\bar{q}' \rightarrow h^0W^\pm$ in the continuum (tho there may be peaks at m_{A^0}). The most interesting decays are $h^0, H^0, A^0 \rightarrow b\bar{b}$ -jets and $\tau^+\tau^-$, and, if above threshold, $H^0 \rightarrow ZZ, W^+W^-$ and h^0h^0 . The following final states should be compared with the Standard Model cross section: $b\bar{b}Z$, $b\bar{b}W^\pm$, $\tau^+\tau^-Z$, $\tau^+\tau^-W^\pm$, $b\bar{b}$, $\tau^+\tau^-$, ZZ , W^+W^- , 3 and 4 b -jets, $2\tau^+ + 2\tau^-$, $b\bar{b}\tau^+\tau^-$, ZW^+W^- , $3Z$, ZZW^\pm and $3W^\pm$. Mass peaks should be searched in the following channels: $Zb\bar{b}$, ZZ , ZZZ , $b\bar{b}$, 4 b -jets and, just in case, $Z\gamma$.

We have discussed the masses of the Higgs particles in the Two Higgs Doublet Model of type II, and have calculated several relevant production cross sections and decay rates. We have also discussed running coupling constants and Grand Unification. If the Two Higgs Doublet Model of type II is part of a Grand Unified Theory, then it does not agree with the observed $\sin^2\theta_W$ nor with the non-observation of proton decay. The MSSM with $n_S = 2$ (which includes the Two Higgs Doublet Model of type II) is in agreement with both the observed $\sin^2\theta_W(m_Z)$, and with the non-observation of proton decay.

Bibliography

- [1] Vernon Barger and Roger Phillips, Collider Physics (Addison Wesley, 1988), pages 452-454; S. Dawson, J. F. Gunion, H.E. Haber and G. Kane, *The Higgs Hunter's Guide* (Addison Wesley, 1990), p. 201.
- [2] Carlos A. Marín and Bruce Hoeneisen, hep-ph/0210167 (2002).
- [3] CDF Collab., Phys. Rev. Lett. **79**, 357 (1997).
- [4] D0 Collab., Phys. Rev. Lett. **82**, 4975 (1999); FERMILAB-Conf-00-294-E.
- [5] LEP Higgs Working Group, <http://lephiggs.web.cern.ch/LEPHIGGS/papers/index.html>; LHWG Note/2001-05.
- [6] *Review of Particle Physics*, K. Hagiwara *et al*, Physical Review **D66**, 010001 (2002).
- [7] Carlos Marín y Guillermo Hernández, Serie de Documentos USFQ **13**, Universidad San Francisco de Quito, Ecuador (1994)
- [8] “CompHEP: A package for evaluation of Feynman diagrams and integration over multiparticle phase space.” A. Pukhov, E. Boos, M. Dubinin, V. Edneral, V. Ilyin, D. Kovalenko, A. Kryukov, V. Savrin, S. Shichanin, A. Semenov, hep-ph/9908288 (1999)
- [9] “The quantum theory of fields”, Volume III, Supersymmetry, Steven Weinberg, Cambridge University Press (2000).

Chapter 4

Higgs production at a muon collider in the Two Higgs Doublet Model of type II

Abstract

We calculate Higgs production cross sections at a muon collider in the Two Higgs Doublet Model of type II. The most interesting productions channels are $\mu^-\mu^+ \rightarrow h^0 Z^0, H^0 Z^0, H^- H^+, A^0 Z^0$ and $H^\mp W^\pm$. The last channel is compared with the production processes $p\bar{p} \rightarrow H^\mp W^\pm X$ and $pp \rightarrow H^\mp W^\pm X$ at the Tevatron and LHC energies, respectively, for large values of $\tan \beta$.

4.1 Introduction

In this article we calculate neutral and charged Higgs production cross sections at a muon collider in the Two Higgs Doublet Model of type II. The Higgs sector of the Minimal Supersymmetric Standard Model (MSSM) is of this type (tho the model of type II does not require Supersymmetry). Higgs doublets can be added to the Standard Model without upsetting the Z/W mass ratio. Higher dimensional representations upset this ratio [1]. Adding a second complex doublet to the Standard Model results in five Higgs bosons: one pseudoscalar A^0 (CP-odd scalar), two neutral scalars H^0 and h^0 (CP-even scalars), and two charged scalars H^+ and H^- . In the Standard Model we only have a single neutral Higgs.

In recent years, some papers have appeared, suggesting the possibility of the construction of a $\mu^-\mu^+$ collider to detect charged or neutral Higgs bosons [[2], [3]]. The main reason is that in a muon collider, the signal could be cleaner than in a hadron collider. In this paper, we analyze this possibility studying some production cross sections like: $\mu^-\mu^+ \rightarrow h^0 Z^0, H^0 Z^0, H^- H^+, A^0 Z^0$ and $H^\mp W^\pm$ (Sections 4.2-4.6).

In Sections 4.5,4.6,4.8,4.9 we will focus our interest in the production of charged Higgs bosons. There are three ways of producing H^\pm . One is via $p\bar{p}$ or pp interactions in a hadron collider. In hadron colliders, the signals are overwhelmed by backgrounds due basically to $t\bar{t}$ production [4]. The other ways to produce charged Higgs are e^-e^+ or $\mu^-\mu^+$ colliders, in which backgrounds are considerably less. In some processes like $\mu^-\mu^+ \rightarrow H^- H^+$ and $e^-e^+ \rightarrow H^- H^+$, there is no difference between the cross sections obtained in an e^-e^+ collider or a $\mu^-\mu^+$ collider. However, in reactions like $\mu^-\mu^+ \rightarrow H^\mp W^\pm$ and $e^-e^+ \rightarrow H^\mp W^\pm$, the total cross section is proportional to the square of the mass of the fermion and then e^-e^+ interactions give us very small cross sections. This motivated us to compare in Section 4.9 the channel $\mu^-\mu^+ \rightarrow H^\mp W^\pm$ (at $\sqrt{s} = 500\text{GeV}/c$ and for large values of $\tan\beta$) with the production processes $p\bar{p} \rightarrow H^\mp W^\pm X$ (at the Tevatron) and $pp \rightarrow H^\mp W^\pm X$ (at the LHC), to check the feasibility of detecting H^\pm using a muon collider.

The influence of radiative corrections in the masses of the Higgs bosons is considered in all the calculations.

4.2 Higgs bosons masses and radiative corrections

The masses of the neutral Higgs particles, calculated at tree level, are [5]:

$$m_{A^0}^2 = m_H^2 - m_W^2 \quad (4.1)$$

$$m_{H^0}^2 = \frac{1}{2} \left[m_Z^2 + m_{A^0}^2 + \left[(m_Z^2 - m_{A^0}^2)^2 + 4m_{A^0}^2 m_Z^2 \sin^2 2\beta \right]^{1/2} \right] \quad (4.2)$$

$$m_{h^0}^2 = \frac{1}{2} \left[m_Z^2 + m_{A^0}^2 - \left[(m_Z^2 - m_{A^0}^2)^2 + 4m_{A^0}^2 m_Z^2 \sin^2 2\beta \right]^{1/2} \right] \quad (4.3)$$

with $0 \leq \beta < \frac{\pi}{2}$

From these relations, the Higgs bosons masses satisfy the bounds:

$$m_{A^0} < m_H \quad (4.4)$$

$$m_H > m_W \quad (4.5)$$

$$m_{h^0} \leq m_Z \quad (4.6)$$

$$m_Z \leq m_{H^0} \leq \sec \theta_W m_H \quad (4.7)$$

The bound given by (4.6) practically has been excluded by the present limits on m_{h^0} obtained by LEP and CDF [6].

The mixing angle α ($-\pi/2 < \alpha \leq 0$) between the two neutral scalar Higgs fields H^0 , h^0 is given by

$$\tan \alpha = - \left[\frac{1+F}{1-F} \right]^{1/2} \quad (4.8)$$

$$F = \frac{(1 - \tan^2 \beta)}{(1 + \tan^2 \beta) G} \left[1 - \frac{m_Z^2}{m_H^2} - \frac{m_W^2}{m_H^2} \right] \quad (4.9)$$

$$G = \left[\left(1 - \frac{m_W^2}{m_H^2} + \frac{m_Z^2}{m_H^2} \right)^2 - 4 \left(\frac{m_Z^2}{m_H^2} \right) \left(1 - \frac{m_W^2}{m_H^2} \right) \left(\frac{1 - \tan^2 \beta}{1 + \tan^2 \beta} \right)^2 \right]^{1/2} \quad (4.10)$$

In terms of m_H and G Equations (4.2) and (4.3) are:

$$m_{H^0}^2 = \frac{1}{2}m_H^2 \left[1 - \frac{m_W^2}{m_H^2} + \frac{m_Z^2}{m_H^2} + G \right] \quad (4.11)$$

$$m_{h^0}^2 = \frac{1}{2}m_H^2 \left[1 - \frac{m_W^2}{m_H^2} + \frac{m_Z^2}{m_H^2} - G \right] \quad (4.12)$$

Taking into account radiative corrections, (4.2) and (4.3) can be written as [see [7], [8]]:

$$\begin{aligned} m_{H^0}^2 = & \frac{1}{2} \{ m_A^2 + m_Z^2 + \Delta_t + \Delta_b \\ & + \{ ((m_A^2 - m_Z^2) \cos 2\beta + \Delta_t - \Delta_b)^2 \\ & + (m_A^2 + m_Z^2)^2 \sin^2 2\beta \}^{1/2} \} \end{aligned} \quad (4.13)$$

$$\begin{aligned} m_{h^0}^2 = & \frac{1}{2} \{ m_A^2 + m_Z^2 + \Delta_t + \Delta_b \\ & - \{ ((m_A^2 - m_Z^2) \cos 2\beta + \Delta_t - \Delta_b)^2 \\ & + (m_A^2 + m_Z^2)^2 \sin^2 2\beta \}^{1/2} \} \end{aligned} \quad (4.14)$$

where:

$$\Delta_b = \frac{3\sqrt{2}m_b^4 G_F (1 + \tan^2 \beta)}{2\pi^2} \ln \left(\frac{M_{sb}^2}{m_b^2} \right) \quad (4.15)$$

and

$$\Delta_t = \frac{3\sqrt{2}m_t^4 G_F (1 + \tan^2 \beta)}{2\pi^2 \tan^2 \beta} \ln \left(\frac{M_{st}^2}{m_t^2} \right) \quad (4.16)$$

M_{sb} and M_{st} are the masses of the sbottom and stop (the scalar superpartners of the bottom and top quarks).

Equation (4.1) is practically unaffected by radiative corrections. According to (4.14) m_{h^0} increases as the value of m_A increases. Then, for very large values of m_A we can set an upper bound for m_{h^0} :

$$m_{h^0}^2 \leq m_{h^0}^2(m_{A^0} \rightarrow \infty) = m_Z^2 \left(\frac{1 - \tan^2 \beta}{1 + \tan^2 \beta} \right)^2 + \frac{\Delta_t \tan^2 \beta}{(1 + \tan^2 \beta)} + \frac{\Delta_b}{(1 + \tan^2 \beta)} \quad (4.17)$$

Taking $m_b = 4.3 \text{ GeV}/c^2$, $m_t = 174.3 \text{ GeV}/c^2$, $M_{st} \sim M_{sb} \sim 1 \text{ TeV}$ [7] and $m_Z = 91.1876 \text{ GeV}/c^2$ we obtain:

$$\Delta_b = 1.123 \times 10^{-6} (1 + \tan^2 \beta) m_Z^2 \quad (4.18)$$

$$\Delta_t = 0.9723 m_Z^2 \frac{(1 + \tan^2 \beta)}{\tan^2 \beta} \quad (4.19)$$

The contribution of the b-quark loop is negligible. Using Equations (4.18) and (4.19), (4.17) can be expressed as:

$$m_{h^0} \leq m_Z \left[\left(\frac{1 - \tan^2 \beta}{1 + \tan^2 \beta} \right)^2 + 0.9723 \right]^{1/2} \quad (4.20)$$

For large values of $\tan \beta$ ($\tan \beta \rightarrow \infty$) we obtain the limit

$$m_{h^0} \leq 1.4044 m_Z = 128.062 \text{ GeV}/c^2 \quad (4.21)$$

The upper bound on m_{h^0} is raised by radiative corrections from m_Z to $128.062 \text{ GeV}/c^2$ for stop masses of order 1 TeV.

Considering radiative corrections, we can write, for the masses of the neutral Higgs scalars:

$$m_{H^0}^2 = \frac{1}{2} m_H^2 \left[1 - \frac{m_W^2}{m_H^2} + \frac{m_Z^2}{m_H^2} + \frac{\Delta_t}{m_H^2} + G_{rc} \right] \quad (4.22)$$

$$m_{h^0}^2 = \frac{1}{2} m_H^2 \left[1 - \frac{m_W^2}{m_H^2} + \frac{m_Z^2}{m_H^2} + \frac{\Delta_t}{m_H^2} - G_{rc} \right] \quad (4.23)$$

$$G_{rc} = \left[\left(1 - \frac{m_W^2}{m_H^2} + \frac{m_Z^2}{m_H^2} \right)^2 - 4 \left(\frac{m_Z^2}{m_H^2} \right) \left(1 - \frac{m_W^2}{m_H^2} \right) \left(\frac{1 - \tan^2 \beta}{1 + \tan^2 \beta} \right)^2 + 2 \left(\frac{\Delta_t}{m_H^2} \right) \left(1 - \frac{m_W^2}{m_H^2} - \frac{m_Z^2}{m_H^2} \right) \left(\frac{1 - \tan^2 \beta}{1 + \tan^2 \beta} \right) + \left(\frac{\Delta_t}{m_H^2} \right)^2 \right]^{1/2} \quad (4.24)$$

With radiative corrections, the value of the α parameter is:

$$\tan \alpha = - \left[\frac{1 + F_{rc}}{1 - F_{rc}} \right]^{1/2} \quad (4.25)$$

$$F_{rc} = \frac{\left[\left(\frac{1 - \tan^2 \beta}{1 + \tan^2 \beta} \right) \left(1 - \frac{m_Z^2}{m_H^2} - \frac{m_W^2}{m_H^2} \right) + \frac{\Delta_t}{m_H^2} \right]}{G_{rc}} \quad (4.26)$$

Additionally we have:

$$\sin 2\alpha = -\frac{2 \tan \beta}{(1 + \tan^2 \beta)} \frac{\left(1 - \frac{m_W^2}{m_H^2} + \frac{m_Z^2}{m_H^2}\right)}{G_{rc}} \quad (4.27)$$

4.3 Production of h^0 , H^0

From the Feynman diagrams in Figure 4.1 and the corresponding Feynman rules given in reference [9], we obtain the differential cross section for the reaction $\mu^- \mu^+ \rightarrow h^0 Z^0$ in the center of mass system

$$\begin{aligned} \frac{d\sigma}{d\Omega}(\mu^- \mu^+ \rightarrow h^0 Z^0) &= \frac{1}{64\pi^2 s^2} G_F^2 m_Z^4 |C_Z|^2 \Lambda^{1/2}(s, m_{h^0}^2, m_Z^2) \\ &\quad \left[(g_A^\mu)^2 + (g_V^\mu)^2 \right] [8sm_Z^2 + \Lambda(s, m_{h^0}^2, m_Z^2) \sin^2 \theta] \end{aligned} \quad (4.28)$$

where

$$\begin{aligned} g_A^\mu &= -\frac{1}{2} \\ g_V^\mu &= -\frac{1}{2} + 2 \sin^2 \theta_W \end{aligned} \quad (4.29)$$

$$\Lambda(a, b, c) = a^2 + b^2 + c^2 - 2ab - 2ac - 2bc \quad (4.30)$$

$$C_Z = \frac{\sin(\beta - \alpha)}{(s - m_Z^2 + im_Z \Gamma_Z)} \quad (4.31)$$

Γ_Z is the total decay width of the Z^0 and θ is the scattering angle in the center of mass system.

The total cross section corresponding to $\mu^- \mu^+ \rightarrow h^0 Z^0$ is obtained integrating Equation (4.28):

$$\begin{aligned} \sigma(\mu^- \mu^+ \rightarrow h^0 Z^0) &= \frac{G_F^2 m_Z^4 (\tan \beta - \tan \alpha)^2}{48\pi s^2 (1 + \tan^2 \alpha) (1 + \tan^2 \beta)} \\ &\quad \times \frac{(1 - 4 \sin^2 \theta_W + 8 \sin^4 \theta_W)}{\left[(s - m_Z^2)^2 + m_Z^2 \Gamma_Z^2 \right]} [12sm_Z^2 + \Lambda(s, m_{h^0}^2, m_Z^2)] \\ &\quad \times \Lambda^{1/2}(s, m_{h^0}^2, m_Z^2) \times (3.8938 \times 10^{11}) \text{ fb} \end{aligned} \quad (4.32)$$

In Figures 4.2 and 4.3, the total cross section for $\mu^- \mu^+ \rightarrow h^0 Z^0$, is plotted as a function m_{h^0} for several values of \sqrt{s} and $\tan \beta$. These total cross

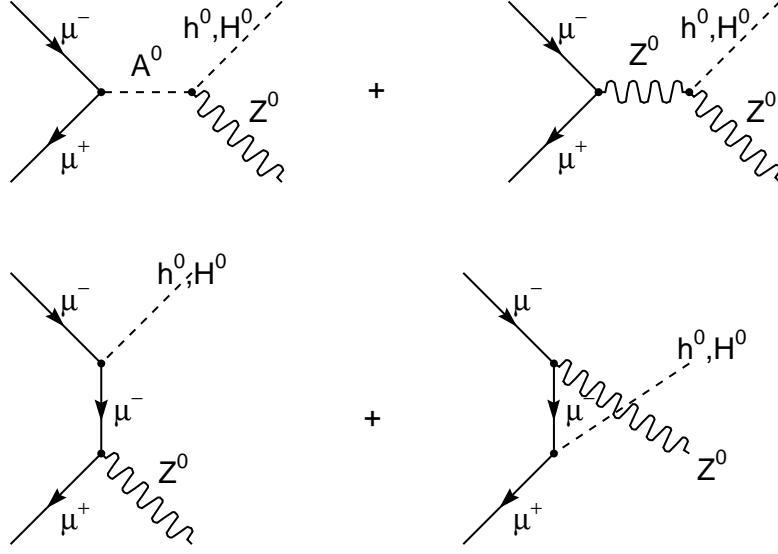


Figure 4.1: Feynman diagrams corresponding to the production of h^0 or H^0 in the channel $\mu^-\mu^+ \rightarrow h^0 Z^0$.

sections were plotted considering the radiative corrections of the masses given by Equations (4.23), (4.24), (4.25) and (4.26). According to these graphs, the total cross section becomes important in the mass interval $118 \leq m_{h^0} \leq 128 [\text{GeV}/c^2]$.

The Standard Model cross section is:

$$\begin{aligned} \sigma(\mu^-\mu^+ \rightarrow h_{SM}^0 Z^0)_{SM} &= \frac{G_F^2 m_Z^4}{48\pi s^2} \frac{(1 - 4\sin^2\theta_W + 8\sin^4\theta_W)}{\left[(s - m_Z^2)^2 + m_Z^2 \Gamma_Z^2\right]} \\ &\quad \times \left[12sm_Z^2 + \Lambda(s, m_{h_{SM}^0}^2, m_Z^2)\right] \\ &\quad \times \Lambda^{1/2}(s, m_{h_{SM}^0}^2, m_Z^2) \times (3.8938 \times 10^{11}) \text{ fb} \end{aligned} \quad (4.33)$$

where h_{SM} is the Standard Model Higgs boson.

The production cross section corresponding to $e^-e^+ \rightarrow h^0 Z^0$ is given by an expression identical to (4.32). In terms of the cross section

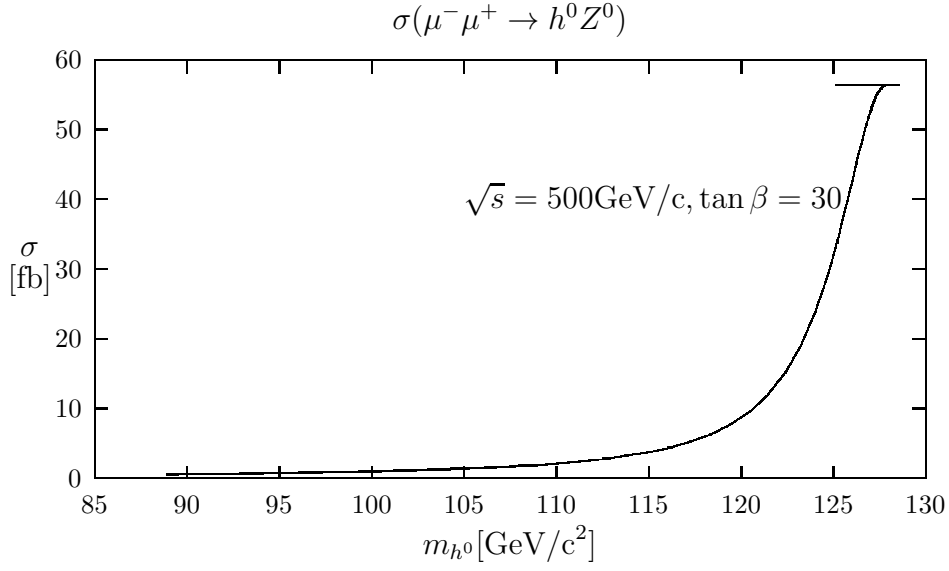


Figure 4.2: Total cross section for the process $\mu^-\mu^+ \rightarrow h^0 Z^0$ as a function of m_{h^0} . We have taken $\sqrt{s} = 500 \text{ GeV/c}$ and $\tan \beta = 30$.

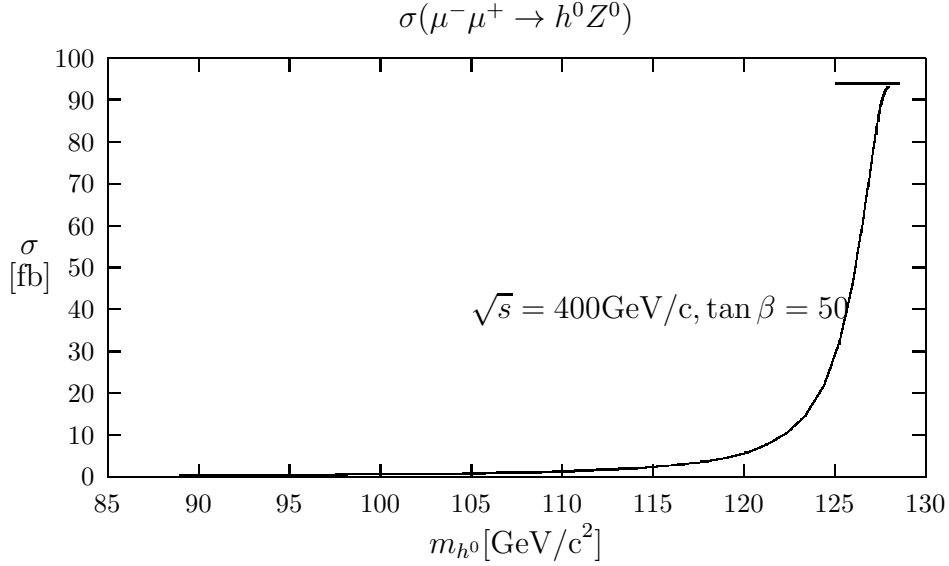


Figure 4.3: Total cross section for the process $\mu^-\mu^+ \rightarrow h^0 Z^0$ as a function of m_{h^0} . We have taken $\sqrt{s} = 400 \text{ GeV/c}$ and $\tan \beta = 50$.

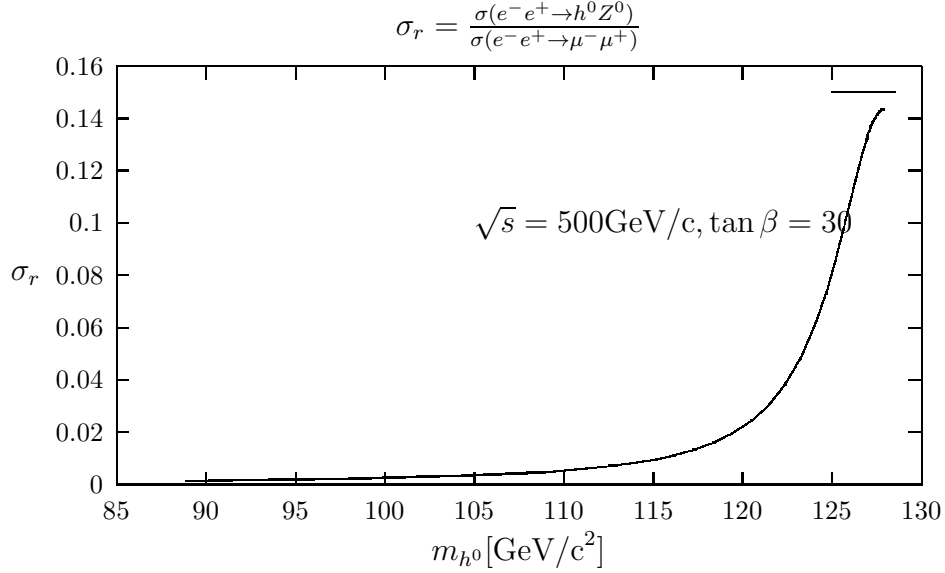


Figure 4.4: Total cross section $\sigma(e^-e^+ \rightarrow h^0 Z^0)$ compared with the cross section $\sigma(e^-e^+ \rightarrow \mu^-\mu^+)$ as a function of m_{h^0} . We have taken $\sqrt{s} = 500\text{GeV}/c$ and $\tan\beta = 30$.

$\sigma(e^-e^+ \rightarrow \mu^-\mu^+)$ we can write:

$$\frac{\sigma(e^-e^+ \rightarrow h^0 Z^0)}{\sigma(e^-e^+ \rightarrow \mu^-\mu^+)} = \frac{1}{128s} \frac{(\tan\beta - \tan\alpha)^2}{(1 + \tan^2\alpha)(1 + \tan^2\beta)} \Lambda^{1/2}(s, m_{h^0}^2, m_Z^2) \times \frac{(1 - 4\sin^2\theta_W + 8\sin^4\theta_W)}{\sin^4\theta_W (1 - \sin^2\theta_W)^2} \frac{[12sm_Z^2 + \Lambda(s, m_{h^0}^2, m_Z^2)]}{[(s - m_Z^2)^2 + m_Z^2\Gamma_Z^2]} \quad (4.34)$$

Equation (4.34) is plotted in Figure 4.4, as a function of m_{h^0} for $\sqrt{s} = 500\text{GeV}/c$ and $\tan\beta = 30$.

The total cross section corresponding to $\mu^-\mu^+ \rightarrow H^0 Z^0$ is obtained from Equation (4.32) replacing $(\tan\beta - \tan\alpha)^2$ by $(1 + \tan\beta \tan\alpha)^2$ in the numerator and m_{h^0} by m_{H^0} . This production cross section is plotted in Figures 4.5, 4.6 as a function of m_{H^0} for $\sqrt{s} = 500\text{GeV}/c$ and $\tan\beta = 30$, without and with mass radiative corrections, respectively. In Figure 4.7 we show the ratio between the production cross section $\sigma(e^-e^+ \rightarrow H^0 Z^0)$ and the cross section $\sigma(e^-e^+ \rightarrow \mu^-\mu^+)$ in terms of m_{H^0} . The radiatively corrected masses total cross section is shown in Figure 4.8. Figures 4.6 and 4.8 show the importance of the radiative corrections of the masses in the processes $\mu^-\mu^+ \rightarrow H^0 Z^0$ and $e^-e^+ \rightarrow H^0 Z^0$.

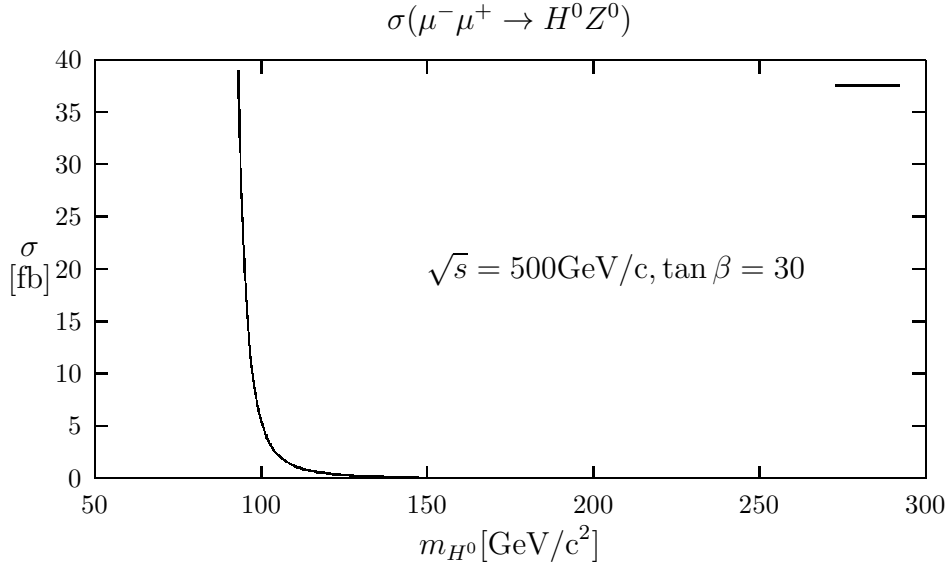


Figure 4.5: Total cross section for the process $\mu^-\mu^+ \rightarrow H^0 Z^0$ as a function of m_{H^0} . The radiative corrections of the masses were not taken into account. We have taken $\sqrt{s} = 500\text{GeV}/c$ and $\tan \beta = 30$.

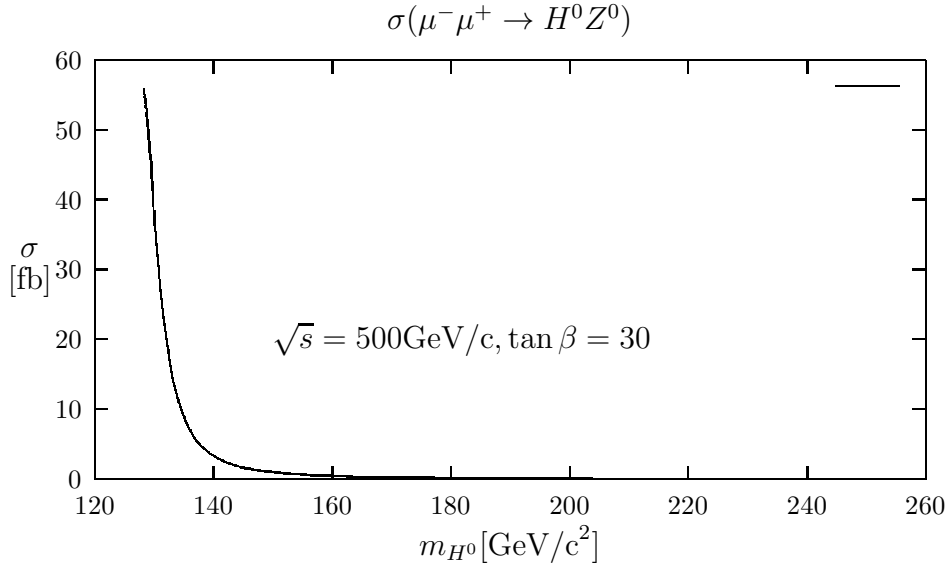


Figure 4.6: Radiatively corrected masses total cross section for the process $\mu^-\mu^+ \rightarrow H^0 Z^0$ as a function of m_{H^0} . We have taken $\sqrt{s} = 500\text{GeV}/c$ and $\tan \beta = 30$.

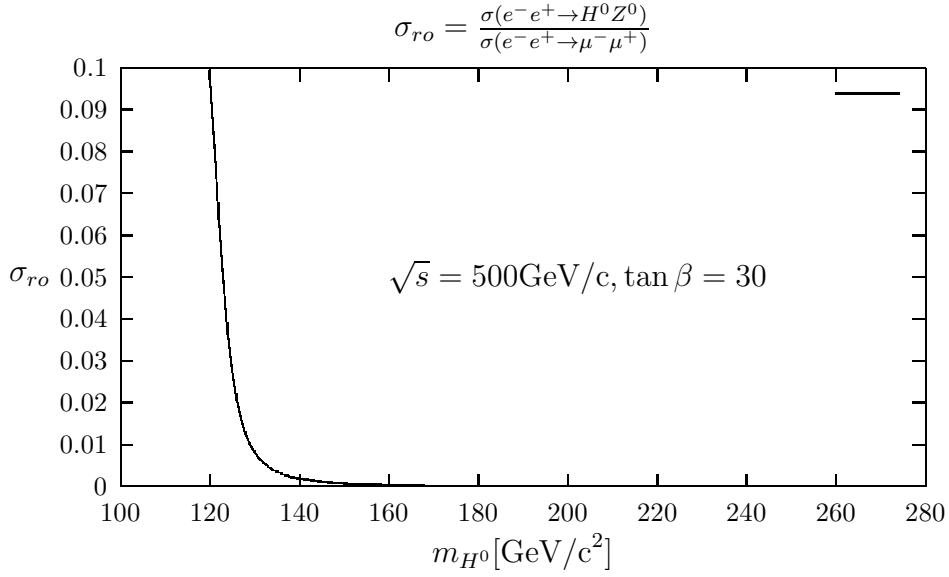


Figure 4.7: Total cross section for the process $e^-e^+ \rightarrow H^0 Z^0$ compared with the cross section $\sigma(e^-e^+ \rightarrow \mu^- \mu^+)$ as a function of m_{H^0} . We have taken $\sqrt{s} = 500 \text{ GeV}/c$ and $\tan \beta = 30$. The radiative corrections of the masses were not taken into account.

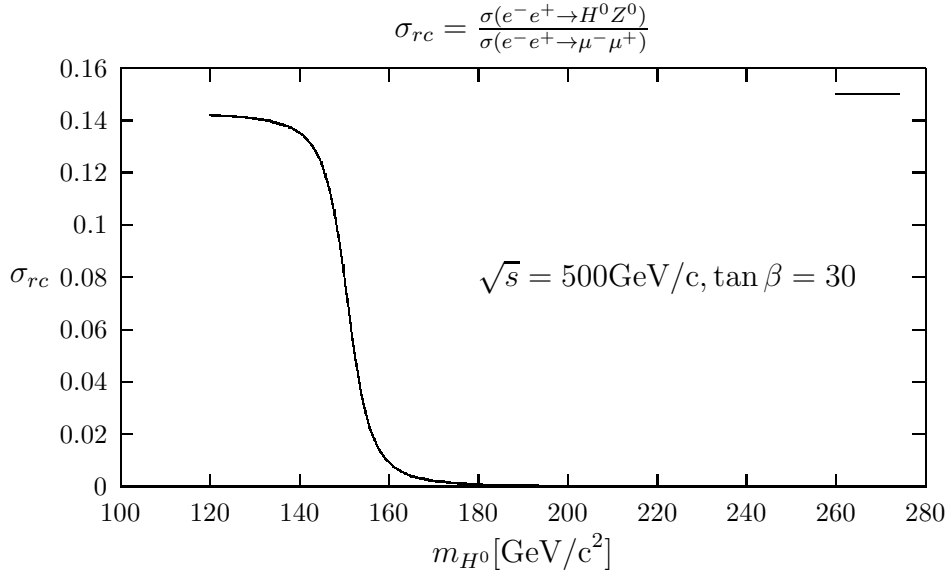


Figure 4.8: Radiatively corrected masses total cross section for the process $e^-e^+ \rightarrow H^0 Z^0$ compared with the cross section $\sigma(e^-e^+ \rightarrow \mu^- \mu^+)$ as a function of m_{H^0} . We have taken $\sqrt{s} = 500 \text{ GeV}/c$ and $\tan \beta = 30$.

4.4 Production of A^0

From the Feynman diagrams of Figure 4.9 and the Feynman rules given in [9], we obtain the differential cross section for the production process $\mu^- \mu^+ \rightarrow A^0 Z^0$ in the center of mass system:

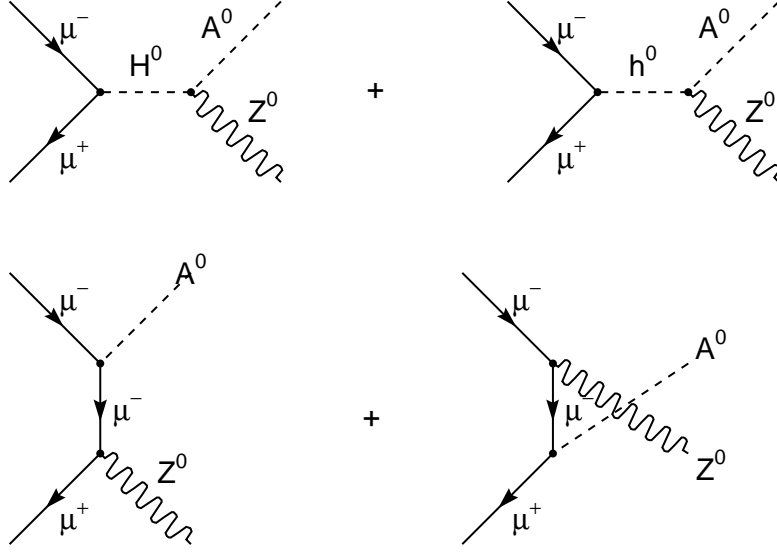


Figure 4.9: Feynman diagrams corresponding to the production of A^0 in the channel $\mu^- \mu^+ \rightarrow A^0 Z^0$.

$$\begin{aligned}
\frac{d\sigma}{d\Omega}(\mu^- \mu^+ \rightarrow A^0 Z^0) &= \frac{1}{64\pi^2 s} \Lambda^{1/2}(s, m_{A^0}^2, m_Z^2) G_F^2 m_\mu^2 \\
&\times \{ C_{Hb}^2 \Lambda(s, m_{A^0}^2, m_Z^2) + [(g_A^\mu)^2 + (g_V^\mu)^2] \\
&[\tan^2 \beta \left(1 + \frac{\Lambda(s, m_{A^0}^2, m_Z^2) m_Z^2 \sin^2 \theta}{2st^2} \right) \\
&+ \tan^2 \beta \left(1 + \frac{\Lambda(s, m_{A^0}^2, m_Z^2) m_Z^2 \sin^2 \theta}{2su^2} \right)] \\
&+ 2g_A^\mu \tan \beta C_{Hb} \left[\frac{m_{A^0}^2 m_Z^2}{t} - \frac{\Lambda(s, m_{A^0}^2, m_Z^2) \sin^2 \theta}{4t} - t \right] \\
&+ 2g_A^\mu \tan \beta C_{Hb} \left[\frac{m_{A^0}^2 m_Z^2}{u} - \frac{\Lambda(s, m_{A^0}^2, m_Z^2) \sin^2 \theta}{4u} - u \right] \\
&+ 2 \tan^2 \beta [(g_V^\mu)^2 - (g_A^\mu)^2] \left[\frac{m_{A^0}^2 m_Z^2}{ut} - \frac{\Lambda(s, m_{A^0}^2, m_Z^2) \sin^2 \theta}{4ut} \right. \\
&\left. + \frac{\Lambda(s, m_{A^0}^2, m_Z^2) m_Z^2 \sin^2 \theta}{2sut} \right] \} \quad (4.35)
\end{aligned}$$

where g_A^μ and g_V^μ are given by (4.29); s, t, u are the Mandelstam invariant variables and

$$C_{Hb} = \frac{\left(\frac{1}{2} \sin 2\alpha + \tan \beta \sin^2 \alpha\right)}{(s - m_{h^0}^2)} - \frac{\left(\frac{1}{2} \sin 2\alpha - \tan \beta \cos^2 \alpha\right)}{(s - m_{H^0}^2)} \quad (4.36)$$

To obtain the total cross section, we integrate Equation (4.35) over the solid angle Ω .

$$\begin{aligned} \sigma(\mu^- \mu^+ \rightarrow A^0 Z^0) &= \frac{G_F^2 m_\mu^2}{16\pi s^2} \{ \Lambda^{1/2}(s, m_{A^0}^2, m_Z^2) [s C_{Hb}^2 \Lambda(s, m_{A^0}^2, m_Z^2) \\ &\quad + 4 \tan^2 \beta \sin^2 \theta_W (1 - 2 \sin^2 \theta_W) (s - 2m_Z^2) + 2s \tan \beta C_{Hb} \\ &\quad \times (m_{A^0}^2 + m_Z^2 - s) + (1 - 4 \sin^2 \theta_W + 8 \sin^4 \theta_W) \\ &\quad \times \tan^2 \beta (s - 4m_Z^2)] + 4m_Z^2 \tan \beta f(s, m_{A^0}^2, m_Z^2) \\ &\quad \times [-s C_{Hb} m_{A^0}^2 + \frac{1}{2} \tan \beta (1 - 4 \sin^2 \theta_W + 8 \sin^4 \theta_W) (m_{A^0}^2 + m_Z^2 - s) \\ &\quad - 4 \frac{\sin^2 \theta_W (1 - 2 \sin^2 \theta_W) \tan \beta m_{A^0}^2 (s - m_Z^2)}{(m_{A^0}^2 + m_Z^2 - s)}] \} \\ &\quad \times (3.8938 \times 10^{11}) \text{ fb} \end{aligned} \quad (4.37)$$

where

$$f(s, m_{A^0}^2, m_Z^2) \equiv \ln \left| \frac{m_{A^0}^2 + m_Z^2 - s + \Lambda^{1/2}(s, m_{A^0}^2, m_Z^2)}{m_{A^0}^2 + m_Z^2 - s - \Lambda^{1/2}(s, m_{A^0}^2, m_Z^2)} \right| \quad (4.38)$$

Note that if $m_{A^0} = \sqrt{s} - m_Z$, then we have, $\Lambda(s, m_{A^0}^2, m_Z^2) = 0$ and $f(s, m_{A^0}^2, m_Z^2) = 0$. Therefore $\sigma(\mu^- \mu^+ \rightarrow A^0 Z^0) = 0$.

Figure 4.10 shows the total cross section $\sigma(\mu^- \mu^+ \rightarrow A^0 Z^0)$ as a function of m_{A^0} for $\sqrt{s} = 500 \text{ GeV}/c$ and $\tan \beta = 30, 50$. The total cross section is not affected by radiative corrections of the masses. From Figure 4.10 we can see that cross sections are important for large values of $\tan \beta$.

The total cross section corresponding to $e^- e^+ \rightarrow A^0 Z^0$ can be obtained from Equation (4.37) replacing m_μ by m_e :

$$\frac{\sigma(e^- e^+ \rightarrow A^0 Z^0)}{\sigma(\mu^- \mu^+ \rightarrow A^0 Z^0)} = \left(\frac{m_e}{m_\mu} \right)^2 = 2.34 \cdot 10^{-5}. \quad (4.39)$$

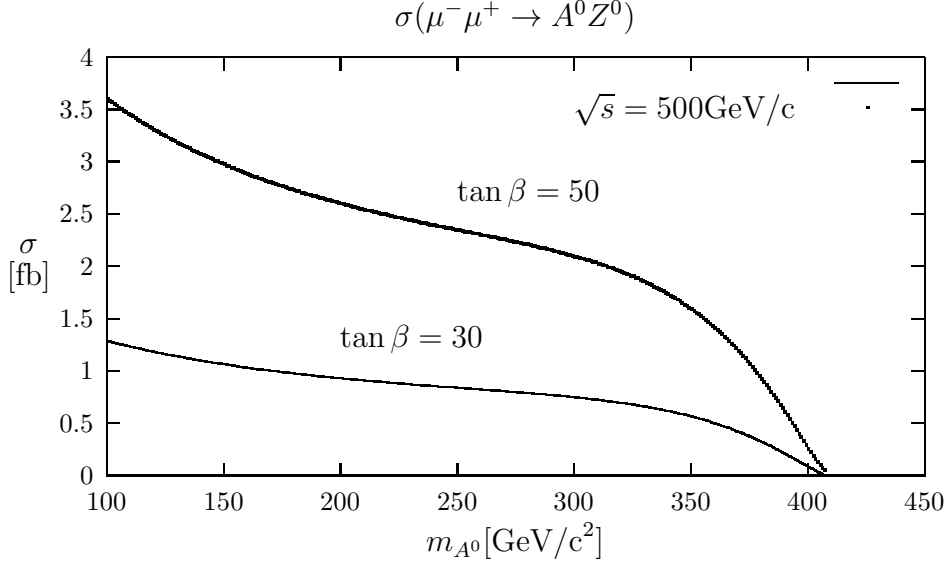


Figure 4.10: Total cross section for the process $\mu^- \mu^+ \rightarrow A^0 Z^0$ as a function of m_{A^0} . We have taken $\sqrt{s} = 500 \text{ GeV}/c$ and $\tan \beta = 30, 50$. The total cross section is not affected by radiative corrections of the masses.

4.5 Production of H^\pm

From the Feynman diagrams of Figure 4.11 we obtain the differential cross section in the center of mass system for the process $\mu^- \mu^+ \rightarrow H^- W^+$:

$$\begin{aligned}
 \frac{d\sigma}{d\Omega}(\mu^- \mu^+ \rightarrow H^- W^+) &= \frac{1}{64\pi^2 s} \Lambda^{1/2}(s, m_H^2, m_W^2) G_F^2 m_\mu^2 \\
 &\times \left\{ [C_{Hb}^2 + C_{Ab}^2] \Lambda(s, m_H^2, m_W^2) + 2 \left(\frac{\tan \beta}{t} \right)^2 \right. \\
 &\times \left[\frac{\Lambda(s, m_H^2, m_W^2) \sin^2 \theta m_W^2}{2s} + t^2 \right] - 2 \left(\frac{\tan \beta}{t} \right) (C_{Ab} + C_{Hb}) \\
 &\times \left[-t^2 - \frac{1}{4} \Lambda(s, m_H^2, m_W^2) \sin^2 \theta + m_W^2 m_H^2 \right] \left. \right\} \quad (4.40)
 \end{aligned}$$

where C_{Hb} is given by Equation (4.36) and

$$C_{Ab} = \frac{\tan \beta}{(s - m_{A^0}^2)} \quad (4.41)$$

The differential cross section corresponding to $\mu^- \mu^+ \rightarrow H^+ W^-$ is obtained from (4.40) by replacing t by u .

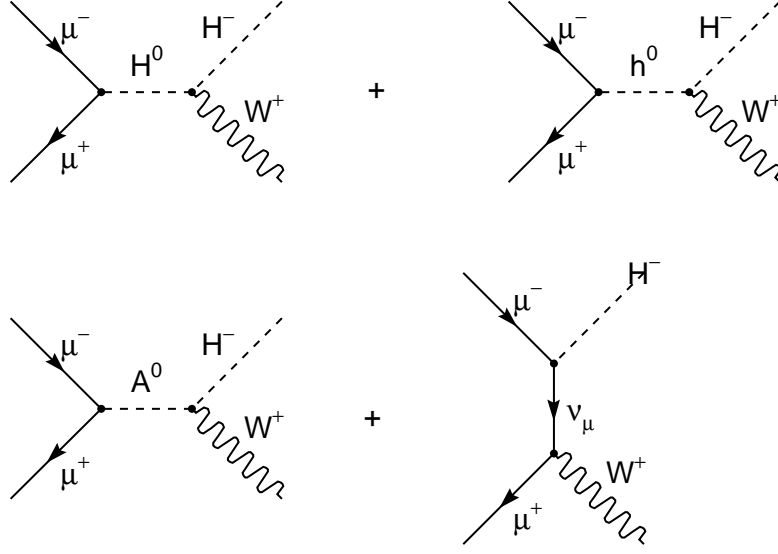


Figure 4.11: Feynman diagrams corresponding to the production of H^- in the channel $\mu^- \mu^+ \rightarrow H^- W^+$.

The integration of (4.40) over the solid angle Ω give us the total cross section:

$$\begin{aligned}
\sigma(\mu^- \mu^+ \rightarrow H^- W^+) &= \frac{G_F^2 m_\mu^2}{16\pi s^2} \{ s \Lambda^{3/2}(s, m_H^2, m_W^2) [C_{Hb}^2 + C_{Ab}^2] \\
&\quad + 2 \tan \beta \Lambda^{1/2}(s, m_H^2, m_W^2) [\tan \beta (s - 4m_W^2) \\
&\quad + (C_{Ab} + C_{Hb}) s (m_H^2 + m_W^2 - s)] + 4m_W^2 \tan \beta f(s, m_H^2, m_W^2) \\
&\quad [\tan \beta (m_H^2 + m_W^2 - s) - (C_{Ab} + C_{Hb}) s m_H^2] \} \\
&\quad \times (3.8938 \times 10^{11}) \text{ fb}
\end{aligned} \tag{4.42}$$

where

$$f(s, m_H^2, m_W^2) = \ln \left| \frac{m_H^2 + m_W^2 - s + \Lambda^{1/2}(s, m_H^2, m_W^2)}{m_H^2 + m_W^2 - s - \Lambda^{1/2}(s, m_H^2, m_W^2)} \right| \tag{4.43}$$

For the process $\mu^- \mu^+ \rightarrow H^+ W^-$ we obtain:

$$\sigma(\mu^- \mu^+ \rightarrow H^+ W^-) = \sigma(\mu^- \mu^+ \rightarrow H^- W^+) \tag{4.44}$$

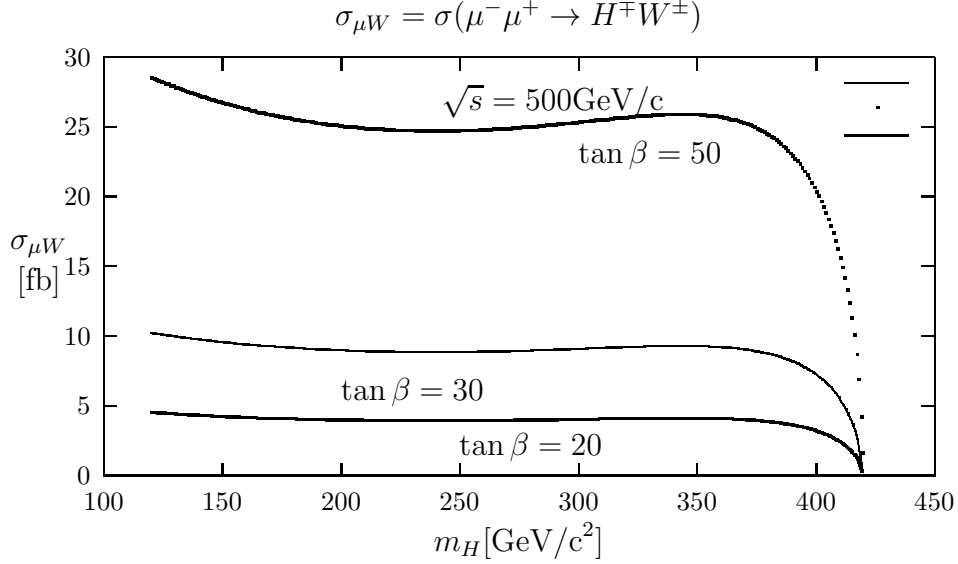


Figure 4.12: Total cross section for the process $\mu^- \mu^+ \rightarrow H^\mp W^\pm$ as a function of m_H . We have taken $\sqrt{s} = 500 \text{ GeV}/c$ and $\tan \beta = 20, 30, 50$. The radiative corrections of the masses are negligible.

and then

$$\sigma(\mu^- \mu^+ \rightarrow H^\pm W^\mp) = 2\sigma(\mu^- \mu^+ \rightarrow H^- W^+) \quad (4.45)$$

Observe that $\sigma(\mu^- \mu^+ \rightarrow H^\pm W^\mp) = 0$ if $m_H = \sqrt{s} - m_W$.

The total cross section corresponding to $\mu^- \mu^+ \rightarrow H^\mp W^\pm$ is given in Figure 4.12 for $\sqrt{s} = 500 \text{ GeV}/c$ and $\tan \beta = 20, 30, 50$. This total cross section is not affected by radiative corrections of the masses. From Figure 4.12 we see that $\sigma(\mu^- \mu^+ \rightarrow H^\mp W^\pm) \gtrsim 5 \text{ fb}$ for $\tan \beta \geq 20$ in the mass interval $100 \leq m_H \leq 400 [\text{GeV}/c^2]$.

For the process $e^- e^+ \rightarrow H^\mp W^\pm$, the total cross section is obtained from Equations (4.42), (4.45) replacing m_μ by m_e . This cross section is smaller than the one plotted in Figure 4.12 by a factor $m_e^2/m_\mu^2 = 2.34 \cdot 10^{-5}$.

Equations (4.37) and (4.42) are in agreement with the cross sections calculated in [3].

4.6 Production of charged Higgs boson pairs

From the Feynman diagrams of Figure 4.13, the differential cross section in the center of mass system corresponding to $\mu^- \mu^+ \rightarrow H^- H^+$ is

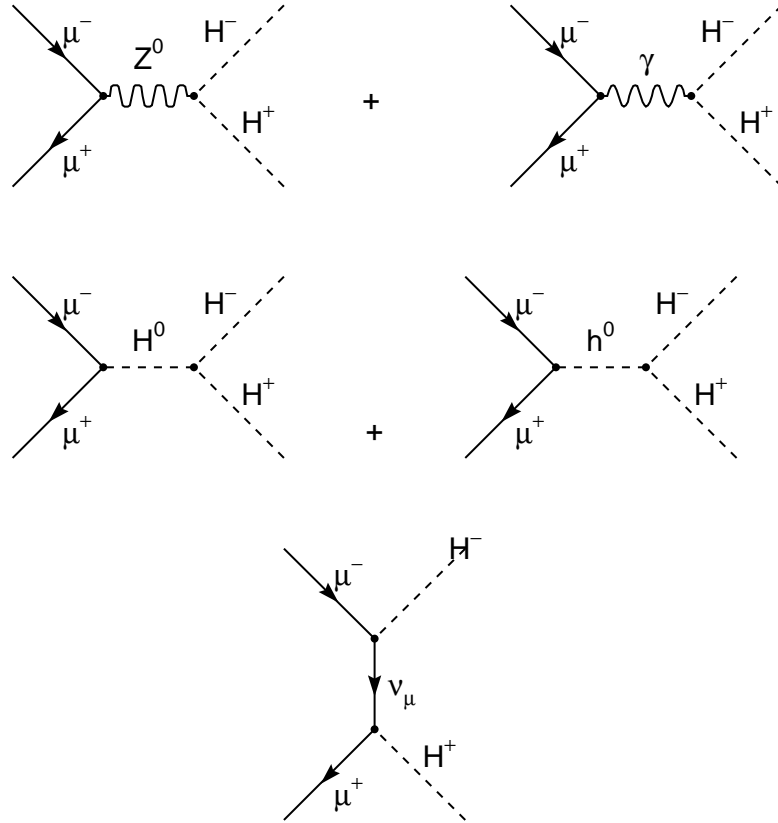


Figure 4.13: Feynman diagrams corresponding to the production of charged Higgs boson pairs in the channel $\mu^- \mu^+ \rightarrow H^- H^+$.

$$\begin{aligned}
\frac{d\sigma}{d\Omega}(\mu^-\mu^+ \rightarrow H^-H^+) &= \frac{G_F^2 m_W^4}{8\pi^2 s} \left(1 - 4\frac{m_H^2}{s}\right)^{1/2} \{s(s - 4m_H^2) \sin^2 \theta \\
&\left[\frac{1}{8} |C_1|^2 [(g_A^\mu)^2 + (g_V^\mu)^2] + 2 \left(\frac{\sin^2 \theta_W}{s}\right)^2 - \left(\frac{\sin^2 \theta_W}{s}\right) \Re(C_1) g_V^\mu \right] \\
&+ 2m_\mu^2 [(s - 4m_H^2) [\frac{|C_1|^2}{4} (\cos^2 \theta (g_V^\mu)^2 - \sin^2 \theta (g_A^\mu)^2) \\
&+ 4 \left(\frac{\sin^2 \theta_W}{s}\right)^2 \cos^2 \theta - 2 \left(\frac{\sin^2 \theta_W}{s}\right) \Re(C_1) g_V^\mu \cos^2 \theta] \\
&+ \frac{1}{4} (C^{Hh})^2 s + (s(s - 4m_H^2))^{1/2} \\
&\times \cos \theta C^{Hh} \left(\frac{1}{2} g_V^\mu \Re(C_1) - 2 \left(\frac{\sin^2 \theta_W}{s}\right)\right)] \}
\end{aligned} \tag{4.46}$$

where g_A^μ and g_V^μ are given by Equation (4.29),

$$C_1 \equiv \frac{\cos(2\theta_W)}{\cos^2 \theta_W} \frac{1}{(s - m_Z^2 + im_Z \Gamma_Z)}, \tag{4.47}$$

$$C^{Hh} = \frac{a_1}{(s - m_{H^0}^2)} - \frac{a_2}{(s - m_{h^0}^2)}, \tag{4.48}$$

$$\begin{aligned}
a_1 &= [\cos^2 \alpha + \frac{\tan \beta \sin 2\alpha}{2} - \frac{m_Z}{2m_W \cos \theta_W} \\
&\frac{(1 - \tan^2 \beta)}{(1 + \tan^2 \beta)} \left(\cos^2 \alpha - \frac{\tan \beta \sin 2\alpha}{2} \right)],
\end{aligned} \tag{4.49}$$

$$\begin{aligned}
a_2 &= [\frac{\tan \beta \sin 2\alpha}{2} - \sin^2 \alpha + \frac{m_Z}{2m_W \cos \theta_W} \\
&\frac{(1 - \tan^2 \beta)}{(1 + \tan^2 \beta)} \left(\sin^2 \alpha + \frac{\tan \beta \sin 2\alpha}{2} \right)]
\end{aligned} \tag{4.50}$$

The integration of (4.46) give us the total cross section for the process $\mu^-\mu^+ \rightarrow H^-H^+$:

$$\begin{aligned}
\sigma(\mu^+\mu^-\rightarrow H^+H^-) &= \sigma(\mu^-\mu^+\rightarrow H^-H^+) = \frac{2m_W^4 G_F^2 \sin^4 \theta_W}{3\pi s} \\
&\left(1 - \frac{4m_H^2}{s}\right)^{3/2} \left\{ \left[1 + \frac{(1 - 2\sin^2 \theta_W)^2 (1 + (4\sin^2 \theta_W - 1)^2)}{64 \sin^4 \theta_W \cos^4 \theta_W}\right] \right. \\
&\times \frac{1}{\left[\left(1 - \frac{m_Z^2}{s}\right)^2 + \left(\frac{M_Z \Gamma_Z}{s}\right)^2\right]} - \frac{(1 - 2\sin^2 \theta_W)(4\sin^2 \theta_W - 1)}{4 \sin^2 \theta_W \cos^2 \theta_W} \\
&\times \frac{\left(1 - \frac{m_Z^2}{s}\right)}{\left[\left(1 - \frac{m_Z^2}{s}\right)^2 + \left(\frac{M_Z \Gamma_Z}{s}\right)^2\right]} \left. + \frac{m_\mu^2}{s} \left[-\frac{((4\sin^2 \theta_W - 1)^2 - 2)}{32 \sin^4 \theta_W \cos^4 \theta_W} \right] \right. \\
&\times \frac{(1 - 2\sin^2 \theta_W)^2}{\left[\left(1 - \frac{m_Z^2}{s}\right)^2 + \left(\frac{M_Z \Gamma_Z}{s}\right)^2\right]} + 2 - \frac{(1 - 2\sin^2 \theta_W)(4\sin^2 \theta_W - 1)}{2 \sin^2 \theta_W \cos^2 \theta_W} \\
&\times \frac{\left(1 - \frac{m_Z^2}{s}\right)}{\left[\left(1 - \frac{m_Z^2}{s}\right)^2 + \left(\frac{M_Z \Gamma_Z}{s}\right)^2\right]} + \frac{3}{4} \frac{s^2 (C^{Hh})^2}{\left(1 - 4\frac{m_H^2}{s}\right)} \left. \right\} \\
&\times (3.8938 \times 10^{11}) \text{ fb}
\end{aligned} \tag{4.51}$$

Neglecting the mass of the muon we can write:

$$\begin{aligned}
\sigma(\mu^+\mu^-\rightarrow H^+H^-) &= \sigma(\mu^-\mu^+\rightarrow H^-H^+) = \frac{2m_W^4 G_F^2 \sin^4 \theta_W}{3\pi s} \\
&\left(1 - \frac{4m_H^2}{s}\right)^{3/2} \left\{ 1 + \frac{(1 - 2\sin^2 \theta_W)^2 (1 + (4\sin^2 \theta_W - 1)^2)}{64 \sin^4 \theta_W \cos^4 \theta_W} \right. \\
&\times \frac{1}{\left[\left(1 - \frac{m_Z^2}{s}\right)^2 + \left(\frac{M_Z \Gamma_Z}{s}\right)^2\right]} - \frac{(1 - 2\sin^2 \theta_W)(4\sin^2 \theta_W - 1)}{4 \sin^2 \theta_W \cos^2 \theta_W} \\
&\times \frac{\left(1 - \frac{m_Z^2}{s}\right)}{\left[\left(1 - \frac{m_Z^2}{s}\right)^2 + \left(\frac{M_Z \Gamma_Z}{s}\right)^2\right]} \left. \right\} \times (3.8938 \times 10^{11}) \text{ fb}
\end{aligned} \tag{4.52}$$

In the last approximation there is no difference with the total cross section corresponding to the process $e^-e^+ \rightarrow H^-H^+$. In Figure 4.14 we have plotted the total cross section given by Equation (4.51) as a function of the mass

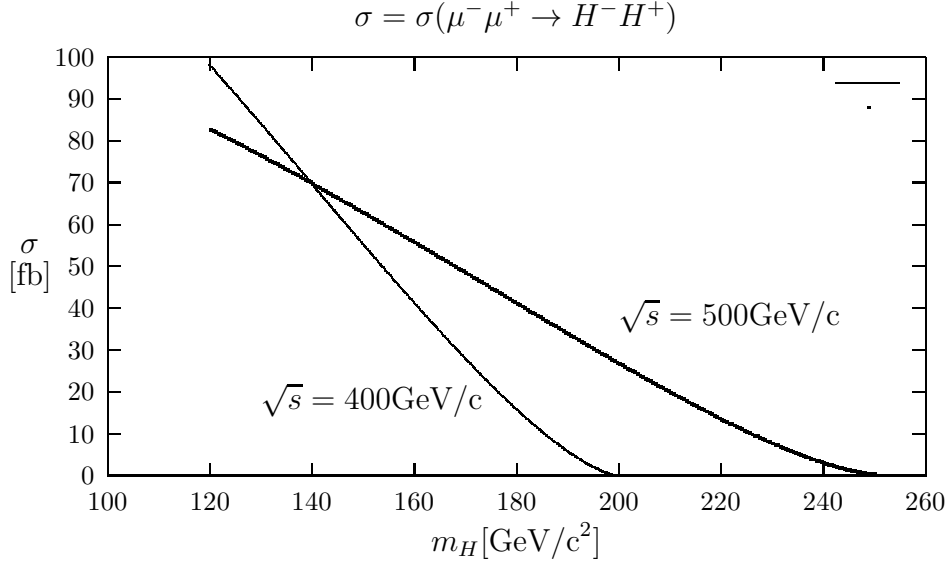


Figure 4.14: Total cross section for the process $\mu^-\mu^+ \rightarrow H^-H^+$ as a function of m_H . We have taken $\sqrt{s} = 400, 500 \text{ GeV}/c$. The total cross section is practically independent of $\tan\beta$. The radiative corrections of the masses are negligible.

of the charged Higgs for $\sqrt{s} = 400, 500 \text{ GeV}/c$. The total cross section is practically independent of $\tan\beta$. The radiative corrections of the masses are also negligible.

In Figure 4.15 we have plotted the total cross section corresponding to the process $\mu^-\mu^+ \rightarrow H^-H^+$ as a function of m_H compared with $\mu^-\mu^+ \rightarrow H^\mp W^\pm$. We have taken $\sqrt{s} = 500 \text{ GeV}/c$.

4.7 $\mu^-\mu^+ \rightarrow t\bar{t}$ annihilation

The main background in the processes $\mu^-\mu^+ \rightarrow H^\pm W^\mp$, assuming $H^+ \rightarrow t\bar{b}$ or $H^- \rightarrow \bar{t}b$ decays, comes from $t\bar{t}$ production.

To lowest order in e^2 the Feynman diagrams corresponding to the process $\mu^-\mu^+ \rightarrow t\bar{t}$ are given in Figure 4.16. The corresponding total cross section is (see reference [10]):

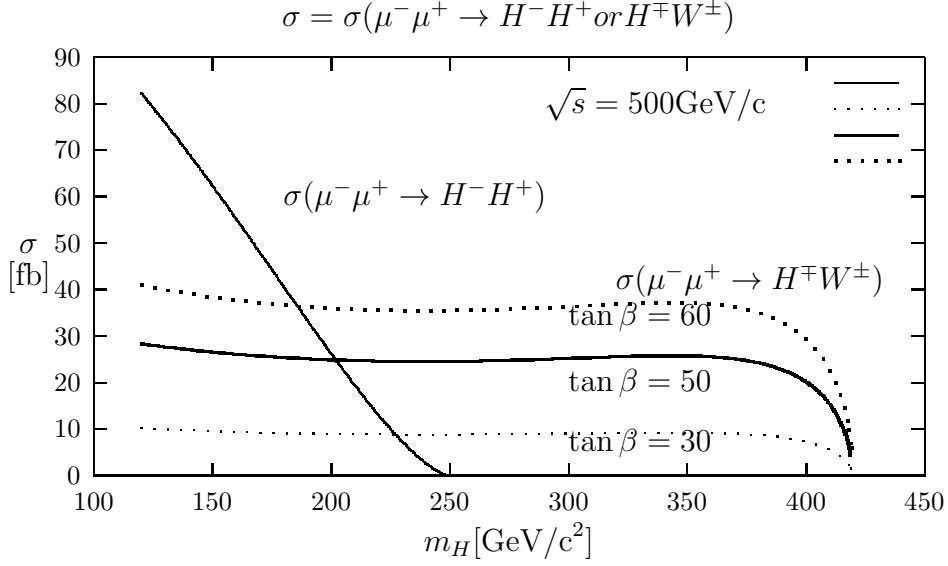


Figure 4.15: Total cross section for the process $\mu^- \mu^+ \rightarrow H^- H^+$ as a function of m_H compared with $\mu^- \mu^+ \rightarrow H^\mp W^\pm$. We have taken $\sqrt{s} = 500 \text{ GeV}/c$ and $\tan \beta = 30, 50, 60$.

$$\begin{aligned}
\frac{\sigma(\mu^- \mu^+ \rightarrow t\bar{t})}{\sigma_0} &= \frac{3}{4} \{ m_t^2 s \left\{ \left[\frac{4}{3s} + \frac{(\frac{8}{3} \sin^2 \theta_W - 1)}{2 \cos^2 \theta_W (s - m_Z^2)} \right]^2 \right. \\
&\quad \left. + \left[\frac{4}{3s} - \frac{(\frac{14}{3} \sin^2 \theta_W - \frac{16}{3} \sin^4 \theta_W - 1)}{\sin^2(2\theta_W) (s - m_Z^2)} \right]^2 \right\} \\
&\quad + 2 \left[\frac{2}{3} + \frac{(\frac{8}{3} \sin^2 \theta_W - 1) s}{4 \cos^2 \theta_W (s - m_Z^2)} \right]^2 + \left[\frac{s^2 \left(1 - \frac{4m_t^2}{s}\right)}{8 \cos^4 \theta_W (s - m_Z^2)^2} \right] \\
&\quad + 2 \left[\frac{2}{3} + \frac{(2 \sin^2 \theta_W - 1) (\frac{4}{3} \sin^2 \theta_W - \frac{1}{2}) s}{\sin^2(2\theta_W) (s - m_Z^2)} \right]^2 \\
&\quad \left. + \frac{\left(1 - \frac{4m_t^2}{s}\right) (2 \sin^2 \theta_W - 1)^2 s^2}{2 \sin^4(2\theta_W) (s - m_Z^2)^2} \right\} \left(1 - \frac{4m_t^2}{s}\right)^{1/2} \quad (4.53)
\end{aligned}$$

where

$$\sigma_0 = \sigma(e^- e^+ \rightarrow \mu^- \mu^+) = \frac{4\pi \alpha_{em}^2}{3s} \quad (4.54)$$

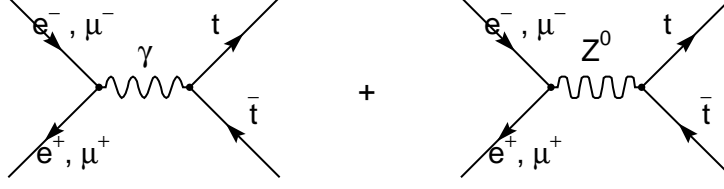


Figure 4.16: Feynman diagrams corresponding to $e^-e^+ \rightarrow t\bar{t}$ and $\mu^-\mu^+ \rightarrow t\bar{t}$ annihilation.

In (4.53) we have neglected Γ_Z that is very small for large values of \sqrt{s} .

Taking $\sin^2 \theta_W = 0.231$, $m_Z = 91.1876 \text{ GeV}/c^2$, $m_t = 174.3 \text{ GeV}/c^2$ and $\sqrt{s} = 500 \text{ GeV}/c$ we get $\sigma(\mu^-\mu^+ \rightarrow t\bar{t}) = 495.1 \text{ fb}$.

The total cross section corresponding to $e^-e^+ \rightarrow t\bar{t}$ is given by the same Equation (4.53).

4.8 $H^\mp W^\pm$ production at a Hadron Collider

4.8.1 $q\bar{q} \rightarrow H^- W^+$ interaction

From the Feynman diagrams of Figures 4.17 and 4.18 we obtain:

$$\begin{aligned}
\frac{d\sigma_I}{d\hat{t}}(q\bar{q} \rightarrow H^- W^+) &= \frac{G_F^2}{48\pi\hat{s}} \{m_q^2 \Lambda(\hat{s}, m_H^2, m_W^2) [(C_{Hb})^2 + (C_{Ab})^2] \\
&+ 2 \sum_{i,j=u,c,t} V_{iq} V_{jq}^* [m_q^2 c_{t_{1i}} c_{t_{1j}} \left(\hat{t}^2 + \frac{\Lambda(\hat{s}, m_H^2, m_W^2) \sin^2 \theta m_W^2}{2\hat{s}} \right) \\
&+ m_i^2 m_j^2 c_{t_{2i}} c_{t_{2j}} \left(2m_W^2 + \frac{\Lambda(\hat{s}, m_H^2, m_W^2) \sin^2 \theta}{4\hat{s}} \right)] + m_q^2 [-2m_H^2 m_W^2 + 2\hat{t}^2 \\
&+ \frac{1}{2} \Lambda(\hat{s}, m_H^2, m_W^2) \sin^2 \theta] (C_{Hb} + C_{Ab}) \sum_{i=u,c,t} \Re(V_{iq}) c_{t_{1i}} \} \quad (4.55)
\end{aligned}$$

for $q = d, s, b$. In Equation (4.55), C_{Hb} and C_{Ab} are given by Equations (4.36) and (4.41) replacing s by \hat{s} . V_{iq} are elements of the CKM matrix.

$$c_{t_{1i}} = \frac{\tan \beta}{(\hat{t} - m_i^2)}, \quad (4.56)$$

and

$$c_{t_{2i}} = \frac{\cot \beta}{(\hat{t} - m_i^2)}. \quad (4.57)$$

On the other hand,

$$\begin{aligned} \frac{d\sigma_{II}}{d\hat{t}} (q\bar{q} \rightarrow H^- W^+) &= \frac{G_F^2}{48\pi\hat{s}} \{ m_q^2 \Lambda(\hat{s}, m_H^2, m_W^2) (\hat{C}_{Ht}^2 + \hat{C}_{At}^2) \\ &+ 2 \sum_{i,j=d,s,b} V_{qi}^* V_{qj} [m_q^2 c_{u_{2i}} c_{u_{2j}} \left(\hat{u}^2 + \frac{\Lambda(\hat{s}, m_H^2, m_W^2) \sin^2 \theta m_W^2}{2\hat{s}} \right) \\ &+ m_i^2 m_j^2 c_{u_{1i}} c_{u_{1j}} \left(2m_W^2 + \frac{\Lambda(\hat{s}, m_H^2, m_W^2) \sin^2 \theta}{4\hat{s}} \right)] + m_q^2 [-2m_H^2 m_W^2 + 2\hat{u}^2 \\ &+ \frac{1}{2} \Lambda(\hat{s}, m_H^2, m_W^2) \sin^2 \theta] (\hat{C}_{At} - \hat{C}_{Ht}) \sum_{i=d,s,b} \Re(V_{qi}) c_{u_{2i}} \} \end{aligned} \quad (4.58)$$

for $q = u, c$.

$$\begin{aligned} \hat{C}_{Ht} &= \left[\frac{(\frac{1}{2} \sin 2\alpha - \sin^2 \alpha (\tan \beta)^{-1})}{(\hat{s} - m_{H^0}^2)} \right. \\ &\quad \left. - \frac{(\frac{1}{2} \sin 2\alpha + \cos^2 \alpha (\tan \beta)^{-1})}{(\hat{s} - m_{h^0}^2)} \right], \end{aligned} \quad (4.59)$$

$$\hat{C}_{At} = \frac{\cot \beta}{(\hat{s} - m_{A^0}^2)}, \quad (4.60)$$

$$c_{u_{1i}} = \frac{\tan \beta}{(\hat{u} - m_i^2)} \quad (4.61)$$

and

$$c_{u_{2i}} = \frac{\cot \beta}{(\hat{u} - m_i^2)}. \quad (4.62)$$

The differential cross section corresponding to the process $q\bar{q} \rightarrow H^+ W^-$ for $q = d, s, b$ is obtained from Equation (4.55) with the replacement $\hat{t} \rightarrow \hat{u}$. For $q = u, c$ we change \hat{u} by \hat{t} in (4.58).

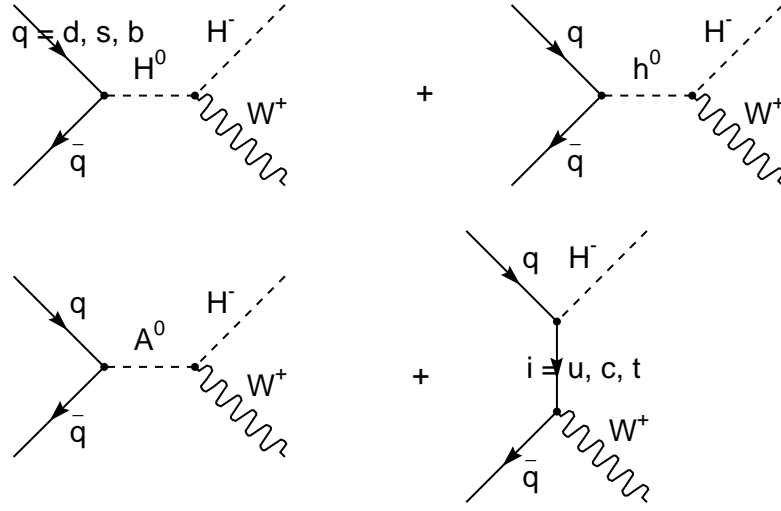


Figure 4.17: Feynman diagrams corresponding to the process $(q\bar{q} \rightarrow H^- W^+)$ for $q = d, s, b$.

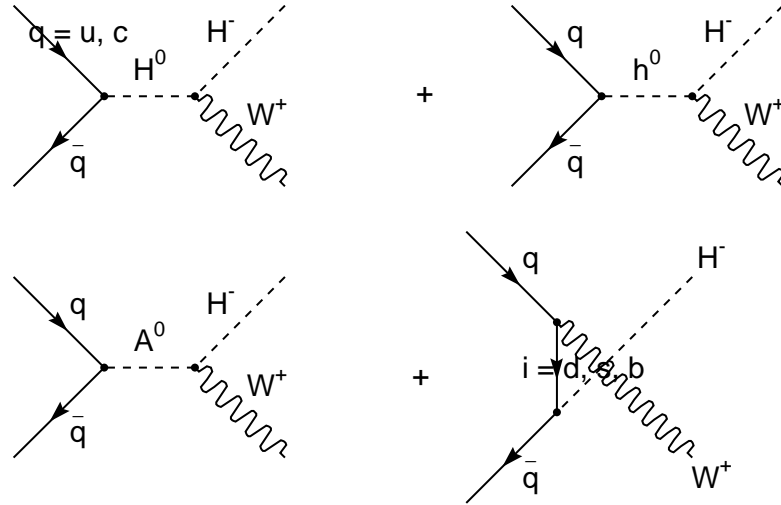


Figure 4.18: Feynman diagrams corresponding to the process $(q\bar{q} \rightarrow H^- W^+)$ for $q = u, c$.

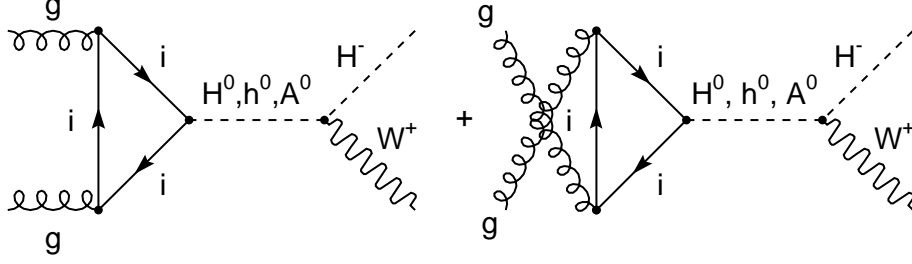


Figure 4.19: Triangle diagrams corresponding to the process $gg \rightarrow H^- W^+$. $i = b, t$.

4.8.2 $gg \rightarrow H^- W^+$ interaction

The differential cross section corresponding to the sum of the triangle diagrams in Figure 4.19 is given by:

$$\begin{aligned}
 \frac{d\sigma_{\Delta}}{d\hat{t}} (gg \rightarrow H^- W^+) &= \frac{\alpha_s^2 G_F^2}{4096\pi^3} \\
 &\times \Lambda(\hat{s}, m_H^2, m_W^2) \left\{ \left| \sum_{i=b,t} \left[\hat{C}_{Hi} (2\tau_i + \tau_i(\tau_i - 1) f(\tau_i)) \right] \right|^2 \right. \\
 &\left. + \frac{1}{2} \left| \sum_{i=b,t} \hat{C}_{Ai} \tau_i f(\tau_i) \right|^2 \right\}
 \end{aligned} \tag{4.63}$$

where

$$\tau_i = \frac{4m_i^2}{\hat{s}} \tag{4.64}$$

and

$$f(\tau_i) = \begin{cases} -2 \left[\arcsin(\tau_i^{-1/2}) \right]^2 & \text{if } \tau_i > 1 \\ \frac{1}{2} \left[\ln \left(\frac{1+(1-\tau_i)^{1/2}}{1-(1-\tau_i)^{1/2}} \right) - i\pi \right]^2 & \text{if } \tau_i \leq 1 \end{cases} \tag{4.65}$$

Due to charge-conjugation invariance

$$\frac{d\sigma_{\Delta}}{d\hat{t}} (gg \rightarrow H^- W^+) = \frac{d\sigma_{\Delta}}{d\hat{t}} (gg \rightarrow H^+ W^-). \tag{4.66}$$

Equations (4.55), (4.58) and (4.63) are in agreement with the differential cross sections calculated in reference [11]. In this reference, the differential

cross section corresponding to the sum of the box diagrams of Figures 4.20 and 4.21, also has been calculated with the aid of the computer packages FEYNARTS, FEYNALC and FF. According to the analysis presented in [11], the dominant subprocesses of $W^\pm H^\mp$ associated production are $b\bar{b} \rightarrow W^\pm H^\mp$ at the tree level and $gg \rightarrow W^\pm H^\mp$ at one loop.

4.8.3 Differential cross section $p\bar{p} \rightarrow H^\mp W^\pm X$

The differential cross section corresponding to the channel $p\bar{p} \rightarrow H^\mp W^\pm X$ is:

$$\begin{aligned} \frac{d^2\sigma}{dyd(p_T)^2}(p\bar{p} \rightarrow H^\mp W^\pm X) &= \sum_f \int_{x_{amin}}^1 dx_a f_f(x_a, m_a^2) f_f(x_b, m_b^2) \\ &\times \frac{x_b \hat{s}}{(m_H^2 - \hat{u})} \frac{d\sigma}{d\hat{t}}(f\bar{f} \rightarrow H^\mp W^\pm) \end{aligned} \quad (4.67)$$

where f is q or g ,

$$x_{amin} = \frac{\sqrt{s}m_T e^y + m_H^2 - m_W^2}{s - \sqrt{s}m_T e^{-y}}, \quad (4.68)$$

$$m_T = (m_W^2 + p_T^2)^{\frac{1}{2}}, \quad (4.69)$$

$$x_b = \frac{x_a \sqrt{s}m_T e^{-y} + m_H^2 - m_W^2}{x_a s - \sqrt{s}m_T e^y}, \quad (4.70)$$

$$\hat{s} = x_a x_b s, \quad (4.71)$$

$$p_T^2 = \frac{\Lambda(\hat{s}, m_H^2, m_W^2) \sin^2 \theta}{4\hat{s}}, \quad (4.72)$$

$$\hat{u} = \frac{1}{2} (m_H^2 + m_W^2 - \hat{s} - \cos \theta \Lambda^{1/2}(\hat{s}, m_H^2, m_W^2)), \quad (4.73)$$

$$\hat{t} = \frac{1}{2} (m_H^2 + m_W^2 - \hat{s} + \cos \theta \Lambda^{1/2}(\hat{s}, m_H^2, m_W^2)), \quad (4.74)$$

$$\hat{u}\hat{t} = m_H^2 m_W^2 + \hat{s} p_T^2, \quad (4.75)$$

and

$$\cos \theta = \left(1 - \frac{4\hat{s}p_T^2}{\Lambda^{1/2}(\hat{s}, m_H^2, m_W^2)} \right)^{1/2} \quad (4.76)$$

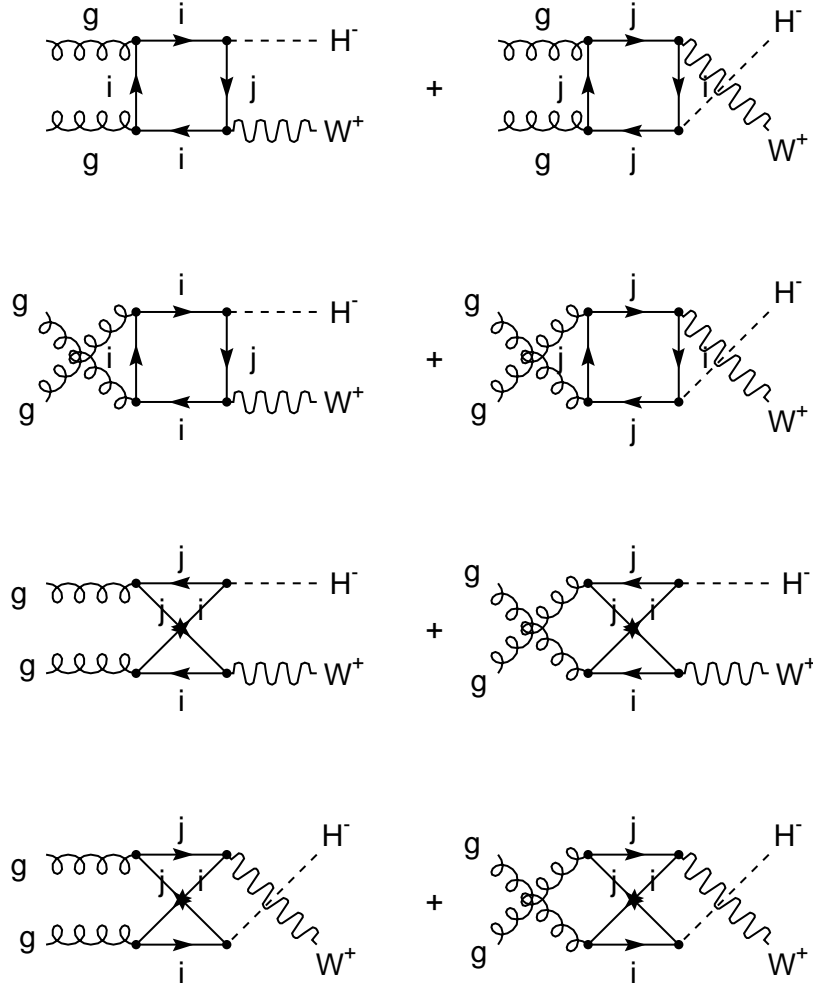


Figure 4.20: Box diagrams corresponding to the process $gg \rightarrow H^- W^+$. $i = d, s, b$; $j = u, c, t$. Continued in Figure 4.21.

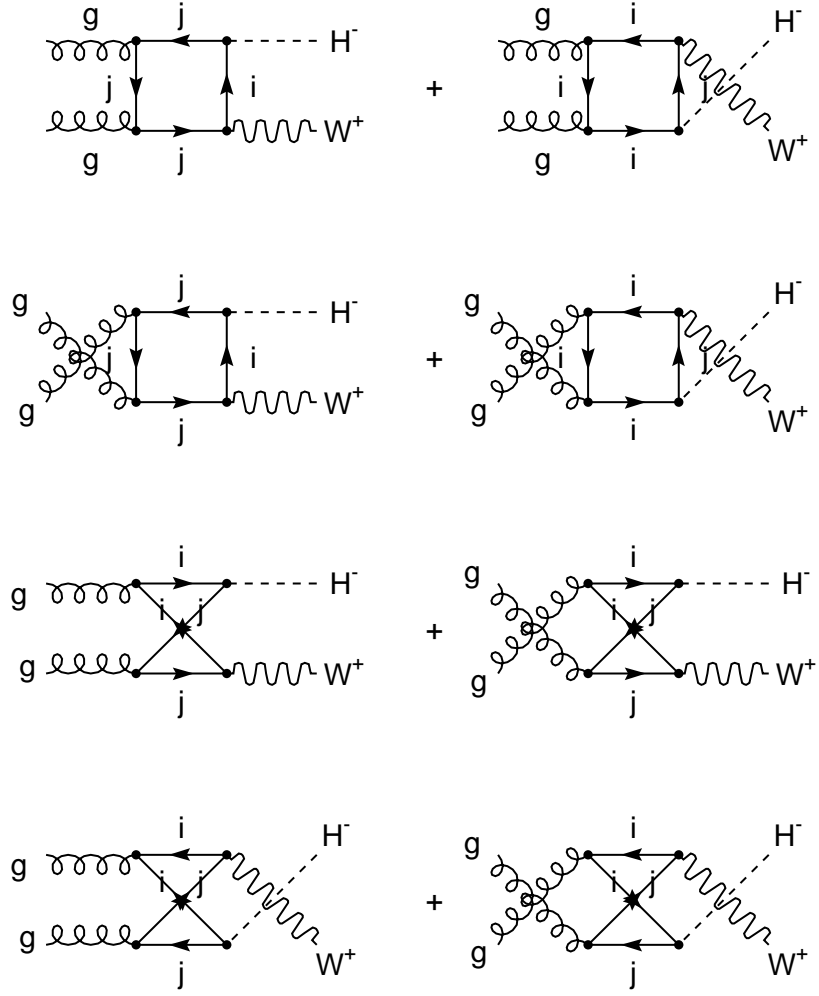


Figure 4.21: Continued from Figure 4.20.

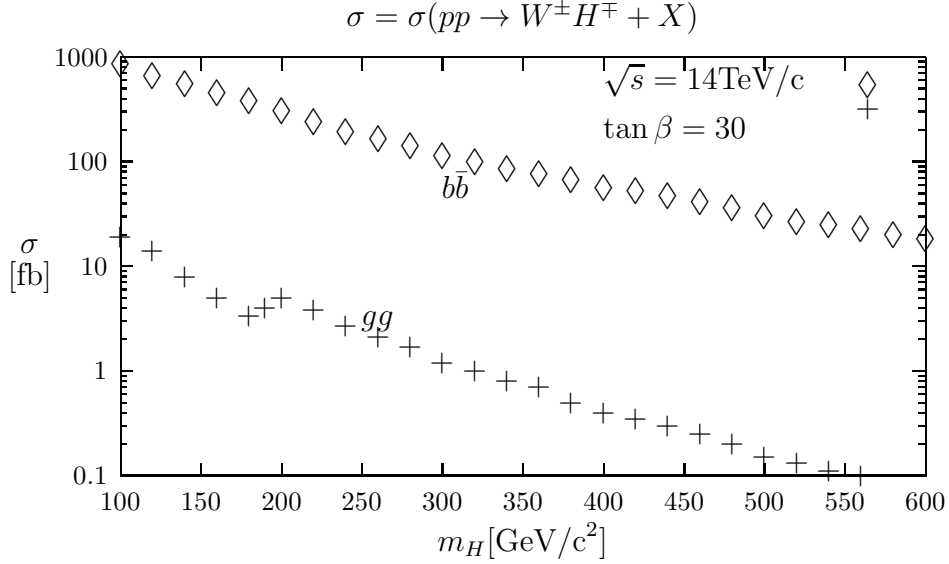


Figure 4.22: Total cross section for the process $pp \rightarrow W^\pm H^\mp + X$ as a function of m_H via $b\bar{b}$ annihilation and gg fusion at LHC energies ($\sqrt{s} = 14\text{TeV}/c$) for $\tan\beta = 30$. Taken from [11].

y is the rapidity of W^\pm , θ is the angle of dispersion in the center of mass system, p_T is the transverse momentum of W^\pm , f_f are the unpolarized parton distribution functions for quarks (antiquarks) or gluons. Finally, m_a^2 or m_b^2 represent the factorization scale.

A similar expression is valid for the reaction $pp \rightarrow H^\mp W^\pm + X$.

In Figure 4.22 (taken from reference [11]) the total cross section σ of $pp \rightarrow W^\pm H^\mp + X$ via $b\bar{b}$ annihilation and gg fusion is plotted as a function of m_H at LHC energies ($\sqrt{s} = 14\text{TeV}/c$) for $\tan\beta = 30$. Other contributions are negligible.

In Figure 4.23 (taken from reference [11]) the total cross section σ of $p\bar{p} \rightarrow W^\pm H^\mp + X$ via $b\bar{b}$ annihilation and gg fusion is plotted as a function of m_H at the Tevatron energy ($\sqrt{s} = 2\text{TeV}/c$) for $\tan\beta = 30$. The contributions of the other partons are negligible.

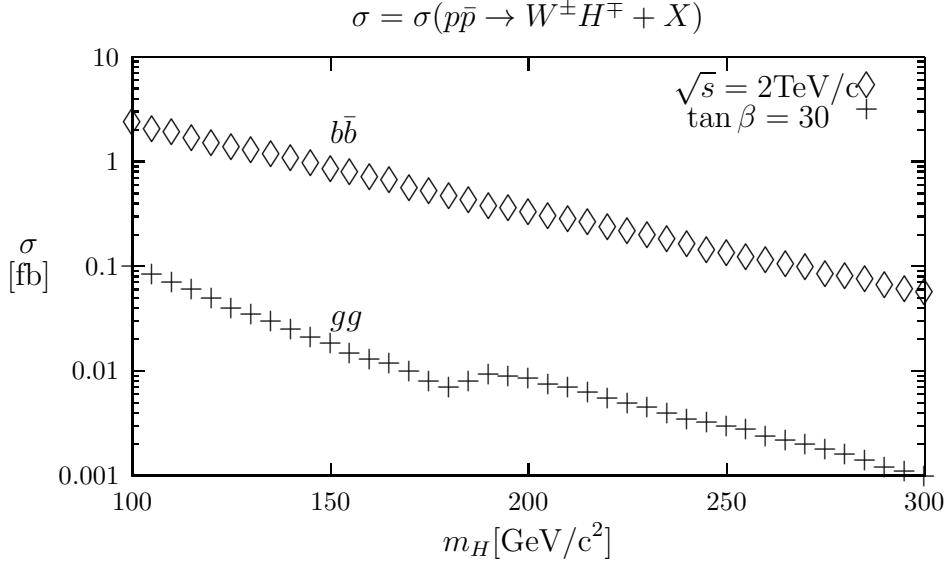


Figure 4.23: Total cross section for the process $p\bar{p} \rightarrow W^\pm H^\mp + X$ as a function of m_H via $b\bar{b}$ annihilation and gg fusion at the Tevatron energy ($\sqrt{s} = 2\text{TeV}/c$) for $\tan\beta = 30$. Taken from [11].

4.9 Comparison between $\mu^-\mu^+ \rightarrow H^\mp W^\pm$ and $p\bar{p}, pp \rightarrow H^\mp W^\pm X$ for large values of $\tan\beta$

Let us compare the channel $\mu^-\mu^+ \rightarrow H^\mp W^\pm$ at $\sqrt{s} = 500\text{GeV}/c$ with the processes $p\bar{p}, pp \rightarrow H^\mp W^\pm X$ at the Tevatron energy ($\sqrt{s} = 2\text{TeV}/c$) and LHC energies ($\sqrt{s} = 14\text{TeV}/c$) respectively for large values of $\tan\beta$ (for example $\tan\beta = 30$).

At the FNAL energy (Figure 4.24), we have: $\sigma(\mu^-\mu^+ \rightarrow H^\mp W^\pm) > \sigma(p\bar{p} \rightarrow W^\pm H^\mp X)$ for $\tan\beta = 30$.

At LHC energies (Figure 4.25), we have: $\sigma(pp \rightarrow W^\pm H^\mp X) > \sigma(\mu^-\mu^+ \rightarrow H^\mp W^\pm)$ for $\tan\beta = 30$.

According to Figure 4.12, $\sigma(\mu^-\mu^+ \rightarrow H^\mp W^\pm) \gtrsim 5\text{fb}$ for $\tan\beta \geq 20$ in the mass interval $100 \leq m_H \leq 400[\text{GeV}/c^2]$, which would be an observable number of H^\pm for luminosities $> 50\text{fb}^{-1}$. In the mass region of interest shown in the figures, the dominant decay mode of H^\pm is $H^+ \rightarrow t\bar{b}$ or $H^- \rightarrow \bar{t}b$. So the main background would be from $t\bar{t}$ production. Reference [4] shows that such a background overwhelms the charged Higgs boson signal in $pp \rightarrow W^\pm H^\mp X$ at the LHC. In fact, in Section 4.7 we have shown that $\sigma(\mu^-\mu^+ \rightarrow t\bar{t}) \approx 495\text{fb}$ for $\sqrt{s} = 500\text{GeV}/c$. In the LHC the background due to $t\bar{t}$

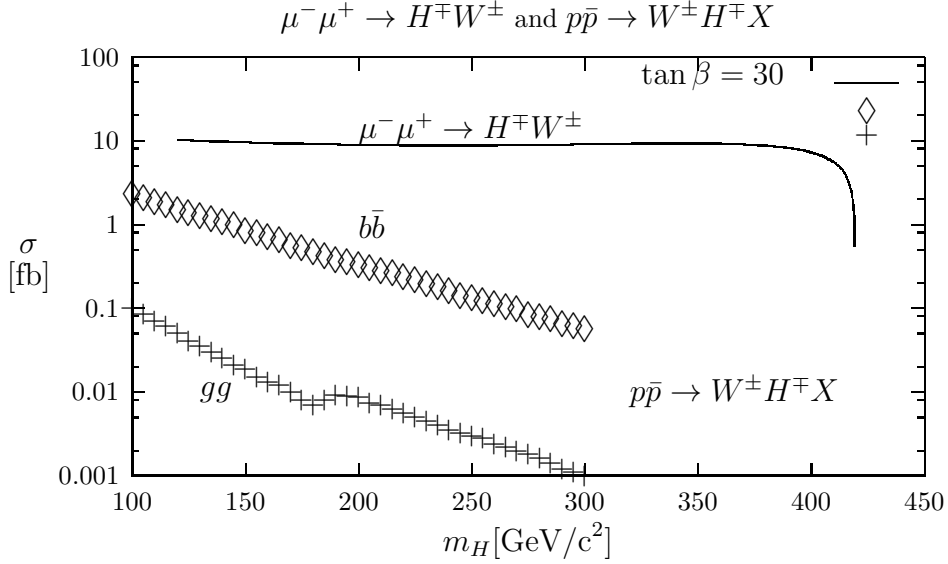


Figure 4.24: Total cross section for the processes $\mu^- \mu^+ \rightarrow H^\mp W^\pm$ and $p\bar{p} \rightarrow W^\pm H^\mp X$ (via $b\bar{b}$ annihilation and gg fusion) as a function of m_H at $\sqrt{s} = 500\text{GeV}/c$ and $\sqrt{s} = 2\text{TeV}/c$, respectively, for $\tan\beta = 30$. Taken partially from [11].

production is of order [4] 800 pb (three orders of magnitude larger than at a muon collider with $\sqrt{s} = 500\text{GeV}/c$). At the FNAL energy ($\sqrt{s} = 2\text{TeV}/c$) something similar happens because $\sigma(p\bar{p} \rightarrow t\bar{t}) = 5.5\text{pb}$ [12].

In the muon collider, the signal of the charged Higgs boson is not overwhelmed.

Then, for large values of $\tan\beta$, the process $\mu^- \mu^+ \rightarrow H^\mp W^\pm$ is a very attractive channel for the search of H^\pm at a $\mu^- \mu^+$ collider.

4.10 Conclusions

The discovery of the Standard Model Higgs is one of the principal goals of experimental and theoretical particle physicists. This is because the Higgs mechanism is a cornerstone of the Standard Model. The search for the Standard Model Higgs will also constrain or discover particles of the Two Higgs Doublet Model of type II.

In this paper we have discussed the masses of the Higgs particles in the Two Higgs Doublet Model of type II, and considered the influence of the radiative corrections on these masses. In the absence of radiative corrections,

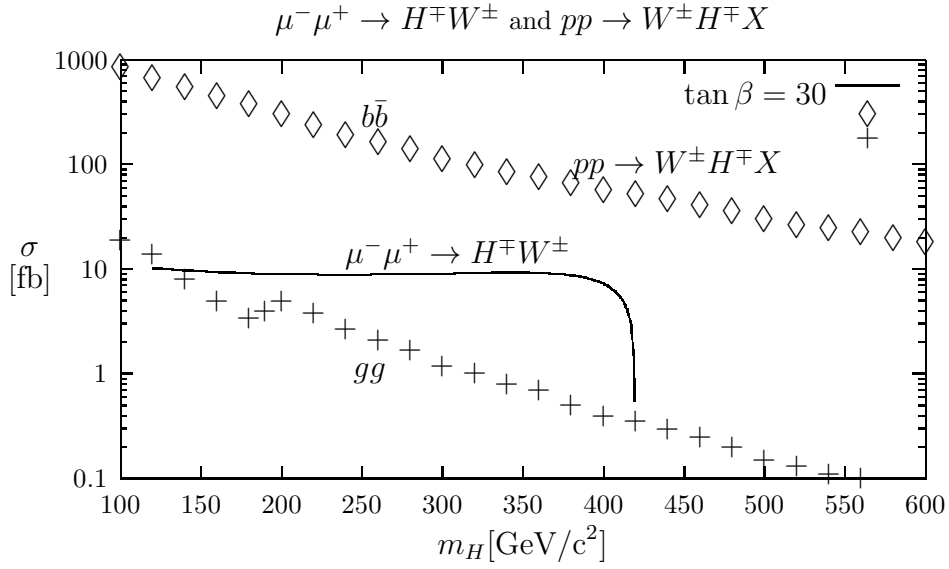


Figure 4.25: Total cross section for the processes $\mu^- \mu^+ \rightarrow H^\mp W^\pm$ and $pp \rightarrow W^\pm H^\mp + X$ (via $b\bar{b}$ annihilation and gg fusion) as a function of m_H at $\sqrt{s} = 500 \text{ GeV}/c$ and $\sqrt{s} = 14 \text{ TeV}/c$, respectively, for $\tan \beta = 30$. Taken partially from [11].

the Higgs boson h^0 obeys the bound $m_{h^0} \leq m_Z$. This bound practically has been excluded by the present limits on m_{h^0} obtained by LEP and CDF [6]. However, when the radiative corrections are taken into account, m_{h^0} increases as the value of m_A increases. As a result, we have a new bound: $m_{h^0} \leq 128.062 \text{ GeV}/c^2$ taking M_{sb} (sbottom mass) and M_{st} (stop mass) of order $1 \text{ TeV}/c^2$.

Considering the radiative corrections of the masses, we have calculated Higgs production cross sections at a muon collider in the Two Higgs Doublet Model of type II. The most interesting production channels are $\mu^- \mu^+ \rightarrow h^0 Z^0, H^0 Z^0, H^- H^+, A^0 Z^0$ and $H^\mp W^\pm$. In the first two channels the radiative corrections of the masses play an important role, which is not true for the other channels. In the reaction $\mu^- \mu^+ \rightarrow h^0 Z^0$, the total cross section becomes important in the mass interval $118 \leq m_{h^0} \leq 128 [\text{GeV}/c^2]$.

The process $\mu^- \mu^+ \rightarrow A^0 Z^0$, would provide an alternative way for searching the A^0 looking for peaks in the $b\bar{b}$ distribution. Another interesting channel could be $\mu^- \mu^+ \rightarrow A^0 h^0$. However, this is highly suppressed for $m_A \geq 200 \text{ GeV}/c^2$ because the total cross section is proportional to the factor

$$\cos^2(\beta - \alpha) = \frac{(1 + \tan \beta \tan \alpha)^2}{(1 + \tan^2 \beta)(1 + \tan^2 \alpha)}$$

(see the Feynman rules given in [9]). This factor decreases as the mass of the A^0 increases.

The most attractive channel is $\mu^- \mu^+ \rightarrow H^\mp W^\pm$, see Figures 4.24 and 4.25. In this reaction $\sigma(\mu^- \mu^+ \rightarrow H^\mp W^\pm) \gtrsim 5 \text{ fb}$ for $\tan \beta \geq 20$ in the mass interval $100 \leq m_H \leq 400 [\text{GeV}/c^2]$, which would give an observable number of H^\pm for luminosities $> 50 \text{ fb}^{-1}$ at $\sqrt{s} = 500 \text{ GeV}/c$.

Because the main background in a hadron collider in the reactions $p\bar{p} \rightarrow W^\pm H^\mp X$ (Tevatron energy) or $pp \rightarrow W^\pm H^\mp X$ (LHC energies) comes from $t\bar{t}$ production, the charged Higgs boson signal would be overwhelmed by such a background. In a muon collider with $\sqrt{s} = 500 \text{ GeV}/c$, the signal of the H^\pm is not overwhelmed. This means, that for large values of $\tan \beta$, the channel $\mu^- \mu^+ \rightarrow H^\mp W^\pm$ is a very attractive channel for the search of charged Higgs bosons at a $\mu^- \mu^+$ collider.

Acknowledgment

I would like to thank Bruce Hoeneisen for the critical reading of this manuscript.

Bibliography

- [1] Bruce Hoeneisen, Serie de Documentos USFQ **26**, Universidad San Francisco de Quito, Ecuador (2001).
- [2] J. Gunion, hep-ph/9802258; V. Barger, hep-ph/9803480.
- [3] A. G. Akeroyd, A. Arhrib, C. Dove, Phys. Rev. D **61**, 071702 (2000).
- [4] Stefano Moretti, Kosuke Odagiri, Phys. Rev. D **59**, 055008 (1999).
- [5] Vernon Barger and Roger Phillips, Collider Physics (Addison Wesley, 1988); S. Dawson, J.F. Gunion, H.E. Haber and G. Kane, The Higgs Hunter's Guide (Addison Wesley, 1990).
- [6] Review of Particle Physics, K. Hagiwara et al., Phys. Rev. D **66**, 010001 (2002).
- [7] "The quantum theory of fields", Volume III, Supersymmetry, Steven Weinberg, Cambridge University Press (2000).
- [8] Zhou Fei et al., Phys. Rev. D **64**, 055005(2001).
- [9] C. Marín and B. Hoeneisen, hep-ph/0402061 v1 (2004).
- [10] C. Marín, Politécnica, **XVII** No. 1, p.79 (1992), Escuela Politécnica Nacional, Quito, Ecuador. DO Note Fermilab (1992).
- [11] A. A. Barrientos Bendezú and B. A. Kniehl, Phys. Rev. D **59**, 015009 (1998).
- [12] V. M. Abazov et al., Phys. Rev. Lett. **88**, 151803 (2002).

Appendix A

Functions S^{WW} , S^{HW} and S^{HH}

If $i \neq j$:

$$S^{WW}(x_W^i, x_W^j) = \frac{x_W^i + x_W^j - \frac{11}{4}x_W^i x_W^j}{(1 - x_W^i)(1 - x_W^j)} + \frac{1}{(x_W^i - x_W^j)} [G(x_W^i, x_W^j) - G(x_W^j, x_W^i)] \quad (\text{A.1})$$

where

$$G(x_W^i, x_W^j) = \frac{(x_W^i)^2 \ln(x_W^i)}{(1 - x_W^i)^2} \left[1 - 2x_W^j + \frac{1}{4}x_W^i x_W^j \right]. \quad (\text{A.2})$$

If $i = j$:

$$S^{WW}(x_W^i, x_W^i) = \frac{x_W^i}{(1 - x_W^i)^2} \left[3 - \frac{19}{4}x_W^i + \frac{1}{4}(x_W^i)^2 \right] + \frac{2x_W^i \ln(x_W^i)}{(1 - x_W^i)^2} \left[1 - \frac{3}{4} \frac{(x_W^i)^2}{(1 - x_W^i)} \right]. \quad (\text{A.3})$$

If $i \neq j$:

$$S^{HH}(x_H^i, x_H^j, x_H^W) = \frac{x_H^i x_H^j}{x_H^W} \left[\frac{J(x_H^i) - J(x_H^j)}{x_H^i - x_H^j} \right] \quad (\text{A.4})$$

with

$$J(x_H^i) = \frac{1}{(1 - x_H^i)} + \frac{(x_H^i)^2 \ln(x_H^i)}{(1 - x_H^i)^2}. \quad (\text{A.5})$$

If $i = j$:

$$S^{HH}(x_H^i, x_H^i, x_H^W) = \frac{(x_H^i)^2}{x_H^W} \left[\frac{1 - (x_H^i)^2 + 2x_H^i \ln(x_H^i)}{(1 - x_H^i)^3} \right]. \quad (\text{A.6})$$

For $i \neq j$:

$$\begin{aligned}
S^{HW} (x_W^i, x_W^j, x_H^i, x_H^j, x_H^W) &= \frac{x_H^i x_H^j}{(x_H^W - 1)(x_H^i - 1)(x_H^j - 1)} \left[1 - \frac{1}{8x_H^W} \right] \\
&+ \frac{x_H^i x_H^j x_H^W}{(x_H^W - 1)(x_H^i - x_H^W)(x_H^j - x_H^W)} \left[\frac{3}{4} \ln(x_H^W) - \frac{7}{8} \right] \\
&+ \frac{(x_H^i)^2 x_H^j}{(x_H^i - x_H^W)(x_H^i - x_H^j)(x_H^i - 1)} \left[\ln(x_H^i) \left(1 - \frac{1}{4} x_W^i \right) + \left(\frac{1}{8} x_W^i - 1 \right) \right] \\
&+ \frac{(x_H^j)^2 x_H^i}{(x_H^j - x_H^W)(x_H^j - x_H^i)(x_H^j - 1)} \\
&\times \left[\ln(x_H^j) \left(1 - \frac{1}{4} x_W^j \right) + \left(\frac{1}{8} x_W^j - 1 \right) \right]. \tag{A.7}
\end{aligned}$$

For $i = j$:

$$\begin{aligned}
S^{HW} (x_W^i, x_W^i, x_H^i, x_H^i, x_H^W) &= (x_H^i)^2 \left[\frac{\ln(x_H^i)}{(x_H^W - 1)(x_H^i - 1)^2} \left(1 - \frac{1}{4x_H^W} \right) \right. \\
&\left. - \frac{3}{4} \frac{x_H^W \ln(x_W^i)}{(x_H^W - 1)(x_H^i - x_H^W)^2} + \frac{1}{(x_H^i - 1)(x_H^i - x_H^W)} \left(1 - \frac{1}{4} x_W^i \right) \right] \tag{A.8}
\end{aligned}$$

Appendix B

Calculation of the box diagrams corresponding to charged Higgs contributions to $B^0 - \bar{B}^0$ mixing in the “Two Higgs Doublet Model of type II”

B.1 Invariant amplitude M^{HH}

In the unitary gauge the invariant amplitude corresponding to the box diagram (HH1) in Figure B.1 is:

$$\begin{aligned}
M_1^{HH} = & i \left(\frac{g}{2\sqrt{2}m_W} \right)^4 \sum_{i,j} \xi_i \xi_j \int \frac{d^4 K}{(2\pi)^4} \bar{v}(\bar{q}) \\
& \left[m_q \tan \beta (1 - \gamma^5) + m_j \cot \beta (1 + \gamma^5) \right] (\not{K} + m_j) \\
& \left[m_b \tan \beta (1 + \gamma^5) + m_j \cot \beta (1 - \gamma^5) \right] u(b) \\
& \cdot \bar{u}(q) \left[m_q \tan \beta (1 - \gamma^5) + m_i \cot \beta (1 + \gamma^5) \right] (\not{K} + m_i) \\
& \left[m_b \tan \beta (1 + \gamma^5) + m_i \cot \beta (1 - \gamma^5) \right] v(\bar{b}) \\
& \times \frac{1}{(K^2 - m_i^2)(K^2 - m_j^2)(K^2 - m_H^2)^2}.
\end{aligned} \tag{B.1}$$

where $\not{K} = \gamma^\mu K_\mu$ and $\xi_i = V_{ib} V_{iq}^*$ ($q = d$ or s and $i, j = u, c, t$). Here we have taken the approximation in which all external momenta are zero in the loop.

Using:

$$(1 + \gamma^5)(1 - \gamma^5) = 0, \quad \gamma^\mu \gamma^5 + \gamma^5 \gamma^\mu = 0, \quad \text{we obtain (in the limit } m_q \rightarrow 0)$$

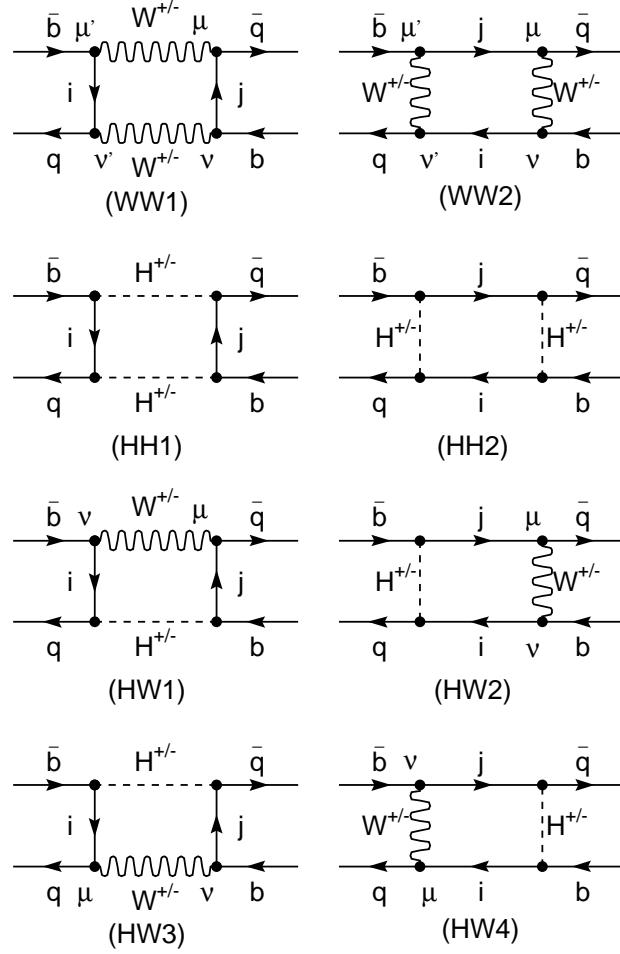


Figure B.1: Feynman diagrams corresponding to $B^0 \leftrightarrow \bar{B}^0$ mixing in the Two Higgs Doublet Model. $q = d$ or s and $i, j = u, c, t$. The diagrams on the right side interfere with a “-” sign.

$$\begin{aligned}
M_1^{HH} = & 4i \left(\frac{g}{2\sqrt{2}m_W} \right)^4 \sum_{i,j} \xi_i \xi_j \{ m_i^2 m_j^2 \cot^4 \beta \bar{v}(\bar{q}) \gamma^\alpha (1 - \gamma^5) u(b) \\
& \cdot \bar{u}(q) \gamma^\beta (1 - \gamma^5) v(\bar{b}) I_{\alpha\beta}^{HH}(i, j) + m_i^2 m_j^2 m_b^2 \bar{v}(\bar{q}) (1 + \gamma^5) u(b) \\
& \cdot \bar{u}(q) (1 + \gamma^5) v(\bar{b}) I^{HH}(i, j) + m_i^2 m_j^2 m_b \cot^2 \beta \bar{v}(\bar{q}) \\
& (\gamma^\alpha (1 - \gamma^5) u(b) \cdot \bar{u}(q) (1 + \gamma^5) + (1 + \gamma^5) u(b) \cdot \bar{u}(q) \gamma^\alpha (1 - \gamma^5)) \\
& v(\bar{b}) I_\alpha^{HH}(i, j) \} \tag{B.2}
\end{aligned}$$

where

$$I_{\alpha\beta}^{HH}(i, j) \equiv \int \frac{d^4 K}{(2\pi)^4} \frac{K_\alpha K_\beta}{(K^2 - m_H^2)^2 (K^2 - m_i^2) (K^2 - m_j^2)} \tag{B.3}$$

$$I_\alpha^{HH}(i, j) \equiv \int \frac{d^4 K}{(2\pi)^4} \frac{K_\alpha}{(K^2 - m_H^2)^2 (K^2 - m_i^2) (K^2 - m_j^2)} \tag{B.4}$$

$$I^{HH}(i, j) \equiv \int \frac{d^4 K}{(2\pi)^4} \frac{1}{(K^2 - m_H^2)^2 (K^2 - m_i^2) (K^2 - m_j^2)} \tag{B.5}$$

The integrals, $I_{\alpha\beta}^{HH}(i, j)$ and $I^{HH}(i, j)$, were calculated in detail in Appendix 2 of reference [1] (replacing m_H by m_W):

If $i \neq j$:

$$I_{\alpha\beta}^{HH}(i, j) = \frac{-i\pi^2 \eta_{\alpha\beta}}{4(2\pi)^4 m_H^2} \left[\frac{J(x_H^i) - J(x_H^j)}{x_H^i - x_H^j} \right] \tag{B.6}$$

where

$$\eta_{\alpha\beta} = \text{diag}(1, -1, -1, -1),$$

$x_H^i = \frac{m_i^2}{m_H^2}$ and $J(x_H^i)$ is given in Equation A.5.

If $i = j$:

$$I_{\alpha\beta}^{HH}(i, i) = \frac{-i\pi^2 \eta_{\alpha\beta}}{4(2\pi)^4 m_H^2} \left[\frac{1 - (x_H^i)^2 + 2x_H^i \ln(x_H^i)}{(1 - x_H^i)^3} \right]. \tag{B.7}$$

If $i \neq j$:

$$I^{HH}(i, j) = \frac{i\pi^2}{(2\pi)^4 m_H^4} \frac{1}{(1 - x_H^i) (1 - x_H^j)} [F(x_H^i, x_H^j) + F(x_H^j, x_H^i) - 1] \tag{B.8}$$

where

$$F(x_H^i, x_H^j) = -\frac{x_H^i \ln(x_H^i) (1 - x_H^j)}{(1 - x_H^i) (x_H^i - x_H^j)}. \quad (\text{B.9})$$

If $i = j$:

$$I^{HH}(i, i) = \frac{-i\pi^2}{(2\pi)^4 m_H^4} \frac{1}{(1 - x_H^i)^2} \left[2 + \frac{(1 + x_H^i)}{(1 - x_H^i)} \ln(x_H^i) \right]. \quad (\text{B.10})$$

The value of the second integral (see Appendix C) is:

For $i \neq j$ and $i = j$:

$$I_\alpha^{HH}(i, j) = 0. \quad (\text{B.11})$$

Neglecting the second term in (B.2) and because $\frac{G_F}{\sqrt{2}} = \frac{g^2}{8m_W^2}$, we have

$$M_1^{HH} = \frac{G_F^2 m_W^2}{32\pi^2} \cot^4 \beta \sum_{i,j} \xi_i \xi_j \bar{v}(\bar{q}) \gamma^\mu (1 - \gamma^5) u(b) \cdot \bar{u}(q) \gamma_\mu (1 - \gamma^5) v(\bar{b}) S^{HH}(x_H^i, x_H^j, x_H^W). \quad (\text{B.12})$$

$S^{HH}(x_H^i, x_H^j, x_H^W)$ for $i \neq j$ and $i = j$ are given in (A.4) and (A.6), respectively.

Note that:

$$\lim_{x_H^i \rightarrow 0} S^{HH}(x_H^i, x_H^j, x_H^W) = 0. \quad (\text{B.13})$$

In a similar way, we can show that the invariant amplitude corresponding to the diagram (HH2) in Figure B.1 is:

$$M_2^{HH} = \frac{G_F^2 m_W^2}{32\pi^2} \cot^4 \beta \sum_{i,j} \xi_i \xi_j \bar{v}(\bar{q}) \gamma^\mu (1 - \gamma^5) v(\bar{b}) \cdot \bar{u}(q) \gamma_\mu (1 - \gamma^5) u(b) S^{HH}(x_H^i, x_H^j, x_H^W). \quad (\text{B.14})$$

According to the Fierz Theorem [2], we can write

$$\begin{aligned} & \bar{v}(\bar{q}) \gamma^\mu (1 - \gamma^5) v(\bar{b}) \cdot \bar{u}(q) \gamma_\mu (1 - \gamma^5) u(b) \\ &= -\bar{v}(\bar{q}) \gamma^\mu (1 - \gamma^5) u(b) \cdot \bar{u}(q) \gamma_\mu (1 - \gamma^5) v(\bar{b}) \end{aligned} \quad (\text{B.15})$$

The total amplitude M^{HH} is then

$$M^{HH} = 2M_1^{HH}. \quad (\text{B.16})$$

Let's consider the amplitude:

$$\langle B^0 | M^{HH} | \bar{B}^0 \rangle = \frac{G_F^2 m_W^2}{4\pi^2} \cot^4 \beta \sum_{i,j} \xi_i \xi_j A S^{HH}(x_H^i, x_H^j, x_H^W) \quad (\text{B.17})$$

where

$$A \equiv \langle B^0 | \bar{v}_L(\bar{q}) \gamma^\mu u_L(b) \cdot \bar{u}_L(q) \gamma_\mu v_L(\bar{b}) | \bar{B}^0 \rangle,$$

$$\bar{v}_L(\bar{q}) \gamma^\mu = \bar{v}(\bar{q}) \gamma^\mu \frac{1}{2} (1 - \gamma^5),$$

$$v_L(\bar{b}) = \frac{1}{2} (1 - \gamma^5) v(\bar{b}),$$

$$\bar{u}_L(q) \gamma_\mu = \bar{u}(q) \gamma_\mu \frac{1}{2} (1 - \gamma^5),$$

$$u_L(b) = \frac{1}{2} (1 - \gamma^5) u(b),$$

For our model, ‘free particles inside the meson’ [1], we have

$$A = \frac{1}{16} \beta_B f_B^2 m_B \quad (\text{B.18})$$

Thus, one obtains

$$\langle B^0 | M^{HH} | \bar{B}^0 \rangle = \frac{\beta_B G_F^2 m_W^2 f_B^2 m_B}{64\pi^2} \cot^4 \beta \sum_{i,j} \xi_i \xi_j S^{HH}(x_H^i, x_H^j, x_H^W) \quad (\text{B.19})$$

B.2 Invariant amplitude M^{HW}

For the box diagram (HW1) of Figure B.1, the corresponding invariant amplitude is given by:

$$\begin{aligned} M_1^{HW} = & -i \left(\frac{g}{2\sqrt{2}} \right)^4 \frac{1}{m_W^2} \sum_{i,j} \xi_i \xi_j \int \frac{d^4 K}{(2\pi)^4} \bar{v}(\bar{q}) \gamma^\mu (1 - \gamma^5) \\ & (\not{K} + m_j) [m_b \tan \beta (1 + \gamma^5) + m_j \cot \beta (1 - \gamma^5)] u(b) \\ & \cdot \bar{u}(q) [m_q \tan \beta (1 - \gamma^5) + m_i \cot \beta (1 + \gamma^5)] \\ & (\not{K} + m_i) \gamma^\nu (1 - \gamma^5) v(\bar{b}) \left(\eta_{\mu\nu} - \frac{K_\mu K_\nu}{m_W^2} \right) \\ & \times \frac{1}{(K^2 - m_W^2) (K^2 - m_H^2) (K^2 - m_i^2) (K^2 - m_j^2)} \end{aligned} \quad (\text{B.20})$$

Using:

$\gamma^\mu \gamma^5 + \gamma^5 \gamma^\mu = 0$, $(1 + \gamma^5)^2 = 2(1 + \gamma^5)$, $(1 - \gamma^5)^2 = 2(1 - \gamma^5)$,
 $\not{K} \not{K} = K^2$, and taking the limit in which $m_q \rightarrow 0$, we can write the invariant amplitude as

$$\begin{aligned}
M_1^{HW} = & -4i \left(\frac{g}{2\sqrt{2}} \right)^4 \frac{1}{m_W^2} \sum_{i,j} \xi_i \xi_j \{ m_i^2 m_j^2 \cot^2 \beta \bar{v}(\bar{q}) \gamma^\alpha (1 - \gamma^5) u(b) \\
& \cdot \bar{u}(q) \left(\gamma_\alpha I^{HW}(i, j) - \frac{1}{m_W^2} \gamma^\beta I_{\alpha\beta}^{HW}(i, j) \right) (1 - \gamma^5) v(\bar{b}) \\
& + m_i^2 m_b \bar{v}(\bar{q}) \gamma^\mu (1 - \gamma^5) \gamma^\alpha u(b) \cdot \bar{u}(q) \gamma_\mu (1 - \gamma^5) v(\bar{b}) (I_\alpha^{HW})^{(1)}(i, j) \\
& - \frac{1}{m_W^2} m_i^2 m_b \bar{v}(\bar{q}) (1 + \gamma^5) u(b) \\
& \cdot \bar{u}(q) \gamma^\alpha (1 - \gamma^5) v(\bar{b}) (I_\alpha^{HW})^{(2)}(i, j) \}
\end{aligned} \tag{B.21}$$

where

$$I^{HW}(i, j) \equiv \int \frac{d^4 K}{(2\pi)^4} \frac{1}{(K^2 - m_W^2)(K^2 - m_H^2)(K^2 - m_i^2)(K^2 - m_j^2)} \tag{B.22}$$

$$I_{\alpha\beta}^{HW}(i, j) \equiv \int \frac{d^4 K}{(2\pi)^4} \frac{K_\alpha K_\beta}{(K^2 - m_W^2)(K^2 - m_H^2)(K^2 - m_i^2)(K^2 - m_j^2)} \tag{B.23}$$

$$(I_\alpha^{HW})^{(1)}(i, j) \equiv \int \frac{d^4 K}{(2\pi)^4} \frac{K_\alpha}{(K^2 - m_W^2)(K^2 - m_H^2)(K^2 - m_i^2)(K^2 - m_j^2)} \tag{B.24}$$

$$(I_\alpha^{HW})^{(2)}(i, j) \equiv \int \frac{d^4 K}{(2\pi)^4} \frac{K^2 K_\alpha}{(K^2 - m_W^2)(K^2 - m_H^2)(K^2 - m_i^2)(K^2 - m_j^2)} \tag{B.25}$$

After momentum integration (see Appendix C), we get

If $i \neq j$:

$$\begin{aligned}
I^{HW}(i, j) &= \frac{-i\pi^2}{(2\pi)^4} \frac{1}{m_H^4} \frac{1}{(x_H^W - 1)} \\
&\times \left[\frac{x_H^W (\ln(x_H^W) - 1)}{(x_H^i - x_H^W)(x_H^j - x_H^W)} + \frac{1}{(x_H^i - 1)(x_H^j - 1)} \right. \\
&+ \frac{(x_H^W - 1)}{(x_H^j - x_H^W)(x_H^j - x_H^i)(x_H^j - 1)} x_H^j (\ln(x_H^j) - 1) \\
&\left. + \frac{(x_H^W - 1)}{(x_H^i - x_H^W)(x_H^i - x_H^j)(x_H^i - 1)} x_H^i (\ln(x_H^i) - 1) \right] \quad (B.26)
\end{aligned}$$

If $i = j$:

$$\begin{aligned}
I^{HW}(i, i) &= \frac{-i\pi^2}{(2\pi)^4} \frac{1}{m_H^4} \frac{1}{(x_H^W - 1)} \left[\frac{x_H^W (\ln(x_H^W) - 1)}{(x_H^i - x_H^W)^2} + \frac{1}{(x_H^i - 1)^2} \right. \\
&+ \frac{(x_H^W - 1) \left[\ln(x_H^i) (x_H^W - (x_H^i)^2) + x_H^i (2x_H^i - x_H^W - 1) \right]}{(x_H^i - x_H^W)^2 (x_H^i - 1)^2} \left. \right] \quad (B.27)
\end{aligned}$$

If $i \neq j$:

$$\begin{aligned}
I_{\alpha\beta}^{HW}(i, j) &= \frac{-i\pi^2}{8(2\pi)^4} \eta_{\alpha\beta} \frac{1}{m_H^2} \frac{1}{(x_H^W - 1)} \\
&\times \left[-\frac{(x_H^W - 1)(x_H^i)^2 (2\ln(x_H^i) - 1)}{(x_H^j - x_H^i)(x_H^i - 1)(x_H^i - x_H^W)} \right. \\
&- \frac{(x_H^W - 1)(x_H^j)^2 (2\ln(x_H^j) - 1)}{(x_H^i - x_H^j)(x_H^j - 1)(x_H^j - x_H^W)} \\
&\left. + \frac{1}{(x_H^i - 1)(x_H^j - 1)} + \frac{(x_H^W)^2 (2\ln(x_H^W) - 1)}{(x_H^i - x_H^W)(x_H^j - x_H^W)} \right] \quad (B.28)
\end{aligned}$$

If $i = j$:

$$\begin{aligned}
I_{\alpha\beta}^{HW}(i, i) &= \frac{-i\pi^2}{8(2\pi)^4} \eta_{\alpha\beta} \frac{1}{m_H^2} \frac{1}{(x_H^W - 1)} \left[\frac{(x_H^W - 1)(x_H^i)}{(x_H^i - 1)^2 (x_H^i - x_H^W)^2} \right. \\
&\times [x_H^i (2x_H^i - x_H^W - 1) - 2\ln(x_H^i) (x_H^i x_H^W + x_H^i - 2x_H^W)] \\
&\left. + \frac{1}{(x_H^i - 1)^2} + \frac{(x_H^W)^2 (2\ln(x_H^W) - 1)}{(x_H^i - x_H^W)^2} \right] \quad (B.29)
\end{aligned}$$

For $i \neq j$ and $i = j$:

$$(I_\alpha^{HW})^{(1)}(i, j) = 0 \quad (\text{B.30})$$

For $i \neq j$ and $i = j$:

$$(I_\alpha^{HW})^{(2)}(i, j) = 0 \quad (\text{B.31})$$

Introducing these integrals in B.21, we find

$$M_1^{HW} = -\frac{G_F^2 m_W^2 \cot^2 \beta}{8\pi^2} \sum_{i,j} \xi_i \xi_j \bar{v}(\bar{q}) \gamma^\mu (1 - \gamma^5) u(b) \cdot \bar{u}(q) \gamma_\mu (1 - \gamma^5) v(\bar{b}) S^{HW}(x_W^i, x_W^j, x_H^i, x_H^j, x_H^W) \quad (\text{B.32})$$

where $S^{HW}(x_W^i, x_W^j, x_H^i, x_H^j, x_H^W)$ is given in (A.7) and (A.8). Note that

$$\lim_{x_H^i \rightarrow 0} S^{HW}(x_W^i, x_W^i, x_H^i, x_H^i, x_H^W) = 0. \quad (\text{B.33})$$

We have another three diagrams. In the limit $m_q \rightarrow 0$, the Fierz transformation shows that all four diagrams contribute equally and then, the total invariant amplitude is:

$$M^{HW} = 4M_1^{HW} \quad (\text{B.34})$$

Therefore, as in (B.19), the matrix element $\langle B^0 | M^{HW} | \bar{B}^0 \rangle$ can be expressed as

$$\langle B^0 | M^{HW} | \bar{B}^0 \rangle = -\frac{\beta_B G_F^2 m_W^2 f_B^2 m_B}{8\pi^2} \cot^2 \beta \sum_{i,j} \xi_i \xi_j S^{HW}(x_W^i, x_W^j, x_H^i, x_H^j, x_H^W). \quad (\text{B.35})$$

B.3 Invariant amplitude M^{WW}

The calculation of the invariant amplitude for the box diagrams (WW) in Figure B.1, was performed in detail in reference [1]:

$$M^{WW} = \frac{G_F^2 m_W^2}{\pi^2} \sum_{i,j} \xi_i \xi_j \bar{v}_L(\bar{q}) \gamma^\mu u_L(b) \cdot \bar{u}_L(q) \gamma_\mu v_L(\bar{b}) S^{WW}(x_W^i, x_W^j) \quad (\text{B.36})$$

Therefore

$$\langle B^0 | M^{WW} | \bar{B}^0 \rangle = \frac{\beta_B G_F^2 m_W^2 f_B^2 m_B}{16\pi^2} \sum_{i,j} \xi_i \xi_j S^{WW}(x_W^i, x_W^j). \quad (\text{B.37})$$

B.4 Mass difference Δm_B

The mass difference between the two states that diagonalize the hamiltonian is:

$$\begin{aligned} \Delta m_B &= m_{B_H} - m_{B_L} = 2|M_{12}| = 2|\langle B^0 | M^{HH} + M^{HW} + M^{WW} | \bar{B}^0 \rangle| \\ &= 2|\langle B^0 | M^{HH} | \bar{B}^0 \rangle + \langle B^0 | M^{HW} | \bar{B}^0 \rangle + \langle B^0 | M^{WW} | \bar{B}^0 \rangle| \end{aligned} \quad (\text{B.38})$$

where H and L stand for Heavy and Light, respectively.

Introducing (B.19), (B.35), and (B.37) in Equation (B.38) (after correcting by a color factor 4/3), we arrive to Equation (2.4).

Appendix C

Integrals

C.1 $I_\alpha^{HH}(i, j)$

From the identity:

$$\frac{1}{abcd} = 3! \int_0^1 \int_0^1 \int_0^1 \frac{x^2 y dx dy dz}{[(1-x)d + x(1-y)c + xy(1-z)b + xyz a]^4} \quad (C.1)$$

where $a, b, c, d \neq 0$; and setting:

$a = (K^2 - m_H^2)$, $b = (K^2 - m_H^2)$, $c = (K^2 - m_i^2)$, $d = (K^2 - m_j^2)$,
it is found that

$$\begin{aligned} & \frac{1}{(K^2 - m_H^2)^2 (K^2 - m_i^2) (K^2 - m_j^2)} \\ &= 3! \int_0^1 \int_0^1 \int_0^1 \frac{x^2 y dx dy dz}{[K^2 + x(m_j^2 - m_i^2) + xy(m_i^2 - m_H^2) - m_j^2]^4} \quad (C.2) \end{aligned}$$

Introducing the last Equation in (B.4), we obtain

$$I_\alpha^{HH}(i, j) = 3! \int_0^1 \int_0^1 \int_0^1 dx dy dz x^2 y \int \frac{d^4 K}{(2\pi)^4} \frac{K_\alpha}{[K^2 + M^2]^4} \quad (C.3)$$

where

$$M^2 = x(m_j^2 - m_i^2) + xy(m_i^2 - m_H^2) - m_j^2 \quad (C.4)$$

Then using [3]

$$I_\mu = \int \frac{d^d K}{(2\pi)^d} \frac{K_\mu}{(K^2 + 2P \cdot K + M^2 + i\epsilon)^\alpha} = -P_\mu I_0 \quad (C.5)$$

$$\begin{aligned}
I_0 &= \int \frac{d^d K}{(2\pi)^d} \frac{1}{(K^2 + 2P \cdot K + M^2 + i\epsilon)^\alpha} \\
&= \frac{i(-\pi)^{d/2} \Gamma(\alpha - \frac{d}{2})}{(2\pi)^d \Gamma(\alpha)} \frac{1}{(M^2 - P^2 + i\epsilon)^{\alpha - \frac{d}{2}}}
\end{aligned} \tag{C.6}$$

With $n = 4$, $\alpha = 4$ and $P_\mu = 0$, we get

$$I_\alpha^{HH}(i, j) = 0. \tag{C.7}$$

C.2 $(I_\alpha^{HW})^{(1)}(i, j)$

Again, using the identity (C.1) for:

$a = (K^2 - m_H^2)$, $b = (K^2 - m_W^2)$, $c = (K^2 - m_i^2)$, $d = (K^2 - m_j^2)$,
we obtain the same integral (C.7), but with

$$M^2 = x(m_j^2 - m_i^2) + xy(m_i^2 - m_W^2) + xyz(m_W^2 - m_H^2) - m_j^2 \tag{C.8}$$

Once more, (C.5) implies

$$(I_\alpha^{HW})^{(1)}(i, j) = 0. \tag{C.9}$$

C.3 $(I_\alpha^{HW})^{(2)}(i, j)$

On account of (C.1), we can write

$$(I_\alpha^{HW})^{(2)}(i, j) = 3! \gamma^\mu \gamma^\nu \int_0^1 \int_0^1 \int_0^1 dx dy dz x^2 y \int \frac{d^4 K}{(2\pi)^4} \frac{K_\mu K_\nu K_\alpha}{[K^2 + M^2]^4} \tag{C.10}$$

then, from [3]

$$\begin{aligned}
I_{\mu\nu\alpha} &= \int \frac{d^d K}{(2\pi)^d} \frac{K_\mu K_\nu K_\alpha}{[K^2 + 2P \cdot K + M^2 + i\epsilon]^\alpha} \\
&= -I_0 \left[P_\mu P_\nu P_\alpha + \frac{(M^2 - P^2)}{2(\alpha - \frac{d}{2} - 1)} (\eta_{\mu\nu} P_\alpha + \eta_{\mu\alpha} P_\nu + \eta_{\nu\alpha} P_\mu) \right]
\end{aligned} \tag{C.11}$$

With $n = 4$, $\alpha = 4$ and $P_\mu = 0$, we get

$$(I_\alpha^{HW})^{(2)}(i, j) = 0. \tag{C.12}$$

C.4 $I^{HW}(i, j)$

Equation (B.22) can be written as:

$$I^{HW}(i, j) = 3! \int_0^1 \int_0^1 \int_0^1 dx dy dz x^2 y \int \frac{d^4 K}{(2\pi)^4} \frac{1}{(K^2 + M^2)^4} \quad (C.13)$$

From (C.6), we have

$$\int \frac{d^4 K}{(2\pi)^4} \frac{1}{(K^2 + M^2)^4} = \frac{i\pi^2}{(2\pi)^4} \frac{1}{3! (M^2)^2} \quad (C.14)$$

and then

$$I^{HW}(i, j) = \frac{i\pi^2}{(2\pi)^4} \int_0^1 \int_0^1 \int_0^1 f(x, y, z) dx dy dz \quad (C.15)$$

where

$$f(x, y, z) = \frac{x^2 y}{[x(m_j^2 - m_i^2) + xy(m_i^2 - m_W^2) + xyz(m_W^2 - m_H^2) - m_j^2]^2} \quad (C.16)$$

Integrating (C.15), we obtain (B.26) and (B.27).

C.5 $I_{\alpha\beta}^{HW}(i, j)$

Equation (B.23) can be written as:

$$I_{\alpha\beta}^{HW}(i, j) = 3! \int_0^1 \int_0^1 \int_0^1 dx dy dz x^2 y \int \frac{d^4 K}{(2\pi)^4} \frac{K_\alpha K_\beta}{(K^2 + M^2)^4} \quad (C.17)$$

Using the integral [3]

$$\begin{aligned} I_{\alpha\beta} &= \int \frac{d^d K}{(2\pi)^d} \frac{K_\alpha K_\beta}{(K^2 + 2P \cdot K + M^2 + i\epsilon)^\alpha} \\ &= I_0 \left[P_\alpha P_\beta + \frac{1}{2} \eta_{\alpha\beta} (M^2 - P^2) \frac{1}{(\alpha - \frac{d}{2} - 1)} \right], \end{aligned} \quad (C.18)$$

we obtain

$$\int \frac{d^4 K}{(2\pi)^4} \frac{K_\alpha K_\beta}{(K^2 + M^2)^4} = \frac{i\pi^2}{2(2\pi)^4} \frac{1}{3! M^2} \eta_{\alpha\beta} \quad (C.19)$$

and therefore, (C.17) becomes

$$I_{\alpha\beta}^{HW}(i, j) = \frac{i\pi^2}{2(2\pi)^4} \eta_{\alpha\beta} \int_0^1 \int_0^1 \int_0^1 g(x, y, z) dx dy dz \quad (\text{C.20})$$

where

$$g(x, y, z) = \frac{x^2 y}{\left[x(m_j^2 - m_i^2) + xy(m_i^2 - m_W^2) + xyz(m_W^2 - m_H^2) - m_j^2 \right]} \quad (\text{C.21})$$

After some long, but trivial calculations, we arrive to Equations (B.28) and (B.29).

Appendix D

$A^0 \rightarrow Z^0 \gamma$ decay

As an example, we derive the expression for the width decay corresponding to the channel $A^0 \rightarrow Z^0 \gamma$. The Feynman diagrams are given in Figure D.1.

D.1 (a) $i = e^-, \mu^-, \tau^-, d, s, b$

In the unitary gauge, the invariant amplitude corresponding to the first Feynman diagram of Figure D.1 is:

$$M_{1a} = -\frac{g^2 e \tan \beta}{4m_W \cos \theta_W} \sum_{i=d,s,b,\dots} N_i Q_i m_i \int \frac{d^d K}{(2\pi)^d} (T) \times \frac{1}{(K^2 - m_i^2) [(K - P_2)^2 - m_i^2] [(K + P_1)^2 - m_i^2]} \epsilon_{1\mu}^* \epsilon_{2\nu}^* \mu^* \quad (D.1)$$

where

$$T = \text{Trace} [\gamma^\mu (g_V^i - g_A^i \gamma^5) (\not{K} + m_i) \gamma^\nu (\not{K} - \not{P}_2 + m_i) \gamma^5 (\not{K} + \not{P}_1 + m_i)] \quad (D.2)$$

and $\mu^* = \mu^{(4-d)/2}$ is a mass parameter. Q_i and m_i are the charge and mass of the particle i , and N_i is a color factor ($N_i = 1$ for leptons, $N_i = 3$ for quarks). P_1 and P_2 are the momenta of the Z^0 and the photon, respectively. Finally, $\epsilon_{1\mu}^*$ and $\epsilon_{2\nu}^*$ are polarization vectors.

Using

$$\gamma^\mu \gamma^5 + \gamma^5 \gamma^\mu = 0, \quad (D.3)$$

$$\gamma^\mu \not{K} + \not{K} \gamma^\mu = 2K^\mu, \quad (D.4)$$

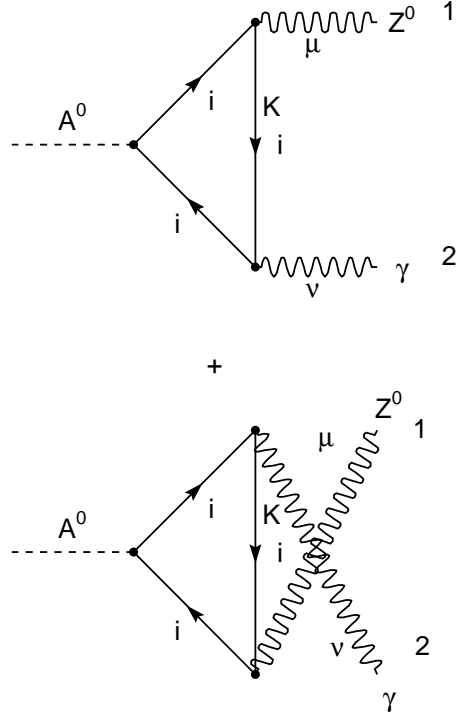


Figure D.1: Feynman diagrams corresponding to the decay $A^0 \rightarrow Z^0 \gamma$. $i = d, s, b, e^-, \mu^-, \tau^-$ or u, c, t .

$$\text{trace}(\text{odd number of } \gamma' s) = 0, \quad (\text{D.5})$$

$$\text{trace}(\gamma^\mu \gamma^\nu) = d\eta^{\mu\nu}, \quad (\text{D.6})$$

$$\text{trace}(\gamma^\mu \gamma^\nu \gamma^\rho \gamma^\sigma) = d(\eta^{\mu\nu} \eta^{\rho\sigma} - \eta^{\mu\rho} \eta^{\nu\sigma} + \eta^{\mu\sigma} \eta^{\nu\rho}), \quad (\text{D.7})$$

$$\text{trace}(\gamma^5 \gamma^\mu \gamma^\nu \gamma^\alpha \gamma^\beta) = -4i\epsilon^{\mu\nu\alpha\beta}, \quad (\text{D.8})$$

$$\text{trace}(\gamma^5 \gamma^\mu \gamma^\nu) = 0, \quad (\text{D.9})$$

and

$$K \not{K} = K^2, \quad (\text{D.10})$$

we can show that

$$\begin{aligned} T = dm_i \{ & -2g_A^i P_1^\mu K^\nu - \frac{4i}{d} g_V^i \epsilon^{\mu\nu\alpha\beta} P_{2\alpha} P_{1\beta} \\ & + g_A^i [-2K^\nu P_2^\mu + 2(P_2 \cdot K) \eta^{\mu\nu}] - g_A^i K^2 \eta^{\mu\nu} \\ & + g_A^i (\eta^{\mu\nu} (P_1 \cdot P_2) - P_2^\mu P_1^\nu + P_1^\mu P_2^\nu) + m_i^2 g_A^i \eta^{\mu\nu} \} \end{aligned} \quad (\text{D.11})$$

From the identity [4]

$$\frac{1}{abc} = 2 \int_0^1 dx \int_0^{1-x} \frac{dy}{[a(1-x-y) + bx + cy]^3} \quad (\text{D.12})$$

where $a, b, c \neq 0$; and setting:

$$a = (K^2 - m_i^2), \quad b = [(K + P_1)^2 - m_i^2], \quad c = [(K - P_2)^2 - m_i^2],$$

we have

$$\begin{aligned} & \frac{1}{(K^2 - m_i^2) [(K + P_1)^2 - m_i^2] [(K - P_2)^2 - m_i^2]} \\ & = 2 \int_0^1 dx \int_0^{1-x} \frac{dy}{[K^2 - m_i^2 + m_Z^2 x + 2K \cdot (P_1 x - P_2 y)]^3} \end{aligned} \quad (\text{D.13})$$

putting $K' = K + (P_1 x - P_2 y)$, and working in the rest frame of A^0 , we get

$$\begin{aligned}
M_{1a} = & -\frac{2g^2 e \tan \beta d}{4m_W \cos \theta_W} \sum_{i=d,s,b,\dots} N_i Q_i m_i^2 \int_0^1 dx \int_0^{1-x} dy \\
& \int \frac{d^d K'}{(2\pi)^d} \left\{ -2g_A^i P_1^\mu K'^\nu - \frac{4i}{d} g_V^i \epsilon^{\mu\nu\alpha\beta} P_{2\alpha} P_{1\beta} - 2g_A^i P_2^\mu K'^\nu \right. \\
& + 2g_A^i \eta^{\mu\nu} \left(P_2 \cdot (K' - (P_1 x - P_2 y)) \right) - g_A^i \eta^{\mu\nu} \left(K' - (P_1 x - P_2 y) \right)^2 \\
& + g_A^i \eta^{\mu\nu} (P_1 \cdot P_2) + m_i^2 g_A^i \eta^{\mu\nu} \} \\
& \times \left[K'^2 - m_i^2 + m_Z^2 x - m_Z^2 x^2 + 2(P_1 \cdot P_2) xy \right]^{-3} \epsilon_{1\mu}^* \epsilon_{2\nu}^* \mu^* \quad (D.14)
\end{aligned}$$

where we have used: $P_1^\mu \epsilon_{2\mu}^* = 0$, $P_1^\mu \epsilon_{1\mu}^* = 0$ and $P_2^\nu \epsilon_{2\nu}^* = 0$.
With the integrals [3]:

$$\int d^d K' \frac{K'^\mu}{[K'^2 - m_i^2 + m_Z^2 x (1-x) + 2(P_1 \cdot P_2) xy]^3} = 0, \quad (D.15)$$

$$\int d^d K' \frac{1}{[K'^2 - m_i^2 + m_Z^2 x (1-x) + 2(P_1 \cdot P_2) xy]^3} = I_0(x, y), \quad (D.16)$$

and

$$\begin{aligned}
& \int d^d K' \frac{K'^2}{[K'^2 - m_i^2 + m_Z^2 x (1-x) + 2(P_1 \cdot P_2) xy]^3} \\
& = I_0(x, y) \frac{d}{2} \frac{[-m_i^2 + m_Z^2 x (1-x) + 2(P_1 \cdot P_2) xy]}{(2 - \frac{d}{2})} \quad (D.17)
\end{aligned}$$

where

$$I_0(x, y) = \frac{i(-\pi)^{d/2} \Gamma(3 - \frac{d}{2})}{2[-m_i^2 + m_Z^2 x (1-x) + 2(P_1 \cdot P_2) xy]^{3-d/2}}; \quad (D.18)$$

we get

$$\begin{aligned}
M_{1a} = & -\frac{2g^2 e \tan \beta d}{4m_W \cos \theta_W (2\pi)^d} \sum_{i=d,s,b,\dots} N_i Q_i m_i^2 \int_0^1 dx \int_0^{1-x} dy I_0(x, y) \\
& \times \left[-\frac{4i}{d} g_V^i \epsilon^{\mu\nu\alpha\beta} P_{2\alpha} P_{1\beta} - 2g_A^i \eta^{\mu\nu} (P_1 \cdot P_2) x + g_A^i \eta^{\mu\nu} (P_1 \cdot P_2) \right. \\
& + m_i^2 g_A^i \eta^{\mu\nu} - g_A^i \eta^{\mu\nu} m_Z^2 x^2 + 2(P_1 \cdot P_2) xy g_A^i \eta^{\mu\nu} \\
& \left. - g_A^i \eta^{\mu\nu} \frac{d[-m_i^2 + m_Z^2 x(1-x) + 2(P_1 \cdot P_2) xy]}{2(2 - \frac{d}{2})} \right] \epsilon_{1\mu}^* \epsilon_{2\nu}^* \mu^* \quad (D.19)
\end{aligned}$$

The invariant amplitude corresponding to the second Feynman diagram of Figure D.1 (crossed diagram) is:

$$\begin{aligned}
M_{2a} = & -\frac{g^2 e \tan \beta}{4m_W \cos \theta_W} \sum_{i=d,s,b,\dots} N_i Q_i m_i \int \frac{d^d K}{(2\pi)^d} (Tra) \\
& \times \frac{1}{(K^2 - m_i^2) [(K - P_1)^2 - m_i^2] [(K + P_2)^2 - m_i^2]} \epsilon_{1\mu}^* \epsilon_{2\nu}^* \mu^* \quad (D.20)
\end{aligned}$$

where

$$\begin{aligned}
Tra = & Trace \left[\gamma^\nu (K + m_i) \gamma^\mu (g_V^i - g_A^i \gamma^5) \right. \\
& \left. [(K - P_1) + m_i] \gamma^5 [(K + P_2) + m_i] \right] \quad (D.21)
\end{aligned}$$

In a similar way, and after performing the calculation of the trace, we can show that

$$\begin{aligned}
M_{2a} = & -\frac{2g^2 e \tan \beta d}{4m_W \cos \theta_W (2\pi)^d} \sum_{i=d,s,b,\dots} N_i Q_i m_i^2 \int_0^1 dx \int_0^{1-x} dy I_0(x, y) \\
& \times \left[-\frac{4i}{d} g_V^i \epsilon^{\nu\mu\alpha\beta} P_{1\alpha} P_{2\beta} + 2g_A^i \eta^{\mu\nu} (P_1 \cdot P_2) x - g_A^i \eta^{\mu\nu} (P_1 \cdot P_2) \right. \\
& - m_i^2 g_A^i \eta^{\mu\nu} + g_A^i \eta^{\mu\nu} m_Z^2 x^2 - 2(P_1 \cdot P_2) xy g_A^i \eta^{\mu\nu} \\
& \left. + g_A^i \eta^{\mu\nu} \frac{d[-m_i^2 + m_Z^2 x(1-x) + 2(P_1 \cdot P_2) xy]}{2(2 - \frac{d}{2})} \right] \epsilon_{1\mu}^* \epsilon_{2\nu}^* \mu^* \quad (D.22)
\end{aligned}$$

Adding Equations (D.19) and (D.22), we obtain

$$M_{1a} + M_{2a} = \frac{4ig^2e \tan \beta}{m_W \cos \theta_W (2\pi)^d} \epsilon^{\mu\nu\alpha\beta} P_{2\alpha} P_{1\beta} \sum_{i=d,s,b,\dots} N_i Q_i m_i^2 g_V^i \int_0^1 dx \int_0^{1-x} dy I_0(x, y) \epsilon_{1\mu}^* \epsilon_{2\nu}^* \mu^* \quad (\text{D.23})$$

In the limit $d \rightarrow 4$, $I_0(x, y)$ is

$$I_0(x, y) = \frac{i\pi^2}{2} \frac{1}{[-m_i^2 + m_Z^2 x(1-x) + 2(P_1 \cdot P_2)xy]} \quad (\text{D.24})$$

Introducing

$$I_i = \int_0^1 dx \int_0^{1-x} \frac{1}{[-m_i^2 + m_Z^2 x(1-x) + 2(P_1 \cdot P_2)xy]} dy, \quad (\text{D.25})$$

we can write

$$M_{1a} + M_{2a} = \frac{g^2e \tan \beta}{8\pi^2 m_W \cos \theta_W} \epsilon^{\mu\nu\alpha\beta} P_{1\alpha} P_{2\beta} \left(\sum_{i=d,s,b,\dots} N_i Q_i m_i^2 g_V^i I_i \right) \epsilon_{1\mu}^* \epsilon_{2\nu}^* \quad (\text{D.26})$$

D.2 b) $i = u, c, t$

In this case, the invariant amplitude is obtained from Equation (D.26) replacing $\tan \beta$ by $\cot \beta$, and then

$$M_{1b} + M_{2b} = \frac{g^2e \cot \beta}{8\pi^2 m_W \cos \theta_W} \epsilon^{\mu\nu\alpha\beta} P_{1\alpha} P_{2\beta} \left(\sum_{i=u,c,t} N_i Q_i m_i^2 g_V^i I_i \right) \epsilon_{1\mu}^* \epsilon_{2\nu}^* \quad (\text{D.27})$$

D.3 Width decay

The total invariant amplitude corresponding to the process $A^0 \rightarrow Z^0 \gamma$ is

$$M = M_{1a} + M_{2a} + M_{1b} + M_{2b} = \frac{g^2e}{8\pi^2 m_W \cos \theta_W} \epsilon^{\mu\nu\alpha\beta} P_{1\alpha} P_{2\beta} \epsilon_{1\mu}^* \epsilon_{2\nu}^* L(\beta) \quad (\text{D.28})$$

where

$$L(\beta) = \tan \beta \sum_{i=d,s,b,\dots} N_i Q_i m_i^2 g_V^i I_i + \cot \beta \sum_{i=u,c,t} N_i Q_i m_i^2 g_V^i I_i \quad (\text{D.29})$$

The absolute value of the invariant amplitude squared and summed over final polarizations is

$$\begin{aligned} \overline{|M|^2} &= \frac{g^4 e^2}{64\pi^4 m_W^2 \cos^2 \theta_W} \epsilon^{\mu\nu\alpha\beta} \epsilon^{\rho\sigma\gamma\delta} P_{1\alpha} P_{2\beta} P_{1\gamma} P_{2\delta} \\ &\quad \left(\sum_{\lambda} \epsilon_{1\mu} \epsilon_{1\rho}^* \right) \left(\sum_{\lambda'} \epsilon_{2\nu} \epsilon_{2\sigma}^* \right) |L(\beta)|^2 \end{aligned} \quad (\text{D.30})$$

Since

$$\sum_{\lambda} \epsilon_{1\mu} \epsilon_{1\rho}^* = -\eta_{\mu\rho} + \frac{P_{1\mu} P_{1\rho}}{m_Z^2}, \quad (\text{D.31})$$

$$\sum_{\lambda'} \epsilon_{2\nu} \epsilon_{2\sigma}^* = -\eta_{\nu\sigma}, \quad (\text{D.32})$$

and because,

$$\epsilon^{\mu\nu\alpha\beta} P_{1\alpha} P_{1\mu} = 0, \quad (\text{D.33})$$

$$\epsilon^{\mu\nu\alpha\beta} \epsilon_{\mu\nu}{}^{\gamma\delta} = -2 \left(\eta^{\alpha\gamma} \eta^{\beta\delta} - \eta^{\alpha\delta} \eta^{\beta\gamma} \right), \quad (\text{D.34})$$

we obtain

$$\overline{|M|^2} = \frac{g^2 e^4 (P_1 \cdot P_2)^2}{32\pi^4 m_W^2 \sin^2 \theta_W \cos^2 \theta_W} |L(\beta)|^2 \quad (\text{D.35})$$

where we have used $g = e/\sin \theta_W$.

The differential decay rate corresponding to the channel $A^0 \rightarrow Z^0 \gamma$ is

$$d\Gamma = \frac{\overline{|M|^2} |\vec{P}_1| d\Omega}{32\pi^2 m_{A^0}^2} \quad (\text{D.36})$$

From the kinematics we can show that

$$|\vec{P}_1| = \frac{m_{A^0}^2 - m_Z^2}{2m_{A^0}}, \quad (\text{D.37})$$

$$P_1 \cdot P_2 = \frac{1}{2} (m_{A^0}^2 - m_Z^2), \quad (\text{D.38})$$

and because, $\frac{G_F}{\sqrt{2}} = \frac{g^2}{8m_W^2}$ and $\alpha_{em} = \frac{e^2}{4\pi}$, we can write

$$\Gamma(A^0 \rightarrow Z^0 \gamma) = \frac{\sqrt{2}G_F \alpha_{em}^2 m_{A^0}^3}{32\pi^3 \sin^2 \theta_W \cos^2 \theta_W} \left(1 - \frac{m_Z^2}{m_{A^0}^2}\right)^3 |L(\beta)|^2. \quad (D.39)$$

With $(P_1 \cdot P_2)$ given by D.38, the value of I_i is

$$I_i = \frac{1}{4m_i^2} I(\tau_i, \lambda_i) \quad (D.40)$$

where

$$I(\tau_i, \lambda_i) \equiv \frac{\tau_i \lambda_i}{(\lambda_i - \tau_i)} (f(\tau_i) - f(\lambda_i)), \quad (D.41)$$

$$\tau_i = \frac{4m_i^2}{m_{A^0}^2}, \quad (D.42)$$

$$\lambda_i = \frac{4m_i^2}{m_Z^2}, \quad (D.43)$$

and

$$f(x) = \begin{cases} -2 [\arcsin(x^{-1/2})]^2 & \text{if } x > 1 \\ \frac{1}{2} \left[\ln \left(\frac{1+(1-x)^{1/2}}{1-(1-x)^{1/2}} \right) - i\pi \right]^2 & \text{if } x \leq 1 \end{cases} \quad (D.44)$$

(note that for $x \ll 1$, we have $f(x) \approx \frac{1}{2} [\ln(\frac{x}{4}) + i\pi]^2$)

Thus, we obtain

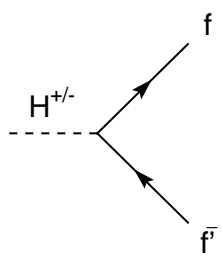
$$\begin{aligned} \Gamma(A^0 \rightarrow Z^0 \gamma) &= \frac{\sqrt{2}G_F \alpha_{em}^2 m_{A^0}^3}{512\pi^3 \sin^2 \theta_W \cos^2 \theta_W} \left(1 - \frac{m_Z^2}{m_{A^0}^2}\right)^3 \\ &\quad \left| \tan \beta \sum_{i=d,s,b,e^-,..} N_i Q_i g_V^i I(\tau_i, \lambda_i) \right. \\ &\quad \left. + \cot \beta \sum_{i=u,c,t} N_i Q_i g_V^i I(\tau_i, \lambda_i) \right|^2 \end{aligned} \quad (D.45)$$

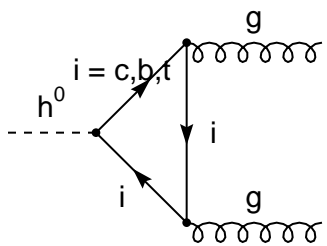
The coefficients g_V^i are given in table 3.1 (Chapter three).

In Equation (D.45), the dominant contributions correspond to the τ^- and the b and t quarks. Thus, (D.45) reduces to Equation (3.44).

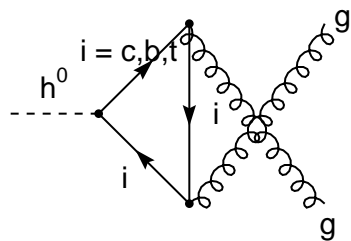
Bibliography

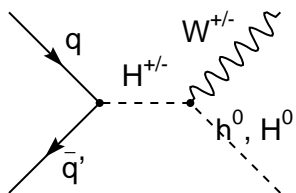
- [1] Carlos Marín and Bruce Hoeneisen, POLITECNICA **XVI**, No. 2, 33 (1990).
- [2] Chris Quigg, Gauge Theories of the Strong, Weak and Electromagnetic Interactions, Addison Wesley (1983), p. 307; Ta-Pei Cheng and Ling-Fong Li, Gauge Theory of Elementary Particle Physics, Oxford University Press (1991), p. 495.
- [3] Stefan Pokorski, Gauge Field Theories, Cambridge University Press (1990), p. 367-369.
- [4] Lewis H. Ryder, Quantum Field Theory, Cambridge University Press (1985), p. 346.





+





+

